UNIVERSITÀ DEGLI STUDI DI PADOVA

DIPARTIMENTO DI INGEGNERIA INDUSTRIALE

CORSO DI LAUREA MAGISTRALE IN INGEGNERIA CHIMICA E DEI PROCESSI INDUSTRIALI

Tesi di Laurea Magistrale in
Ingegneria Chimica e dei Processi Industriali

TECHNICAL ANALYSIS OF A COMBINED JUICE CONCENTRATION PROCESS INVOLVING OSMOTIC EVAPORATION, MEMBRANE DISTILLATION AND DIRECT CONTACT EVAPORATION

Relatore: ***Prof. Fabrizio Bezzo, Universitá degli studi di Padova***
Correlatori: ***Prof. Cristiano Piacsek Borges, COPPE/UFRJ***
Prof. Paulo Laranjeira da Cunha Lage, COPPE/UFRJ

Laureando*: *ENRICO FAVARO

ANNO ACCADEMICO 2012 – 2013

In memory of my Grandfather,
to the love of my parents and brother, steady wind at my back

Riassunto

La Tesi è stata svolta nel centro di ricerca e post laurea COPPE dell'Università Federale di Rio de Janeiro, all'interno di un programma di accordi bilaterali con l'Università di Padova.

Lo scopo della Tesi è di integrare il lavoro fatto all'interno della COPPE da Ribeiro Jr. (2005) e Ongaratto (2012) valutando la fattibilità di un nuovo processo di concentrazione di succo di frutta, basato su evaporazione osmotica (OE), distillazione a membrana (MD) e evaporazione per contatto diretto (DCE).

La tecnica più diffusa per la concentrazione di succhi è la tradizionale evaporazione a multiplo effetto, che raggiunge temperature sufficientemente elevate da compromettere vitamine, aromi, colore e porta ad un prodotto finale con caratteristiche di "cotto".

Le tecniche di concentrazione a membrana permettono di operare la concentrazione di succhi di frutta a basse temperature, preservando quindi le caratteristiche del prodotto fresco.

In questa Tesi, è stato studiato in particolare il processo combinato di MD+OE, che sfrutta l'effetto sinergico del gradiente di pressione osmotica e di temperatura per raggiungere elevati gradi di concentrazione della soluzione di saccarosio (scelta per motivi di praticità). L'agente osmotico scelto è il pirofosfato di potassio, che in seguito alla diluizione subita durante la concentrazione del succo, necessita di essere rigenerato; a questo scopo è stato scelto il processo DCE, che rispetto alle convenzionali tecniche di concentrazione è più semplice e la sua maggiore efficienza non è intaccata dall'uso di liquidi incrostanti o corrosive come possono essere le soluzioni saline. Inoltre, considerando che il liquido si concentra ad una temperatura dai 10 ai 30 °C al di sotto della sua temperatura di ebollizione e la possibilità di usare gas di combustione come vettore termico, è evidente l'ulteriore abbattimento dei costi di gestione.

Nel processo di rigenerazione con gas di combustione altamente ricco di CO2, l'agente osmotico si satura di CO2, il che potrebbe rappresentare un problema nel momento in cui quest'ultima attraversi la membrana, trasferendosi al succo durante il processo di concentrazione a membrana.

Al fine di conoscere la solubilità della CO2 nelle soluzioni coinvolte nel processo a membrana, sono stati effettuati dei saggi preliminari in acqua, soluzione di saccarosio e soluzione di pirofosfato di potassio, a varie concentrazioni.

Il processo MD è stato eseguito usando una corrente di acqua calda e una corrente di acqua fredda satura di CO2, mentre il processo MD+OE è stato eseguito usando una soluzione di saccarosio e una soluzione di pirofosfato di potassio satura di CO2; In

entrambi i casi sono stati misurati i flussi di CO2 e acqua permeati attraverso la membrana.
Un semplice modello basato sulla legge di Fick ha permesso di quantificare il contributo del gradiente di temperatura e del gradiente di pressione osmotica sul flusso di permeato.
Nel processo DCE, una corrente di aria riscaldata tramite una resistenza è stata utilizzata per evaporare rispettivamente acqua e una soluzione di cloruro di sodio; il sale è stato scelto in base alla più semplice reperibilità del coefficiente di attività. Un modello predittivo semplificato applicato ai bilanci di massa e energia ha permesso di confrontare i dati sperimentali con quelli della simulazione e di calcolare la percentuale di calore latente fornito tramite scambio bifasico.

Abstract

This Thesis was developed during a student exchange at COPPE/UFRJ with the aim of complementing Ribeiro Jr. (2005) and Ongaratto (2012) works involving a new route of fruit juice concentration made-up by a combined osmotic evaporation and membrane distillation process (OE+MD) and direct contact evaporation (DCE) for draw regeneration. OE+MD allows solution concentration without needing high temperature and then is suitable for thermo labile solutions concentration, preserving flavours, vitamins and colour. Due to the absence of walls separating fluids, DCE is desirable for the concentration of saline solutions.

Hollow fibers of polypropylene have been used to carry out MD (hot water - CO2 saturated cold water) and OE+MD (sucrose solution - CO2 saturated draw). In MD process, CO2 flux was great, while water flux resulted 0.592 Kg/h K m^2. In OE+MD process, while CO2 flux was negligible, water flux resulted 1.718 Kg/h K m^2.

Osmotic pressure gradient and temperature gradient contributions to water flux were analyzed using Fick's law. As a result it has been discovered that CO2 does not represent a serious contamination problem if potassium pyrophosphate is used in combined OE+MD.

Regarding DCE, hot air was used for water and draw concentration. In the first case, model simulation showed a good agreement with experimental data, and the quantity of heat provided by biphasic exchange is similar in both cases.

Table of contents

List of Figures

List of Tables

List of simbols

OE: Osmotic evaporation;
MD: Membrane distillation;
DCE: Direct contact evaporation;
ΔP_{lv} : pressure difference in the liquid-vapour interface;
r_{max} : maximum value of membrane pore size;
γ_{lv} is the liquid-vapour surface tension;
B : geometric factor, unitary for the cylindrical shape;
Π = Osmotic pressure;
Φ = Osmotic coefficient;
i = Van't Hoff factor;
M = Mean molarity;
R = Gas universal constant ;
J_w: Water flux through the membrane;
$J_{w,T}$: Permeate flux due to temperature gradient;
$J_{w,\pi}$: Permeate flux due to osmotic pressure gradient;
A_m: Membrane area;
M_p: Permeated mass through the membrane;
ΔT_a: Average temperature gradient between the two solutions;
$\Delta \Pi_a$: Average concentration gradient between draw and sucrose solution;
$k_{m,t}$: Mass transfer coefficient relative to the temperature gradient;
$k_{m,\Pi}$: Mass transfer coefficient relative to the osmotic pressure gradient;
T^{res} : Oven resistance temperature;
T^{ove} : Temperature of gas coming from oven;
T^{in} : Temperature of gas entering the column;
T^{L}: Temperature of the liquid in the column;
T^{out} : Temperature of gas coming out from the top of the column;
T^{amb}: Ambiental temperature;
T^{cold} Temperature of gas leaving the condenser;
$u\%$: Relative humidity of gas flux coming out from the top of the column;
G: entering total gas flow rate;
$m_w{}^c$: Mass flow rate of condensed water;
$m_w{}^e$: Mass flow rate of evaporated water;
m^{inc}: Mass flow rate of uncondensed water, leaving the condenser;
m_i^{in} : Mass flow rate of component i entering the column;

m_i^{out} : Mass flow rate of component i leaving the column;
m_{the}^{ev}: Evaporated water mass flow rate (thermo hygrometer data based);
m_{VLE}^{ev}: Evaporated water mass flow rate (VLE calculation based);
m_{wei}^{ev}: Evaporated water mass in interval (i) (balance data based);
M_j (i): Mass amount of component j flowed during a 15 minutes generic interval (i) of m_j flow rate;
P^{top} : Pressure at the top of the column;
p_w : Water partial pressure;
RI: refraction index;
$_a$: Referring to air;
$_w$: Referring to water;
z_i^{in} : Mass fraction of component i in the stream entering the column;
z_i^{out} : Mass fraction of component i in the stream leaving the column;
y_w^{inc}: Mass fraction of water in the stream leaving the condenser;
y_i^{in} : Molar fraction of component i in the stream entering the column;
y_i^{out} : Molar fraction of component i in the stream leaving the column;
y_w^{inc}: Molar fraction of water in the stream leaving the condenser;
MW_i : Averaged component i molecular weight;
γ_w : Water activity coefficient;
$\emptyset_w$: Water fugacity coefficient;
x_w : Molar fraction of water in NaCl solution;
x_{NaCl} : Molar fraction of NaCl in NaCl solution;
f_w^0 : Water fugacity;
P_w^{sat}: Water vapor pressure at saturation;
P^{atm}: Ambient pressure;
$e_{wei}^{ev}(i)$: Relative error between $M_{wei}^{ev}(i)$ and $M_{the}^{ev}(i)$;
$e_{VLE}^{ev}(i)$: Relative error between $M_{VLE}^{ev}(i)$ and $M_{the}^{ev}(i)$;
q^{in}: Heat flow rate entering the column;
q_i^{in}: Heat flow rate of component i entering the column;
q^{out}: Heat flow rate leaving the column;
q_i^{out}: Heat flow rate of component i leaving the column;
q_w^{ev}: Latent heat flow rate leaving the column;
$q_{conduct}$: Heat flow rate provided by sparger conduction;
Q : Heat amount flowed during a 15 minutes generic time interval (i) of q flow rate;
$C_{p,i}^{in}$: Specific heat of component i at T^{in};
$C_{p,i}^{out}$: Specific heat of component i at T^{L};
λ_m: Water latent heat at T^{L};
$_{wei}$: Referring to weight experimental data;

$_{the}$: Referring to thermo hygrometer experimental data;

$_{VLE}$: Referring to VLE prediction model.

Chapter 1

Introduction

This Master thesis work was carried out from August 2012 to February 2013, with the supervision of Ricardo Schmitz Ongaratto, Prof. Cristiano Piacsek Borges and Paulo Laranjeira da Cunha Lage at COPPE (Alberto Luiz Coimbra Institute for Graduate Studies and Research in Engineering) of the Federal University of Rio de Janeiro.
In particular, activity was conducted in two research departments: PAM (Permeation through membranes) directed by Prof. Borges and TFD (Thermo-fluid dynamics) directed by Prof. Lage.

1.1 Background and motivation

People are looking for healthy food to counter poor health caused by busy lifestyles, insufficient exercise and fast food; as a consequence, people all over the world are recognising that diet is important to their health.
In particular, fruits contain many health-promoting factors such as fibers and large amounts of minerals, vitamins, flavonoids and phenolic acids (Ribeiro et al., 2009).
Low fruit and vegetable intake is among the top ten risk factors contributing to mortality, according to evidence presented in *World Health Report* (World Health Organization, 2003).
On a global level, up to 2.7 million lives could potentially be saved each year with sufficient fruit and vegetable consumption; in fact, as part of the daily diet, they could help prevent major non communicable diseases such as cardiovascular diseases and certain cancers.
Worldwide, low fruits and vegetables intake is estimated to cause about 19% of gastrointestinal cancer, about 31% of ischemic heart disease and 11% of stroke.
The global burden attributable to low fruit and vegetable consumption translates in about 85% of cardiovascular diseases and 15% of cancers.
Global sales for food and drink in the “naturally healthy” category reached US$103 billion in 2004 (Euromonitor, 2005).
As a consequence, the global market for fruit and vegetable juices is growing and is forecast to reach 72.29 billion litres by the year 2017 (Global Industry Analysts, 2012).

World orange juice imports for 2006 are valued at $2.2billion, with frozen concentrated orange juice valued at $880 million and not frozen orange juice valued at $1.3billion. Brazil accounts for nearly 84% of total orange exportations (Global Trade Atlas, 2007).
Due to its geographical location, Brazil has great production potential of tropical fruits. Most of these fruits are delicate and have low durability, deteriorating with heating or during transportation, which turns difficult their commercialization and application in food industry.
Another complicating factor is the seasonal nature of certain fruits, which are available just a few months during the year.
Juices and pulps industrial processing is a way to promote an economically profitable production, stocking and transport of fruits throughout the whole year, independently of seasonality or raw material source (FAO, 2001).
It is observed by consumer trends that juice market yet can grow, aided by the improvement of processed product sensorial qualities and combined with marketing strategies in order to meet consumer expectations.

1.2 State of the art and future perspective

Advanced nations consumers desire to have a juice with a freshly squeezed product flavour.
Nowadays, classic or vacuum evaporation are the most economically interesting concentration techniques; their major problem is represented by a set of chemical-physical reactions promoted by relatively high temperature that results in changes in nutritional facts, color, flavor and aroma of such a thermal sensible mix as fruit juice (Cliff et al., 2000, Myrna et al., 1990 and Schreier, 1981).
Remembering that orange juice aroma is the result of a 200 compounds mix (Kato et al., 2003) the aim of creating artificial aroma with the purpose to pretend natural aroma is a hard challenge if economical issues are taken in account.
By focusing on improvement of product quality, many bench scale processes have been developed: membrane distillation (Gunko et al., 2006), direct osmosis (Jacobs et al., 1988), reverse osmosis (Zhang et al., 1991) membrane evaporation (Smith et al., 1986) and nanofiltration (Bagley et al., 2002 and Bánvölgyi, 2006). At the moment the most studied processes are osmotic evaporation and freeze concentration (Merory et al., 1968 and Little et al., 1977). In particular a good future perspective is represented by OE and MD, which justifies this study.

1.3 Objective

The aim of this work is to experimentally investigate a process for fruit juice concentration that results in a final product with superior sensorial characteristics, in respect of traditional vacuum concentration.

The purpose is to validate operating conditions of an integrated system involving a combined OE+MD process for fruit juice concentration and DCE for regenerating the draw coming from membrane separation process.

In OE+MD process, carbon dioxide permeation from draw to juice/sugar solution is studied.

In DCE step, draw is regenerated by bubbling CO2 rich gas (simulating combustion process gas) and process efficiency is studied.

1.4 Test organization

Chapter 1 is an introduction part explaining background, motivation, state of the art and the purpose of the study. In Chapter 2, a general overview about the concentration of fruit juices explaining principles and feasibility of the processes available nowadays is presented. Chapter 3 contains a literature survey that widely describes the principles and underlines the variables playing in two different processes: membrane separation processes focusing on OE+MD and multiphase processes focusing on bubbling columns.

Chapter 4 describes the experimental bench-scale apparatus and the experimental procedure for OE+MD and DCE.

Experimental results and mathematical modeling for OE+MD and DCE are explained respectively in Chapter 5 and 6.

In Chapter 7, conclusions, limitations and further perspectives of work are exposed. This thesis ends with Chapter 8 reporting annexes used in this work.

Chapter 2

Concentration of fruit juices: general overview

Fruit juices commercial production started in the XX century in Europe with the Boehi process of apple juice stocking and diffusion of industrialized juices started in United States only in 1929.
During WWII, juice commercial production had a big growth that continued for the following years, helped by new technologies application.
Nowadays, people are looking for healthy foods and as a consequence the fruit juice market is showing a big growth (Global Industry Analysts, 2012).
In fruit juices as in most of foods, water is the major ingredient (between 75 and 97 percent in weight) (Nevo Foundation, 1996) so concentration process as a preservative technique leads to a reduction of elaboration, stocking and transportation costs, thanks to a remarkable volume reduction. Also, water activity reduction in concentrated juice gives a better stability at microbial deterioration.
The effect of this technology is to purchase a concentrated product with preserved nutritional facts and quality, that could be reconstituted simply by adding water.
In fact, this is a hard goal to achieve because during water removal phase, a series of non reversible reactions and loss of compounds takes place.

2.1 Legislation

Recent guidelines (UK Food Standards Authority, 2003) provide an extension of the description of ‘fruit juice from concentrate’ that leads to stricter limitations. The following designation is given:
The product obtained by replacing, in concentrated fruit juice, water extracted from that juice during concentration, and by restoring the flavors and, if appropriate, pulp and cells lost from the juice but recovered during the process of producing the fruit juice in question or fruit juice of the same kind; in which the water added must display such chemical, microbiological, organoleptic and, if appropriate, other characteristics as will guarantee the essential qualities of the juice; and the product must display organoleptic

and analytical characteristics at least equivalent to those of an average type of fruit obtained from fruit or fruits of the same kind.

2.2 Thermal separation

Thermal evaporation is the older way to concentrate juices and one of the most commons basic unit operations in liquid food production. In this process, the concentration raise of solution is obtained through solvent removal at his boiling temperature, by purchasing a sufficient amount of energy for the molecules to win intermolecular attraction forces.
Usually, heating fluid in food industry is saturated steam that condenses by exchanging his latent heat with liquid that is evaporating. Then, it is a latent heat exchange (of condensation and of evaporation) (Ordóñez, 2005 apud Ongaratto, 2012).

2.2.1 Classic evaporation

Classic evaporation process is the simplest kind of thermal concentration process, it operates at 1 atmosphere in open pan evaporators. Open pan evaporators consist of a container open to the atmosphere in which fluid is heated by a flame or by steam through a coil or external jacket.
High temperatures lead to chemicals reactions, like lipids oxidation and the Maillard reaction between sugars and aminoacids, able to change colour and flavour. Others problems are fouling at the heat exchange walls that require cleaning every 6 hours and aroma loss with the vapour flux (Umano et al., 1992)
Aroma is such a complex mixture of hundreds of organic substances that are found in very little concentrations (of the order of mg/L or μg/L) and give the characteristic fragrance and taste of fruit.
Low volatility of these compounds promotes their transference to aqueous vapour phase during evaporation process and so there is an additional cost on recovering the volatile materials and in blending them in the finished concentrate (Werkhoff et al., 1998, Mannheim, 1975 and Smith, 2006 apud Ongaratto, 2012).
A serious drawback of classic evaporation is the high energy intensity required for vaporization.

2.2.2 Thermally accelerated short time evaporator (TASTE)

TASTE belongs to the falling film multiple-effect evaporators class and is widely used particularly to concentrate substances known to be sensitive and easily spoiled when submitted to high temperature, even for short times.

It usually uses a great number of evaporating stages (up to 8) with a progressively lowering temperature and pressure that dramatically reduces steam consumption per each unit of evaporated water.

In general evaporation takes place inside vertical tubes and the process fluid to be evaporated flows downwards by gravity as a continuous film. The fluid creates a film along the tube walls, progressing downwards (falling) and allowing very high heat transfer coefficients (Figure 2.1).

Evaporation takes place at very low mean temperature differences between heating medium and process stream, typically between 3 - 6K, therefore these devices are ideal for heat recovery in multi stage processes (Chun et al. 1971)

A further advantage of the falling film evaporator is the very short residence time of the liquid and the absence of superheating of the same. Not considering the vapour

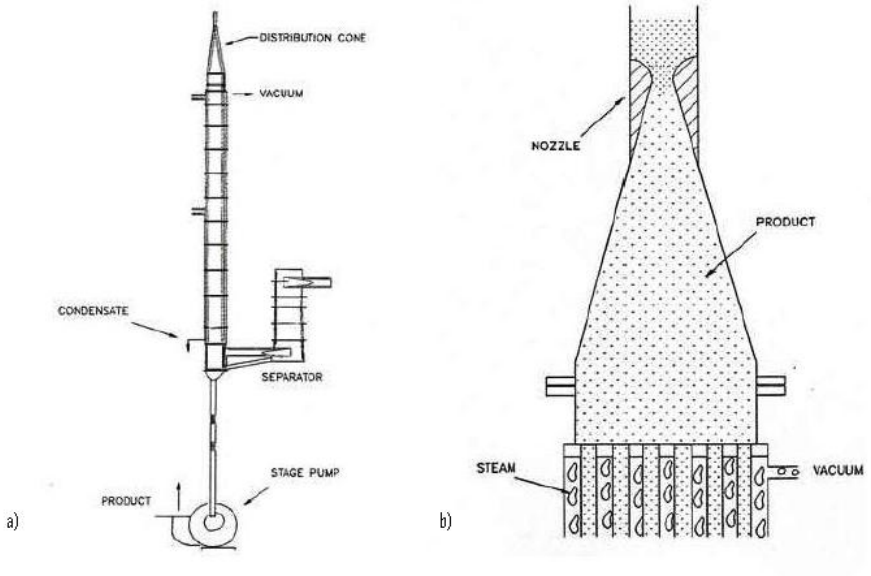

Figure 2.1 *TASTE evaporator: a) Single effect: b) Distribution cone (FMC Technologies Italia S.p.A.).*

separator, the residence time inside the tubes is measured in seconds.

TASTE is also characterised by very low pressure drops, therefore is often used in deep vacuum applications. Generally, it operates at vacuum in the temperature range between 40°C and 85°C with a multiple effect system (Umano et al., 1992)

In juice concentration, TASTE is the more economically competitive and the most developed from a technical point of view but it shows, although in a smaller magnitude, the same disadvantages seen in classic evaporation.

2.3 Membrane separation

Starting in the late sixties, membrane processes gradually have found their way into industrial applications and serve as viable alternatives for more traditional processes

like distillation, evaporation or extraction. Based on the main driving force, which is applied to accomplish the separation, many membrane processes can be distinguished. An overview of the driving forces and the related membrane separation processes is given in Table 2.1.

Table 2.1 *Driving forces and their related membrane separation processes.*

Driving force	Membrane process
Pressure difference	Microfiltration
	Ultrafiltration
	Nanofiltration
	Reverse osmosis
Chemical potential difference	Pervaporation
	Pertraction
	Dialysis
	Gas separation
	Vapour permeation
	Liquid membranes
Electrical potential difference	Electro dialysis
	Membrane electrophoresis
	Membrane electrolysis
Temperature difference	Membrane distillation

2.3.1 Forward osmosis

A schematic representation of the FO process is shown in Figure 2.2.

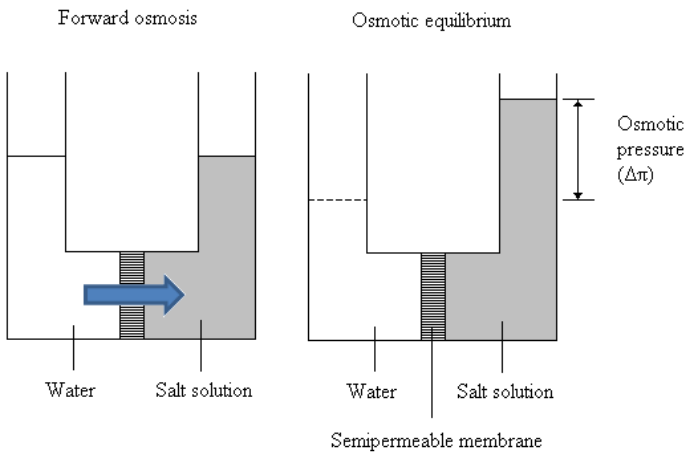

Figure 2.2 *Schematic illustration of forward osmosis.*

Osmosis is the transport of water across a selectively permeable membrane, from a region of higher water chemical potential to a region of lower water chemical potential.

It is driven by a difference in solute concentrations across the membrane that allows passage of water, but rejects most solute molecules or ions.
Forward osmosis (FO or direct osmosis) is a membrane based process that operates juice concentration at low temperatures and pressure, preserving flavor, aroma and color of fresh juice.
FO uses an osmotic agent to create an osmotic pressure gradient across the membrane and so water is removed from fruit juice (Jiao et al., 2004).
FO membranes are dense, with a thickness of 25-100 μm. One of FO disadvantages is salt diffusion trough the membrane, that happens if a saturated solution is used (Popper et al., 1966 apud Ongaratto, 2012).

2.3.2 Reverse osmosis

In reverse osmosis (RO) juice dewatering is obtained by applying a pressure gradient through a dense selective membrane. Pressure gradient utilized are in the order of 24-100 bar (Zhang et al. 1991 apud Ongaratto, 2012).
RO overcomes traditional evaporation because of low thermal degradation of the product, reduction of energy consumption and low capital investment. (Jiao et al., 2004).
RO shows lower loss of aroma compounds but membrane surface is likely to material deposition, with consequent flux reduction (Gostoli et al., 1999, Ramteke et al., 1993).
The major disadvantage is that the maximal concentration that can be achieved is 30 percent of soluble solids, because of the steep increase of juice osmotic pressure, during concentration process. (Das Gupta et al., 1996, Medina et al., 1988 apud Ongaratto, 2012).

2.3.3 Membrane distillation

Membrane distillation (MD) is characterized by a via vapor phase non-isothermal water transport between two water solutions at different temperatures, separated by a microporous hydrophobic membrane. Thanks to membrane properties, as long as the pressure does not exceed a limit value, liquid water is not allowed to flow through the pores. The driving force is the difference in water fugacity between the two membrane interfaces, due to temperature gradient which sets up a pure water flow through the membrane, from high to low temperature (Sheng et al. 1991 apud Ongaratto, 2012).
The process occurs at atmospheric pressure and temperature employed may be much lower than the normal solutions boiling temperature.
Liquid-vapor equilibrium is kept on both side of the pore, that being at different temperatures will be characterized by different vapor pressures. This condition

promotes water evaporation in the hot side and water vapor condensation in the cold side, generating the vapor flux. A schematic representation of the MD process is shown in Figure 2.3.

Water transport origin in this kind of process is a difference in water chemical potential created by a vapor pressure difference. This is produced by a temperature difference

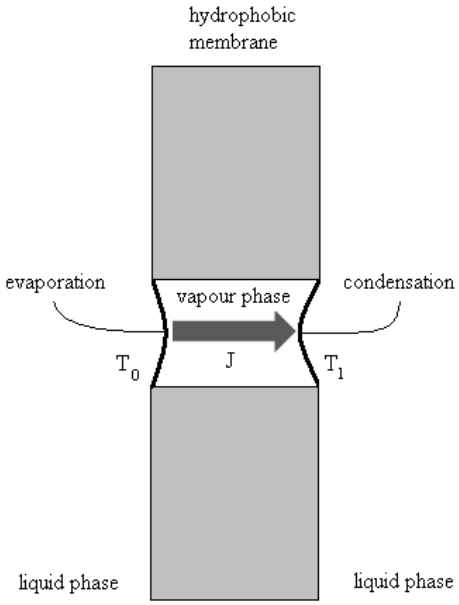

Figure 2.3 *A schematic representation of the MD process.* T_1*, temperature at the hot side:* T_0*, temperature at the cold side:* J*, flux of the vapour phase.*

between the two solutions facing the membrane, but could also be produced by different concentrations between the two aqueous solutions, and in this case the process is called "osmotic distillation" if the system is kept in isothermal conditions and the difference in concentration is produced by non-volatile solutes (Mengual, 1993 and Sheng et al., 1991 apud Ongaratto, 2012).

MD efficiency shows a slight decrease with increasing salt (or other inorganic solutes) concentration, because of a decrease in vapor pressure.

Another drawback is the little temperature gradient that can be applied without causing juice degradation.

2.3.4 Nanofiltration

NF cut-off (300-500 g/mole) lies between that of reverse osmosis and ultrafiltration, so it is used to achieve a separation between sugars, other organic molecules and multivalent salts on one hand and monovalent salts and water on the other.

NF is suitable for juice concentration, because it retains more components than the ultrafiltration that, being characterized by a membrane pore size between 2 nm and 0.05 μm and operating pressures between 1 and 10 bar, is used to separate colloids like

proteins from small molecules like sugars and salts. (Bánvölgyi, 2006 and Timmer, 2001 apud Ongaratto, 2012). A schematic representation of the NF process is shown in Figure 2.4.

The advantage of NF over reverse osmosis is that on average it requires 21% less energy expenditure (A.P. Echavarrıa et al., 2011). With these properties, the most important application of NF areas can be defined:

– removal of monovalent ions from waste water, reaction mixtures in which NaCl is formed and whey;

– separation between ions with different valences;

– separation of low- and high-molecular weight components. (Timmer, 2001)

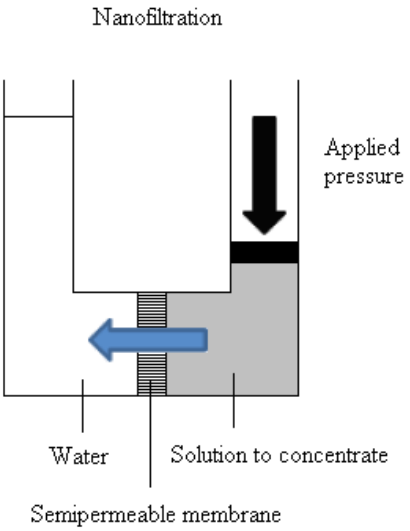

Figure 2.4 *A schematic representation of the NF process.*

2.3.5 Freeze concentration

In freeze concentration (FC) water is removed in the solid state of ice crystals and technique is effective because a solute in solution has a lower melting point of pure ice and can be separated from the water (ice) component as the temperature approaches the melting point of pure ice.

Because of low process temperatures and high viscosities of the fruit juices, the maximum achievable concentration is 40–45 °Brix which is much lower than that achieved during the evaporation process (Raghavarao et al., 2005).

Fruit juice viscosity increase retards the crystallization rate and makes the pumping of the juice concentrate and ice crystals washing very difficult.

In addition, this technique is not suitable to handle liquid foods with high pulp content.

FC has been utilized in food industry for over 30 years, but the equipment and operational costs are very expensive. (Smith, 2006, Nonthanum, 2008)
A schematic representation of the FC process is shown in Figure 2.5.

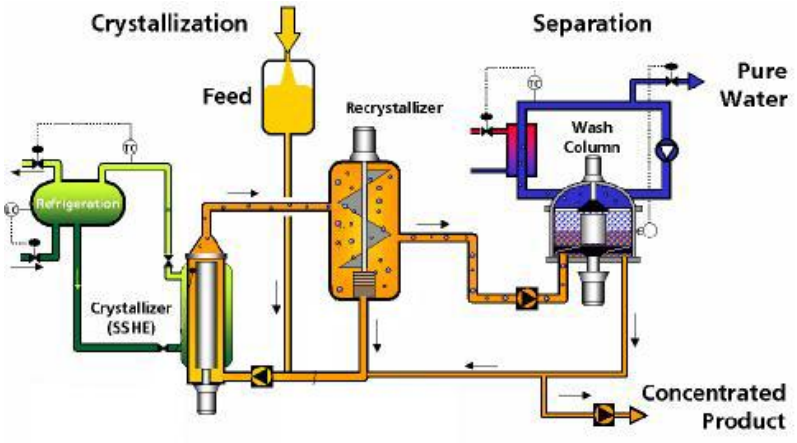

Figure 2.5 *Basic single-stage freeze concentration process based on the Niro developed and patented principles of separate nucleation and growth (Niro Process Technology, 2002).*

2.3.6 Osmotic evaporation

OE is a membrane separation technique that preserves the final product quality, because operates at low temperatures; in fact the driving force is due to the pressure difference between juice and draw.
OE is a kind of direct osmosis that uses a hypertonic solution (generally draw) to remove water; a microporous hydrophobic membrane is used (Figure 2.6).
In comparison to FO, OE does not suffer of salt transference from draw to the solution to be concentrate, as long as the pressure gradient applied through the membrane does not exceed a limit value.

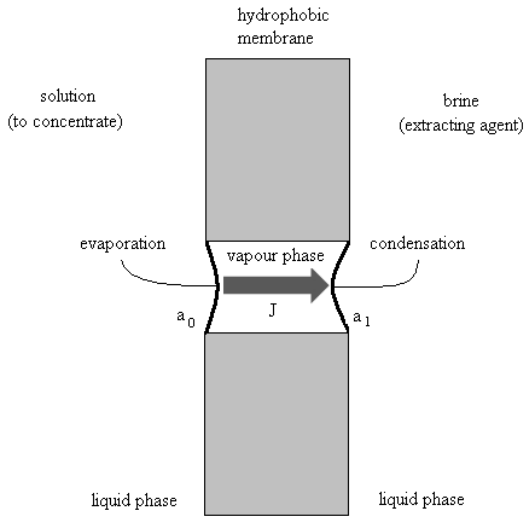

Figure 2.6 *A schematic representation of the OE process.* a_1*: activity of solvent at diluted solution side;* a_2*: activity of solvent at draw side;* J*: flux of the vapour phase.*

Differently from FO, OE can work with no osmotic pressure limits and so is able to achieve concentration degrees typical of a conventional thermal evaporation. (Gostoli, 1999 apud Ongaratto, 2012).
OE process is similar to MD, with the advantage of being able to work at ambient temperature. The driving force is chemical potential, derived by the concentration difference between the two solution.
With the aim of improving process efficiency, OE can be coupled with MD, in other words by applying a temperature gradient over the natural osmotic gradient due to the characteristics of the two solutions (Hongvaleerat et al., 2008, Onsekizoglu et al., 2010, Thanedgunbaworn et al., 2007 apud Ongaratto, 2012).
The main problem of OE is the impossibility to work with diluted draw. Corrosion and the important salt amount needed, make draw regeneration by conventional evaporation an expensive step.

2.4 Purpose of integrated process

2.4.1 Coupled process of combined OE+MD and draw regeneration

With the aim of improving water flux across the membrane, OE and MD processes were coupled. This process consists in conducting membrane separation using a draw colder than the sucrose solution.
In this way, driving forces of two processes (osmotic pressure gradient and temperature gradient) are summed.

2.4.2 Regeneration of draw by DCE

This step is directed to remove from draw the water stream extracted from fruit juice. Draw coming from combined OE+MD process has been diluted and before being recirculated, needs to be regenerated with the cheapest concentration process, in order to keep the economical competitiveness of the whole fruit juice concentration process.

2.5 Considerations

As long as the target of the technology studied in this work is to yield a superior product, it is clear that thermal processes like classical evaporation and TASTE, although are able to achieve a high concentration degree, cannot however preserve natural flavor, aroma, color and the whole set of healthy compounds naturally contained in fruit juice.

NF, RO and MD processes do not reach an interesting concentration degree.
FC allows a sufficient concentration degree that is limited by the difficult ice separation; For this reason and for an economical issue, the process does not yet represent a worthy option.
If saturated draw is used, FO can achieve interesting concentration degrees but this condition promotes salt diffusion through the membrane, making the process clearly unviable for food processing.
In Table 2.2, retention degree of principal membrane separation processes was schematized. In Table 2.3, key features of principal fruit juice concentration processes were schematized, using "P" and "R" for indicating respectively permeated and rejected.

Table 2.2 *Retention degree of different membrane processes.*

Technology	Water	Salts	Macromolecules	Suspended solids
Microfiltration	P	P	P	R
Ultrafiltration	P	P	R	R
Nanofiltration	P	Part. P	R	R
Reverse osmosis	P	R	R	R
Forward osmosis	P	R	R	R
Osmotic evaporation	P	R	R	R
Membrane distillation	P	R	R	R

DCE offers some advantages when compared to conventional methods of evaporation; Because of its high efficiency of heat transfer, the unit is more compact and of easy construction and maintenance and fixed costs are significantly lower (Watson, 1966). Furthermore, thanks to the absence of walls that separate the two fluids, there are no efficiency loss due to problems of fouling, and that is why DCE is preferred for concentration of fouling and corrosive solutions like draw.
Also, the vigorous agitation resulting from bubbling maintains a uniform temperature throughout the solution and the solvent vaporizes at temperatures of 10 to 30 °C below its boiling point (Kurz and Guthoff, 1988).
DCE process characteristics allow the use of exhausted combustion gas or submerged combustion, turning the concentration process far more efficient and cheap than using steam.

Table 2.3 *Key features of principal fruit juice concentration processes.*

Technology	Thermal Degrad.	Maximum concentration (°B)	Source
Classical evaporation	yes	50-60	Hermann et al., 2005
TASTE	yes	65-75	FMC S.p.A.
Nanofiltration	no	25-30	Raghavarao et al., 2004
Reverse osmosis	no	25-30	Raghavarao et al., 2005
Forward osmosis	no	45-60	Wong and Winger, 1999
Osmotic evaporation	no	70	Hogan et al., 1998
Membrane distillation	no	25-30	Raghavarao et al., 2005
Freeze concentration	no	40-45	Raghavarao et al., 2005

Chapter 3

Process description

In this chapter, with the aim of analyzing the respective features and understand the whole integrated process (scheme in Figure 3.1), descriptions of MD, OE and DCE are presented.

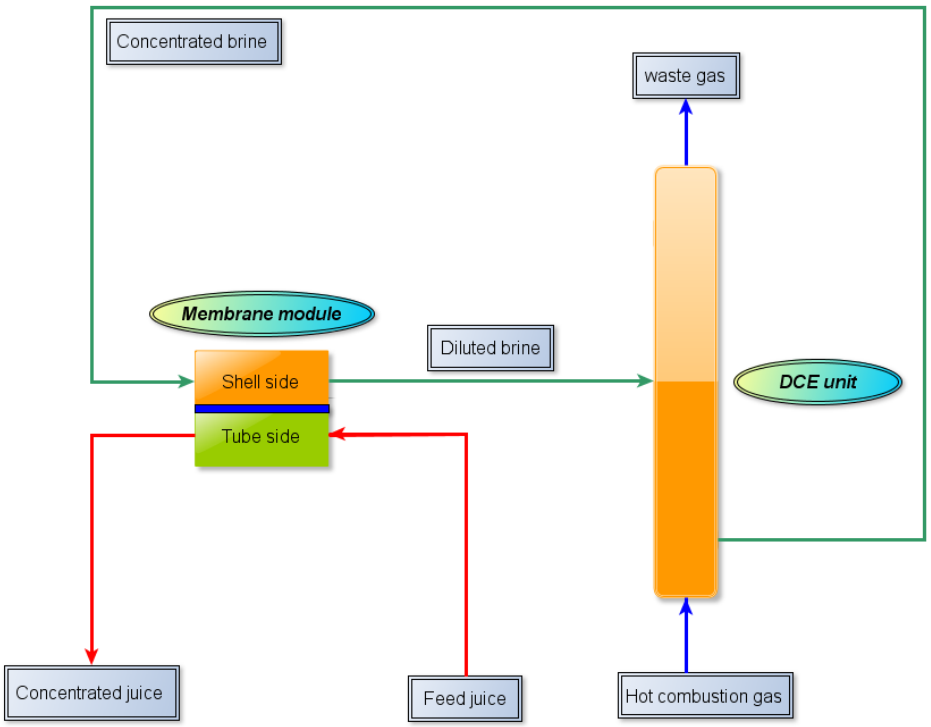

Figure 3.1 *Simplified scheme of juice membrane concentration, integrated with DCE draw regeneration.*

3.1 COMBINED OE+MD PROCESS

The aim of this section is to describe combined OE+MD process basic principles, technology and process variables.

3.1.1 Process description

In combined OE+MD, hot fruit juice to be concentrated and cold hypertonic solution (draw) are placed side by side, separated by a microporous polymeric membrane with

hydrophobic characteristics. As water activity in juice is greater than its activity in draw, water tends to migrate to the latter, seeking equal chemical potential. Membrane is hydrophobic and then, it does not allow the water in the liquid state to permeate through the pores (surface tension of water is greater than the interfacial tension of the material which composes the membrane).

However, water in the vapor state water can permeate through membrane pores.

Interfaces formed by the liquid phases and the retained gas in the pores are considered in thermodynamic equilibrium. Thus, the driving forces generating the mass transfer of water vapor through the porous medium are the difference in vapor pressure and in osmotic pressure between both interfaces.

In practical terms, water evaporates in phase I at the interface with the membrane and condenses in phase II at the other interface. To understand the difference between OE and MD, two figures are reported (Figure 3.2 and 3.3). Figure 3.2 shows an outline describing the principle of OE process where a microporous and hydrophobic membrane separates both solutions.

In Figure 3.2, three regions may be identified in membrane proximities: (1) boundary layer of the feeding solution to be treated; (2) membrane pore filled with gas; (3) boundary layer of the extraction solution. OE is an evaporative process where simultaneous mass and heat transfer are observed with its respective concentration and

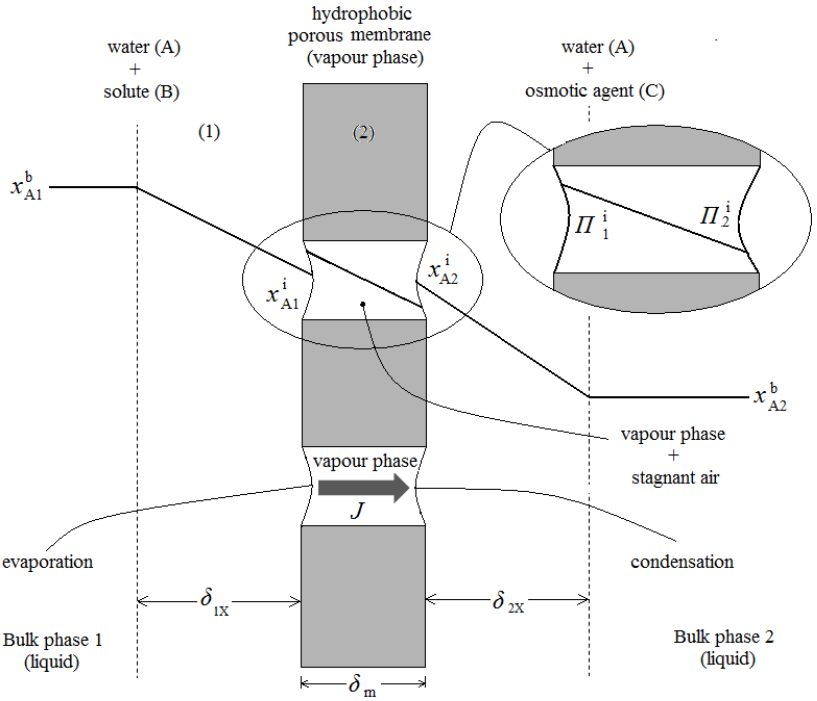

Figure 3.2 *OE water molar fraction profile respectively in phase 1 (juice) and phase 2 (draw); Partial pressure profile of water in stagnant air phase (membrane). Where:* x_{A1}^{i} *: Water molar fraction at interface between phase 1 and membrane (gas phase);* x_{A2}^{i} *: Water molar fraction at interface between phase 2 and membrane (gas phase);* Π_1^i *: Solution osmotic pressure at interface between phase 1 and membrane (gas phase);* Π_2^1 *: Solution osmotic pressure at interface between phase 2 and membrane (gas phase);* δ_{1X} *: Boundary layer thickness in phase 1;* δ_{2X} *: Boundary layer thickness in phase 2;* δ_m *: Membrane thickness.*

temperature profiles. Temperature profile is due to temperature polarization, which involves latent heat transfer through the membrane. Latent heat transfer decreases evaporation interface temperature and increases condensation interface temperature. Figure 3.2 outlines concentration profile through the membrane in OE: water vapour flux finds resistance in the membrane, but beyond this resistance it has to be taken in account that offered by solute concentration increase at juice interface with the membrane, and that provided by water concentration increase at the interface between membrane and hypertonic solution. This phenomenon is called concentration polarization.

As water vapour pressure decreases with increasing feed solute concentration and increases with hypertonic solution dilution, there will be a process driving force drop, with consequent permeate flux drop.

This effect can be minimized by improvement of hydrodynamic flow of the feed and hypertonic solution. An increase in Reynolds number (Re) on both sides will decrease polarized layers membrane thickness.

Water evaporation between phase 1 and membrane produces a solution cooling in the region close to the membrane.

In phase 2, close to the membrane, water vapour condensation generates a heating of this region. This phenomenon is called temperature polarization, and the temperature gradient formed will hinder the concentration gradient.

Membrane used should have a little thickness and a high heat conduction coefficient so that thermal equilibrium is reached quickly near the membrane (Lefebvre, 1992, apud Martins, 2006).

Even small temperature differences can significantly counteract chemical potential gradient and should therefore be minimized (Kunz et al., 1996 apud Martins, 2006).

Temperature polarization is less dependent on the operating conditions in respect of polarization concentration (Bill et al., 2005).

Regarding aroma transfer through the membrane during OE, its low concentration in fruit juices (only few mg/L) and low affinity to salt (Le Thanh et al., apud Martins, 2006) reduces the possibility of loss. Beyond, these components have a lower diffusivity in liquid phases and gas than water. Thus, in principle, flavours transfer is not significant, compared to water transfer. However, some studies have shown some aroma loss during concentration (Courel et al. 2001; Shaw et al. 2001; Vaillant et al., 2001, Ali et al. 2003 apud Martins, 2006).

In Figure 3.3 is represented a MD process scheme, where the driving force is the temperature gradient between hot and cold solution.

This difference induces a vapour pressure difference between the two solutions and causes the water vapour flux across the membrane from hot to cold water.

As said before, coupling OE and MD signify adding osmotic pressure gradient and temperature gradient effect, producing a greater permeated flux of water.

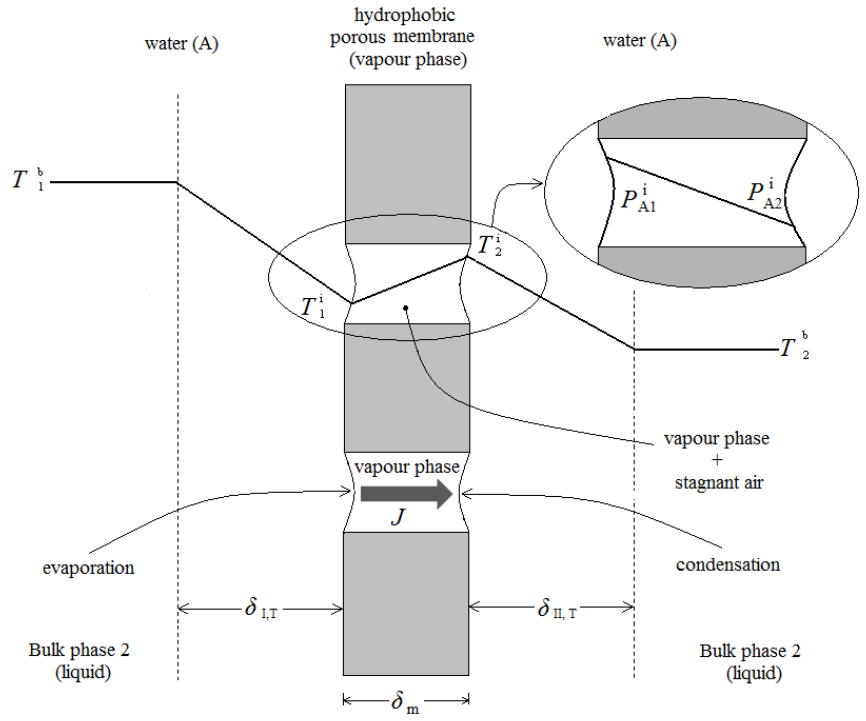

Figure 3.3 *MD temperature profile in phase 1 (juice), membrane and phase 2 (draw). Where:* T_1^b *: Temperature of phase 1 bulk region;* T_2^b *: Temperature of phase 2 bulk region;* T_1^i*: Interface temperature between phase 1 and membrane (gas phase);* T_2^i*: Interface temperature between phase 2 and membrane (gas phase);* P_{A1}^i *: Water partial pressure at interface between phase 1 and membrane (gas phase);* P_{A2}^i *: Water partial pressure at interface between phase 2 and membrane (gas phase);* $\delta_{1,T}$ *: Boundary layer thickness in phase 1;* $\delta_{2,T}$ *: Boundary layer thickness in phase 2;* δ_m *: Membrane thickness; J : vapor water flux from phase 1 to phase 2.*

3.1.2 Process variables

3.1.2.1 Membranes

Combined OE+MD membranes must be microporous and made of a hydrophobic polymer. Distribution of pore diameter, porosity and thickness should be conctrolled. Polymer hydrophobicity is desired to impede liquid entrance in the membrane under required operating conditions.

If pressure gradient is great enough to permit intrusion of liquid into the pores, the passage of juice or hypertonic solution through the membrane will occur and no more separation will follow.

Liquid intrusion into the pores is described by Young-Laplace equation (3.1) and is related to pore size, liquid surface tension and the affinity for the material that composes the membrane.

This latter feature may be related to wetness of the membrane in contact with the two liquids involved in the process. Membrane wettability characterization is therefore suggested as an important issue (Courel et al. 2001, apud Martins, 2006).

$$\Delta P_{lv} = \frac{-2B\gamma_{lv}cos\theta}{r_{max}} \quad (3.1)$$

Where, ΔP_{lv} and r_{max} are respectively pressure difference in the liquid-vapour interface and maximum value of membrane pore size; γ_{lv} and B are respectively the liquid-vapour surface tension and a geometric factor, unitary for the cylindrical shape.

The larger is average membrane pore diameter, the greater will be water vapour flow. However, if the pores are too large, the liquid in contact with the membrane can penetrate them, even at low pressures. Porosity is also another variable that is directly related to the flow.

The smaller is the thickness, the lower will be the path to be crossed by water vapour molecules and the higher will be permeate flow.

Membranes are prepared with commercially manufactured non-polar polymers such as PVDF (polyvinylidene fluoride), PP (polypropylene) and PTFE (polytetrafluoroethylene fluoroethylene), known commercially as Teflon.

Membrane pore diameter the can vary from 0.2 to 1.0 μm, while overall porosity lies between 60-80% and thickness usually is around 80-250 μm (Petrotos et al., 2001).

3.1.2.2 Hydrodynamics of solutions

Hydrodynamic conditions in the region next to membrane surface play an important role in water flow. The best hydrodynamic conditions are associated with higher values of Reynolds (Re), which are obtained with higher flow rates.

Furthermore, use of turbulence promoters (baffles that are inserted into the feed and/or filtrated channels) also improves hydrodynamic conditions.

Solute concentration polarization layer at juice-membrane interface is decreased with the increase of solution flow velocity, resulting in improved process performance.

Similarly, increasing hypertonic solution flow rate, thickness of the boundary layer near the interface with the membrane is reduced, allowing the establishment of a larger difference in chemical potential between membrane faces.

3.1.2.3 Temperature

Although membrane separation process can be conducted isothermally, in other words keeping the same temperature for the two solutions, temperature is an important

variable because when a temperature gradient is imposed between two sides of the membrane, the conditions of vapor-liquid equilibrium are affected.
Moreover, even though activity coefficients are little affected by temperature, this strongly affects the agitation of the molecules and therefore water vapour diffusivity trough pores. Thus, it is expected that an increase in operating temperature increases the permeate flux.
A desirable operating temperature is that which ensures a good water flow without the components involved being deteriorated. Particularly for solutions containing flavours, is important that a temperature value that minimizes the volatiles loss, is applied.

3.1.2.4 Osmotic agent influence

A saline solution is usually used as hypertonic solution. The salt choice should be availed following a set of criteria. According to Michaels et al., 1998, the salt chosen must:

- reduce the vapour pressure of the solution to provide a high potential difference for the chemical separation;
- be chemically stable in solution at all temperatures to which it will be exposed;
- not be destructive to the membrane even in concentrations up to saturation;
- be non-volatile at all temperatures to which the solution will be submitted;
- not toxic at the concentrations used in the solution;
- have no taste or smell detectable at the concentrations used;
- being chemically inert to the volatile substances of the feed solution;
- not be corrosive to the materials that make up the system;
- be characterized by a high solubility in a wide range of temperature;
- be commercially available in large quantities and possess low cost.

Larger differences in chemical potential can be achieved with saturated electrolyte, such as $MgSO_4$ or $MgCl_2$ and from mixtures of different salts (Kunz et al. 1996 apud Martins, 2006).

3.1.2.5 Solute concentration

Solute concentration in food is a very important variable. As juice is concentrated, the solids content increases and so the solution becomes more viscous. Due to increased solids content, a decrease in permeate flux of water vapor is observed.
Unlike what happens with draw, water activity in juice is not much affected in the usual concentration range (10 to 70 °Brix) and therefore does not significantly affect the permeate flux. However, increase in solute content leads to a higher viscosity and a lower diffusion coefficient (Courel et al. 2000 apud Martins, 2006).

Hypertonic solution concentration has an important role in the process, because osmotic pressure depends on the concentration of solute in the solution.

The driving force of the process, which is a chemical potential gradient due to a vapour pressure difference between membrane sides, increases with draw water activity reduction, which has a strong dependency on the salt content. Thus, the lower the concentration of hypertonic solution, the higher the water activity and lower flows are obtained.

Figure 3.4 shows osmotic pressure variation for sucrose and a set of salts (Sourirajan, 1970 apud Martins, 2006).

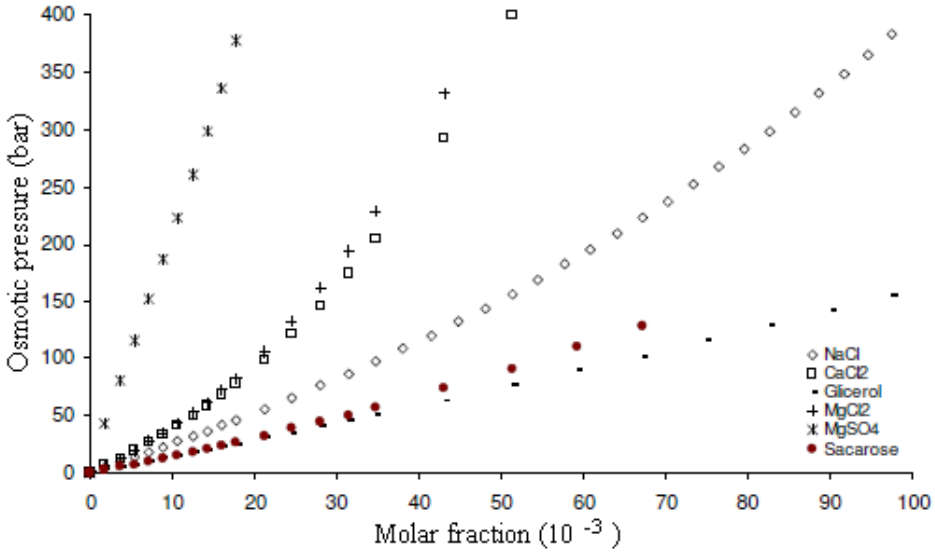

Figure 3.4 *Osmotic pressure variation for sucrose and a set of salts (Sourirajan, 1970 apud Martins, 2006).*

According to Courel et al. (2000), this activity effect is much stronger than the increase in flow that might be expected due to improvement of transport properties: when it takes place draw dilution, density and viscosity tends to decrease while the diffusion coefficient increases, but effect in water activity is more pronounced for draw.

3.1.3 State of the art

Due to deteriorating effects caused by traditional concentration process on solutions containing thermo sensitive compounds typical of food products, many studies concerning OE have developed on the last two decades. In particular, due to low temperature of OE, most of applications are focused on juice processing.

Table 3.1 shows results regarding permeate fluxes obtained in a set of recent studies realized applying OE and MD on fruit juice concentration; experiments were carried out with the purpose of evaluating technique viability the and principal process variables influence.

Table 3.1 *Recent studies of OE and MD applied to juice processing.*

Feed solution	Osm. agent	Membrane	Operating conditions	Flux (kg/m^2h)	Source
Grape juice (15.7 to 66 °B) Apple juice (11 to 57 °B)	$CaCl_2$ (5.6 M)	PP tubular 0.2 µm 10.2 m^2	T_{feed} (35°C) T_{draw} (37°C)	1.17 (both juices)	Cissé et al. (2011), apud Ongaratto et al. (2012)
Cherry juice (14.7 to 60.8 °B)	$CaCl_2$ (43%)	hollow fiber 0.1µm 0.2 m2	T_{feed} and T_{draw} (30°C) F_{feed} and F_{draw} (36 L/h)	0.86	Racz et al. (2011)
Apple juice (12 to 44 °B)	$CaCl_2 \cdot 2H_2O$ (0 a 65%)	PP hollow fiber 0.2 µm 0.1 m^2	ΔT between feed and draw (10 to 30°C) F_{feed} and F_{draw} (10 to 30 L/h)	0.064 to 1.462	Onsekizoglu et al. (2010a) apud Ongaratto et al. (2012)
Apple juice (12 to 65 °B)	$CaCl_2 \cdot 2H_2O$ (65%)	PP hollow fiber 0.2 µm 0.1 m^2	T_{feed} (25 to 30°C) T_{draw} (10 to 25°C) F_{feed} and F_{draw} (30 L/h) Feed fiber side Draw shell side	-	Onsekizoglu et al. (2010b) apud Ongaratto et al. (2012)
Water Great morinda juice (8 to 32 °B)	$CaCl_2$ (2 to 6 M)	PP hollow fiber 0.3 µm 0.58 m^2	T_{feed} and T_{draw} (30°C) F_{feed} and F_{draw} (6 to 60L/h) Feed shell side Draw fiber side	0.118 to 0.390 (Water) 0.058 to 0.374 (Juice)	Valdés et al. (2009) apud Ongaratto et al. (2012)
Pineapple juice (12.6 to 62 °B)	$CaCl_2 \cdot 2H_2O$ (2 to 10 M)	PP flat 0.2 µm 0.01 m^2	T_{feed} and T_{draw} (25°C) F_{feed} and F_{draw} (1.5 to 6 L/h) V_{alim} (0.94x10-3 to 3.75x10-3 m/s) V_{draw} (1.12x10-2 to 4.5x10-3 m/s)	0.36 to 2.12	Badu et al. (2008) apud Ongaratto et al. (2012)
Orange juice (30 to 60 °B)	$CaCl_2 \cdot 2H_2O$ (60%)	PP hollow fiber	T_{feed} and T_{draw} (25°C) F_{feed} (28.7 L/h)	-	Galaverna et al. (2008) apud Ongaratto et al. (2012)

		1.4 m^2	F_{draw} (30.3 L/h) Feed shell side Draw fiber side		
Pineapple juice (12 to 60 °B)	$CaCl_2$ (5.5 to 6 M - a_w 0.435 to 0.329)	PTFE flat 0.2 µm 0.005 m^2	T_{feed} (20 and 35ºC) T_{draw} (20ºC) V_{alim} (1.25 m/s) V_{draw} (2 and 3 m/s – Re 1897 and 2924)	2 to 13	Hongvalee-rat. et al. (2008) apud Ongaratto et al. (2012)
Kiwi juice (9.4 to 66.6 °B)	$CaCl_2 \cdot 2H_2O$ (60%)	PP hollow fiber 1.4 m^2	T_{feed} and T_{draw} (25ºC) F_{feed} – V_{alim} (24 L/h – $2.71x10^{-3}$ m/s) F_{draw} – V_{draw} (31 L/h – $2.44x10^{-2}$ m/s)	1.3	Cassano et al. (2007) apud Ongaratto et al. (2012)
Water Glucose solution (3 to 18 °B) Sucrose solution (3 to 18 °B)	NaCl (10 to 23%)	PA aromatic flat 0.08 m^2	T_{feed} (22°C) T_{draw} (31°C) F_{feed} (630 L/h) F_{draw} (115 L/h)	0.1 to 4.5 (Water) 0.4 to 2 (Sucrose)	Dova et al. (2007) apud Ongaratto et al. (2012)
Fructose solution (35 to 55 °B) Grape juice (35 to 55 °B)	$CaCl_2 \cdot 2H_2O$ (43%)	PVDF hollow fiber 0.2 µm 0.013 m^2	T_{feed} (25 a 55°C) T_{draw} (25 a 55°C) V_{alim} (0.1 to 0.5 m/s – Re 12 to 116) V_{draw} (0.1 to 0.5 m/s – Re 7 to 54)	0.58 to 2.02 (Solution and juice)	Thanedgun-baworn et al. (2007) apud Ongaratto et al. (2012)
Sucrose solution (30 to 60 °B)	$CaCl_2$ (50%), NaCl (24.6%)	PTFE flat 0.45 µm 0.00125 m^2	T_{feed} and T_{draw} (35°C) A_{feed} and A_{draw} (400 rpm)	0.7 to 5.0	Warczok et al. (2007) apud Ongaratto et al. (2012)
Sucrose solution (12 to 62 °B) Orange juice (11 to 62 °B)	$CaCl_2$ (4.9 M)	PP hollow fiber 0.2 µm 0.16 m^2	T_{feed} and T_{draw} (25ºC) Re_{alim} (45.3) $Re_{salmoura}$ (19) Feed shell side Draw fiber side	0.72 (Solution) 0.36 (juice)	Alves et al. (2006) apud Ongaratto et al. (2012)

Orange juice (5 to 55 °B)	$CaCl_2 \cdot 2H_2O$ (2 to 10 M), NaCl (2 to 6 M)	PP flat 0.2 µm 0.012 m^2	T_{feed} and T_{draw} (25°C) F_{feed} and F_{draw} (1.5 to 6 L/h) V_{alim} (0.94x10-3 to 3.75x10-3 m/s) V_{draw} (1.12x10-2 to 4.5x10-3 m/s)	0.18 to 1.55	Badu et al. (2006) apud Ongaratto et al. (2012)
Sucrose solution (20 to 65 °B) Apple juice (20 to 65 °B)	$CaCl_2 \cdot 2H_2O$ (3.5 to 6 M)	PP tubular 0.2 µm 0.036 m^2	T_{feed} (35. 40 and 45°C) T_{draw} (25°C) F_{feed} (10 and 100mL/min) F_{draw} (20 mL/min) Feed shell side Draw fiber side	0.06 to 0.40 (Solution) 0.4 (Juice)	Bélafi-Bakó et al. (2006) apud Ongaratto et al. (2012)
Orange juice (11.8 to 33 °B)	NaCl (20%)	PP hollow fiber 0.2 µm 0.02 m^2	T_{feed} (30°C) T_{draw} (14°C) Feed fiber side Draw shell side	0.51 to 0.77	Martins (2006) apud Ongaratto et al. (2012)
Sucrose solution (10 to 60 °B)	NaCl (12 to 20%)	PTFE flat 0.45 µm 0.00206 m^2	T ambiente A_{alim} (0 a 200 rpm) $A_{salmoura}$ (0 a 150 rpm)	0 to 0.49	Martins (2006) apud Ongaratto et al. (2012)
Sucrose solution (10 to 60 °B)	NaCl (10 to 35%)	PP hollow fiber 0.2 µm 0.02 m^2	T_{feed} (24 to 44°C) T_{draw} (15°C) F_{fiber} – V_{fiber} (22 to 89 L/h – 0.15 to 0.61 m/s) F_{shell} – V_{shell} (21 to 39.5 L/h – 0.05 to 0.1 m/s) Feed and draw on fiber and shell side	0.07 to 1.64	Martins (2006) apud Ongaratto et al. (2012)
Pineapple juice Lime juice	NaCl (2 to 6 M) $CaCl_2 \cdot 2H_2O$ (2 to 14 M)	PP flat 0.05 and 0.2 µm 0.0116 m^2	T_{feed} (28 to 38°C) T_{draw} (28°C) $F_{feed\ and}$ F_{draw} (25 to 100 mL/min)	0.2 to 2.7 (both juices)	Nagaraj et al. (2006) apud Ongaratto et al. (2012)
Sucrose solution	$CaCl_2 \cdot 2H_2O$ (60%)	PP tubular 0.2	T_{feed} and T_{draw} (21°C)	0.3 to 0.6 (Solution)	Rektor et al. (2006) apud Ongaratto et al.

(10 to 54 °B)		µm	F_{feed} and F_{draw}		(2012)
Grape juice		0.1 m^2	(45 L/h – Re 283.2)	0.3	
(10 to 34 °B)				(Juice)	
Melon juice	$CaCl_2$	PP	T_{feed} (26°C)	0.57	Vaillant et al. (2005) apud Ongaratto et al. (2012)
(7 to 55 °B)	(5.3 to 5.6	hollow fiber	T_{draw} (31°C)		
	M)	0.2 µm	V_{alim} (0.2 m/s)		
		10 m^2	V_{draw} (0.02 m/s)		
Water	$CaCl_2.2H_2O$	PP	T_{feed} and T_{draw} (25 and	0.06 to 0.21	Alves et al. (2004) apud Ongaratto et al. (2012)
	(2.8 a	hollow fiber	30°C)	(Water)	
Sucrose	6 M)	0.2 µm	Re_{alim} (0.3 to 9)		
solution		0.16 m^2	$Re_{salmoura}$ (5 to 57)	0.10 to 0.54	
(12 to 60 °B)			Feed shell side	(Solution)	
		PP	Draw fiber side		
		tubular			
		0.2 µm			
		0.036 m^2			
Water	Propylen	PP	T_{feed} and T_{draw} (25°C)	0.35 to 1.7	Celere et al. (2004) apud Ongaratto et al. (2012)
	glycol	hollow fiber	F_{feed} (50 L/h)		
	(35 to 75%),	0.2 µm	F_{draw} (10 to 100 L/h)		
	Glycerol	0.04 m^2	Feed and draw on fiber		
	30 to 70%),		and shell side		
	Glycerol-				
	NaCl				
	(NaCl/glycer				
	ol ratio				
	0.34),				
	CaCl2				
	(15 to 35%)				
Camu camu	$CaCl_2$	PTFE	T_{feed} (35°C)	6 to 11	Rodrigues et al. (2004) apud Ongaratto et al. (2012)
juice	(4 to 5.2 M)	flat	T_{draw} (20°C)		
(6.6 to 6.4 °B)		0.2 µm			
		0.004 m^2			
Sucrose	$CaCl_2$	PP	T_{feed} and T_{draw} (20 to	0.31 to 0.78	Ali et al. (2003) apud Ongaratto et al. (2012)
solution	(3.5 to 5.1	hollow fiber	35°C)		
(18 to 34 °B)	M)	0.03 µm	V_{alim} (0.05 to 0.1 m/s)		
		1.4 m^2	V_{draw} (4.2x10-3 m/s)		
			Feed fiber side		
			Draw shell side		

Orange juice (22 to 60 °B) Carrot juice (13 to 63 °B)	$CaCl_2$ (4.1 to 4.5 M)	PP hollow fiber 0.3 µm 0.032 m^2	T_{feed} and T_{draw} (26°C) F_{feed} (28 L/h) F_{draw} (69 L/h) Feed shell side Draw fiber side	0.48 (orange) 0.1 (carrot)	Cassano et al. (2003) apud Ongaratto et al. (2012)
Water	Glycerol (8.3M), $CaCl_2$ (3.2M), NaCl (3.4M)	-	T_{feed} and T_{draw} (25°C) A_{alim} and A_{draw} (100 to 600 rpm)	2.6 to 3.0 (glycerol) 3.0 to 3.4 ($CaCl_2$)	Alves et al. (2002)
Water	Saline solution not informed (0 to 5 M)	PP hollow fiber 0.2 µm 10 m^2	T_{feed} (25 to 45°C) T_{draw} (20 to 40°C) F_{feed} (35 L/h) F_{draw} (50 L/h) Feed fiber side Draw shell side	0.5 to 4.0	Wang et al. (2001) apud Ongaratto et al. (2012)
Water Passion fruit juice (14.6 to 60 °B)	$CaCl_2$ (5.3 M)	PTFE flat 0.2 µm	T_{feed} and T_{draw} (30°C) V_{alim} (0.24 m/s) V_{draw} (1.8x10-3 m/s) Feed fiber side Draw shell side	0.75 (Water) 0.5 (Juice)	Vaillant et al. (2001) apud Ongaratto et al. (2012)
Sucrose solution (0 to 65 °B)	$CaCl_2.2H_2O$ (45.5%)	hollow fiber 0.1 m^2	T_{feed} and T_{draw} (20 to 35°C) V_{alim} (0.1 to 2.7 m/s) V_{draw} (0.2 to 2.2 m/s – Re 154 to 1540)	0.5 to 23	Courel et al. (2000) apud Ongaratto et al. (2012)
Grape juice (20 to 72 °B)	$CaCl_2.2H_2O$ (40%)	PP hollow fiber 0.2 µm 0.1 m^2	T_{feed} and T_{draw} (20°C) F_{feed} (40.8 L/h) F_{draw} (48.6 L/) Feed shell side Draw fiber side	0.3 to 0.5	Bailey et al. (2000) apud Ongaratto et al. (2012)
Water	NaCl (25%) $MgCl_2$ (30%)	PP hollow fiber 0.2 µm 0.1 and 0.04 m^2	T_{feed} (35 to 50°C) T_{draw} (25 to 50°C) F_{feed} (30 L/h) F_{draw} (93 L/h) Feed fiber side Draw shell side	0.3 to 2.2	Gostoli (1999) apud Ongaratto et al. (2012)

Tomato juice	NaCl (22.24%), $CaCl_2$ (29.97%), $Ca(NO_3)_2$ (29.00%), Glucose (62.86%), Sucrose (58.25%), Polyethylene glycol (49.97%)	PA aromatic tubular 0.1 m^2	T_{feed} (25 to 58ºC) T_{draw} (25ºC) F_{feed} (109 to 502 L/h) F_{draw} (560 L/h)	0.446 to 3.10 (NaCl solution)	Petrotos et al. (1998) apud Ongaratto et al. (2012)

Where, T and F are respectively temperature and flow rate; A and V are respectively agitation and velocity.

OE and MD processes were already studied for many kind of fruit juice, focusing on the most traditional and with wider volume of production and market like orange (Alves et al., 2006; Badu et al., 2006; Cassano et al., 2003; Galaverna et al., 2008; Martins, 2006) grapes (Bailey et al., 2000; Cissé et al., 2011; Rektor et al., 2006; Thanedgunbaworn et al., 2007) and apple (Bélafi-Bakó et al., 2006; Cissé et al., 2011; Onsekizoglu et al., 2010a; Onsekizoglu et al., 2010b).

On the other hand, due to the superior quality of fruit juice produced by OE and MD, this process is gaining special interest for treating less popular fruits that have however a great potential on international customer market, like for example great morinda (Valdés et al., 2009), kiwi (Cassano et al., 2007), lime (Nagaraj et al., 2006), melon (Vaillant et al., 2005), camu-camu (Rodrigues et al., 2004), passion fruit (Vaillant et al., 2001), sour cherry (Racz et al. 2011).

Possible membrane configurations used are hollow fiber, tubular and flat. The best performance on industrial applications is obtained using hollow fiber or tubular membranes, which shows a higher surface-volume ratio.

Commonly in OE and MD, for membrane production are used non-polar materials with low surface energy such PE, PVDF, PP and PTFE with pore diameter around 0.2 μm (Peinemann et al., 2010).

Others polymers like aromatic polyamides (PA aromatic) were studied for sucrose concentration (Dova et al., 2007 apud Ongaratto, 2012) and tomato juice (Petrotos et al., 1998, apud Ongaratto, 2012).

In the studies presented in the state of art are usually adopted sodium and calcium chloride as osmotic agent: this is justified by their low cost and toxicity that promote the use in food processing.
Others studies were carried out using different osmotic agent like propylene glycol, glycerol and glycerol/sodium chloride (Celere et al., 2004 apud Ongaratto, 2012) magnesium chloride (Gostoli, 1999 apud Ongaratto, 2012), glucose, sucrose and polyethylene glycol (Petrotos et al., 1998 apud Ongaratto, 2012).

3.2 DIRECT CONTACT EVAPORATION

The aim of this section is to describe DCE process basic principles, technology and process variables.

3.2.1 Process description

3.2.1.1 Equipment

A direct contact evaporator (DCE) is a simple construction equipment, basically consisting of a column of liquid (continuous phase) through which superheated gas bubbles (dispersed phase) bubbles (Figure 3.5). At the column base lays the sparger, in which are formed bubbles. Usually, are used perforated tubes, metallic plates and perforated or porous spargers. In other words, it is a non-isothermal bubble column.

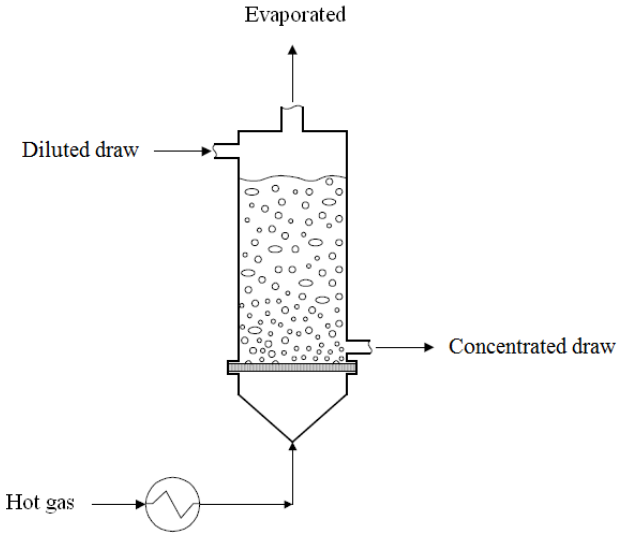

Figure 3.5 *Schematic representation of a direct contact evaporator (Adapted from Lage et al., 2004).*

3.2.1.2 Basic principles

Bubbling process can be divided in two steps: formation and ascension of bubbles.

In formation step, bubble keeps growing stuck to the sparger orifice that is feeding her with new gas; when a critical volume is achieved, bubble detachment takes place and the bubble starts its way through the liquid, heading to the top of the column.

Other theories introduce also two additional stages: detachment, in which there is an abrupt change in internal fluid dynamic conditions, due to end of the injection, and the emersion in which the bubble disappears after reaching the top of the liquid column (Clift et al. 1978 apud Ongaratto, 2012).

During bubble ascension, a natural flow of energy takes place from inside the bubble to the surface, which generally represents the major fraction of the total energy received by the liquid.

The remaining heat amount is transferred by the sparger and the gas chamber walls, since their temperature is intermediate between those of the gas and the liquid.

This energy may be transmitted either in the form of sensible heat, causing an increase in temperature, as in the form of latent heat, promoting vaporization and generating thus a mass flow from the surface to the interior of the bubble.

Energy distribution between the two ways of transfer is a function of composition and liquid temperature, since the component i amount liable to pass to the dispersed phase is proportional to i component saturation pressure in the gas-liquid interface (Burdick et al. 1949 apud Ongaratto, 2012).

Consequently, the higher the temperature of the continuous phase, the greater the total energy fraction will be used in evaporation until an equilibrium temperature is reached, in which almost all of the energy will be transmitted to the liquid as latent heat; the heat transfer without evaporation will take place only to compensate equipment heat losses.

According to Raoult law, as the molar fraction of component i in the liquid phase increases, then the molar fraction of i in equilibrium with the vapour phase becomes greater; so, a greater total energy fraction available will be spent for component i vaporization.

The absence of surfaces separating fluids gives direct contact evaporators a number of advantages over traditional equipment. Direct contact between fluids allows achieving heat transfer efficiencies of about 95% (Watson, 1966). This occurs because there is no heat transfer resistance associated with metallic walls.

The high efficiency of heat exchange can be verified by the temperature difference between liquid and gas at the outlet of the equipment, which usually ranges from 2 to 5 º C (Swindin et al., 1949; Williams et al., 1997 apud Ongaratto, 2012).

Unlike what occurs with traditional shell-and-tube units in DCE there is no efficiency of heat exchange gradual reduction due to fouling or corrosion, which enables the use of the same concentration of corrosive or fouling solutions (Wilke et al. 1963 apud Ongaratto, 2012).

Moreover, the equipment is more compact and of simpler construction, with fixed and maintenance costs considerably smaller (Cronan, 1956 apud Ongaratto, 2012).
Moggio et al., (1955) apud Ongaratto, 2012 stress that simplicity reduces the possibility of failure and also reduces downtime for cleaning and maintenance.
Depending on the solution to be concentrated, the interfacial area for mass and heat transfer can vary significantly depending on the design of the sparger, which gives greater operational flexibility to the product.
DCE is particularly attractive for thermo labile solutions concentration, since hot gas bubbling through the solution allows solvent vaporization at temperatures sensibly below their boiling point; the equilibrium continuous phase temperature lies generally between 10 and 30 °C below solvent boiling point. (Kurz, 1987 apud Ongaratto, 2012).
This is because the non-condensable gases contribute to a large part of each bubble total content, and therefore solvent vapour partial pressure is smaller than total system pressure (Zaida et al. 1986).
The vigorous agitation resulting from bubbling maintains a uniform temperature throughout the solution, eliminating potential points of superheat and promoting the solution concentration. Together, these two factors greatly reduce thermo labile compounds degradation during solution concentration.
In Table 3.2, a qualitative comparison between features of DCE and shell-and-tube evaporator is shown. It should be emphasized that, by working with direct contact between fluids, the contamination possibility should be considered.
Indeed contamination of the gas phase is the major "bottleneck" which hinders the spread of DCE in industry, particularly in the food industry.
Therefore, contamination should be eliminated, which increases the production cost because of the need for purified gas and limiting the application of the process to products with high added value, or may be tolerated.
In the latter case vent gases could be used, which would greatly lower the process cost.
In addition, evaporator needs to operate at a pressure value next to heating gas stream pressure, which may result in additional costs to the process (Jacobs, 1988 apud Ongaratto, 2012).
Depending on the solution surface tension, bubbling can lead to foaming and may impair the equipment operation (Cronan, 1956 apud Ongaratto, 2012).
In some cases the liquid entrainment by gas bubbling can be very significant, from 10 to 100 times greater than in traditional evaporators (Rey, 1961 apud Ongaratto, 2012).

Table 3.2 *Qualitative comparison between features of DCE and shell-and-tube evaporator.*

	DCE	Shell-and-tube evaporator
Corrosion effect on efficiency	no	yes
Fouling effect on efficiency	no	yes
Thermo labile solution	yes	no
Failure frequency	low	high
Heat transfer efficiency	high	Obstacled by walls
Maintenance downtime	low	high
Cleaning downtime	low	high
Contamination problem	possible	rare
Entrainment	high	low
Pressure gradient limits	yes	no

3.2.2 Hydrodynamics

DCE possesses two hydrodynamic parameters of primary importance, which are actually correlated: bubbling regime and gas hold up.

The former is straightly connected to gas superficial velocity and directs affects heat and mass transfer processes (Heijnen et al., 1984; Vandu et al., 2004) while the latter is used to calculate the dispersed phase residence time and together with the mean bubble diameter allows the calculation of the interfacial area. (Heijnen et al., 1984, Shah et al., 1982, Deckwer et al., 1993).

3.2.1.1 Gas hold-up

Gas hold-up (ε) is defined as the gas volume fraction in the mixture. This parameter is used to calculate the dispersed phase residence time and, together with the average diameter of the bubbles allows determining the interfacial area, being therefore a key design parameter (Deckwer et al., 1993; Shah et al., 1982).

Mathematically, the overall ε can be expressed by equation (3.2):

$$\varepsilon = \frac{\pi N_T}{6V_T} \int_0^\infty d_e^3 F(d_e) d(d_e) \qquad (3.2)$$

Where: V_T and d_e are respectively the biphasic mixture volume and the bubble equivalent diameter. N_T and F are respectively the total number of bubbles and normalized bubble size distribution function within the column.

The analysis of equation (3.2) shows that any factor that affects the average size of bubbles, like for example, sparger characteristics, liquid phase properties and the coalescence and breakage phenomenon will produce changes in the value of ε.

3.2.1.3 Bubbling regimes

Flow regime or bubbling regime depends basically on the gas velocity (u_g) defined as the ratio between the volumetric flow of gas fed into the column and the cross-sectional area thereof (Figure 3.6).

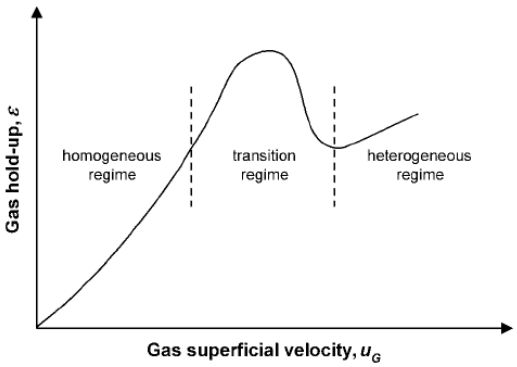

Figure 3.6 *Identification of bubbling regimes with the aid of general relationship between gas hold-up and superficial velocity in a bubble column (Ribeiro C.P. 2005).*

For low u_g values, equipment operates in homogeneous bubbling regime, in which there is little variation in bubbles size and the breakage and coalescence phenomena are negligible because bubbles ascend along trajectories substantially vertical or with small transverse oscillations (Maruyama et al. 1981; Ruzicka et al., 2001).

The extent of coalescence and breakage phenomena is very small, so that gas bubbles size and retention depend on distributor design parameters and on the gas-liquid system physical properties. Bubble concentration and thus gas retention are substantially uniform in the radial direction.

As the u_g rises, the system leaves homogeneous regime and entry a transitional regime, where both bubble formation frequency and bubbles size increase, reducing the average distance between bubbles and thus promoting their interaction.

Accordingly, coalescence and breakage phenomenon will acquire major importance, leading to a wider bubble size range. This is the heterogeneous regime, characterized by

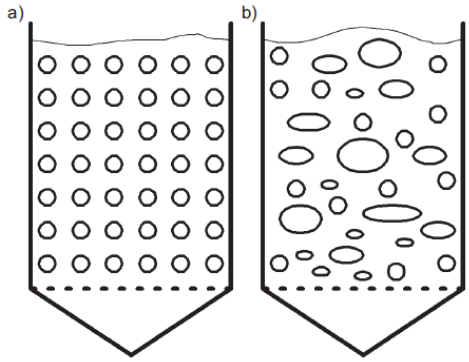

Figure 3.7 *Basic bubbling regimes in a DCE: a) homogeneous; b) heterogeneous (Ribeiro C.P. 2005).*

a parabolic gas hold-up profile with a maximum value in the centre of the column, due to the presence of larger bubbles (Figure 3.7)
In this condition, sparger influence on bulk bubble size distribution falls.

3.2.3 State of the art

Many experimental studies regarding DCE hydrodynamics were developed. The most recent data are reported in Table 3.7, which show that heat transfer efficiency never falls under 80%.
Another interesting issue emerging is that DCE can operate with a liquid temperature considerably lower that its boiling point for the working pressure.
The biggest lack of DCE is foaming but this can be fixed by using an antifoaming agent or a mechanic system.

Table 3.3 *Recent studies of DCE process.*

C.P.	D.C.	T_L (°C)	M_{ev} (kg/hm^2)	μ (%)	C.D.	Features	Source
$FeSO_4$ (7%)-H_2SO_4 (18.4%) solution	combustion gas	130	-	91	2.8	Heat recovery from evaporated flux	Swindin et al. (1949) apud Ongaratto, 2012
Citrus peel solution (12%)	combustion gas	60-89	30-4275	86-88	2.67	Gas flow rate effect studied	Burdick et al. (1949)
Sulphyte solution (6.3%)	combustion gas	102	780	80	12	Charring observed	Owen et al. (1955)
Tap water	combustion gas	82	18-41	-	-	Gas flow rate effect studied	Iver et al. (1971)
Pickle draw (18% solids)	combustion gas	-	231	84	-	Foaming and entrainment observed	Durkee et al. (1973)
Protein solution (6-8%)	combustion gas	76	74-108	86	5	No foaming or bake-on effect	Luedicke et al. (1979) apud Ribeiro et al. (2004)
Water	hot air	48-52	4-7	-	-	T_L. M_{ev}. H_b	Andrade et al.

						measured in homogeneous bubbling regime	(1985) apud Ribeiro et al. (2004)
Skim and whole milk (8.2-12.1%)	hot air and N_2	37-39	33-120	-	4.6	Foaming can be fixed by rising operative pressure	Zaida et al. (1986)
Water and NaCl solution	combustion gas	76-78	19-22	90-100	-	T_L. M_{ev}. H_b measured in homogeneous bubbling regime	Queiroz et al. (1990) apud Ribeiro et al. (2004)
Water	hot air	65-69	10-76	89-98	-	T_L. M_{ev}. H_b. ε measured using two kind of spargers varying gas flow rate. in homogeneous and heterogeneous bubbling regime	Ribeiro et al. (2004)
Sucrose solution (11.2%)	hot air	63-67	11-35	92-95	6.1	T_L. M_{ev}. H_b. ε measured varying gas flow rate	Ribeiro et al. (2004)
Synthetic fruit juice (11.2%)	hot air	57-66	15-37	94-97	6.7	T_L. M_{ev} studied. High concentration degree obtained without reduction of $M_{ev.}$ experimental data for water and synthetic juice	Ribeiro et al. (2005)
Water. Synthetic juice (11.2% sucrose)	hot air	67	18-36	-	4.8	T_L. M_{ev}. H_b. ε studied. Sucrose inhibits bubble coalescence. Heat limited operation.	Ribeiro et al. (2007)
Water. NaCl solution (22%).	hot air	70-89	15-86	-	-	T_L. M_{ev}. H_b were studied considering ebullioscopic increase effect. gas	Ongaratto et al. (2012)

$CaCl_2$ solution (72%). $K_4P_2O_7$ (142%)	flow rate effect

Where, C.P. and D.P are respectively continuous phase and dispersed phase; T_L and M_{ev} are respectively liquid temperature and mass flow rate of evaporated; μ and C.D. are respectively heat transfer efficiency and concentration degree.

Chapter 4

Experimental work

Experimental methodology employed in tests of OE and MD concentration of sucrose solution, as well as experimental methodology employed for draw regeneration through DCE were presented in this chapter.

4.1 MD AND COMBINED OE+MD PROCESSES

Bench-scale unit used in membrane separation, solutions preparation criterion, cleaning procedure and experimental procedure followed for experiments were described in this section.

Operational conditions adopted were presented for both carbon dioxide solubility test and for carbon dioxide and water membrane permeability test.

4.1.1 Bench-scale unit

The experimental device used in this study was assembled in the lab and is constituted by a system of two independent circuits for the circulation of the solutions: one for the solution to be concentrated (water or juice) and the other for the draw.

The two circuits are connected to a hollow fiber membrane contactor, unique point of meeting between the two solutions.

Both circuits have a peristaltic pump (Cole-Parmer 75211-10, EUA) which circulates the fluid from the agitated vessel (1, Figure 4.1) into the membrane module.

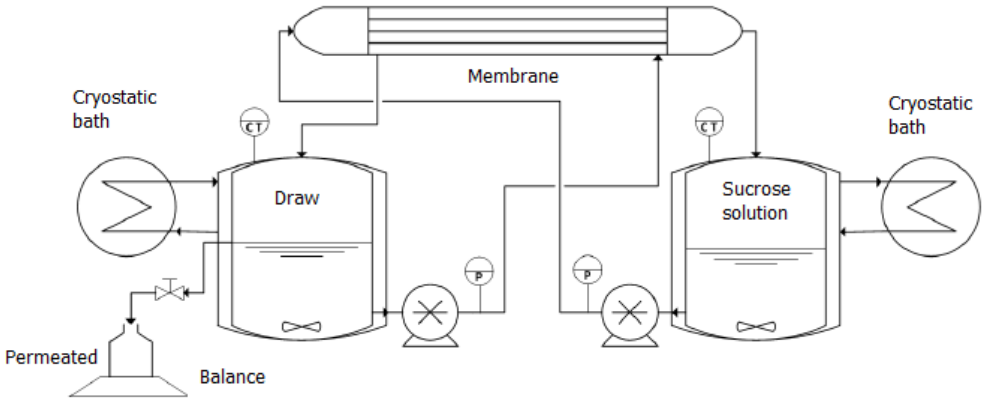

Figure 4.1 *Graphical representation of the bench-scale OE unit (Ongaratto, 2012).*

The solution to be concentrated and the draw are fed in counter current in the membrane module, the former passes through the tube side, while the latter passes through the shell side. Both vessels are cylindrical, jacketed, sealed, are made of polymethyl methacrylate (PMMA) and have a capacity volume of 900 mL. The vessels external jacket presents two holes (2, 3) connected to a heating-cooling system (thermostatic bath) in order to maintain both solutions at constant temperature. For the solution to be concentrated is used a thermostatic bath R6L Polystat model (Cole Parmer, USA) while for the saline is used model 20LE (Lauda, Germany). Hypertonic solution tank has a drain (4) used from time to time remove the exceeding draw. Tanks dimensions can be seen in Figure 4.2, in which only the hypertonic solution tank is shown.

Tanks of solution to concentrate and draw are the same in dimensions but except for the

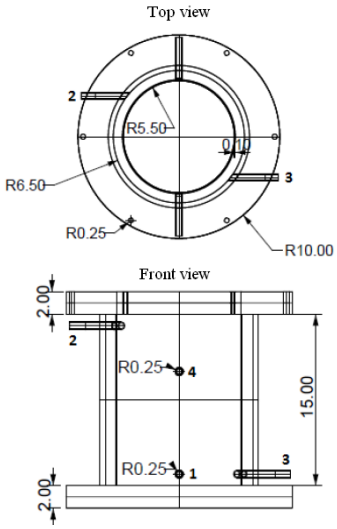

Figure 4.2 *Graphical representation of the vessel (Ongaratto, 2012).*

presence of the drain (4) that is only on the draw tank.

On the lid of each tank there are three openings (not shown), for solution sample collection, for solution return from the membrane and the third input to accommodate the conductivity electrode which determines solution conductivity. Figure 4.3 represents the OE unit.

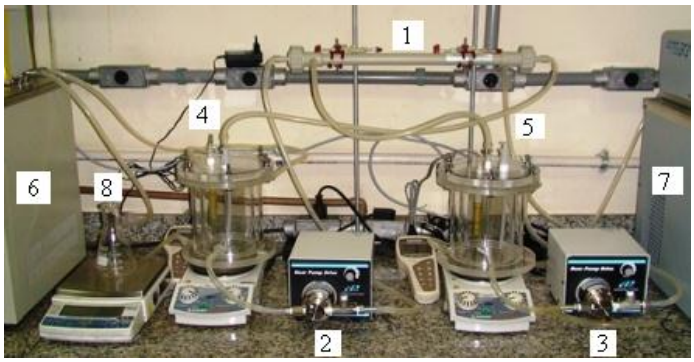

Figure 4.3 *Bench-scale unit: 1) Membrane module, 2) draw pump, 3) sucrose solution pump, 4) Draw tank, 5) Sucrose solution tank, 6) Criostatic bath for draw, 7) Crisostatic bath for sucrose solution, 8) Balance with permeated liquid.*

Membrane

Membrane is a commercial module with hollow fibers MD model 020 CP 2N (Microdyn, Germany) containing 40 Polypropylene capillary fibers, each having an outer diameter of 2.8 mm and a internal of 1.8 mm so that the fiber wall thickness is 0.5 mm. Module has the effective length of 0.5 m, total permeation area of 0.1 m^2 and pore diameter 0.2 mμ. The characteristics of these modules were presented in the Table 4.1.

Table 4.1 *Characteristics of membrane module.*

Feature	Description
Module	MD 020 CP 2N (Microdyn, Germany)
Configuration	Tubes and shell
Length of the fiber (m)	0.5
Inner diameter of the Shell (m)	0.025
Membrane area (m^2)	0.1
Membrane material	Polypropylene
Type	Hollow fiber
Number of fibers	40
Nominal pore diameter (μm)	0.2
Inner diameter of the fiber (mm)	1.8
Outer diameter of the fiber (mm)	2.8
Membrane thickness (mm)	0.5
Cross area available for the tube and shell side flow (m^2)	0.1

4.1.2 Experimental procedure

4.1.2.1 Solutions preparation

Solutions were prepared at room temperature, by weighing the solute in the semi-analytical balance (Gehaka, accuracy 0.001 g), adding distilled water and stirring until complete solute dissolution. Solutions were then adjusted to volume in calibrated flasks. Sucrose used for the solution preparation is from Vetec, while for draw preparation is used food grade potassium pyrophosphate (Halal).

Sucrose solution

Sucrose solution is prepared dissolving ~160g of commercial sucrose in distilled water and adjusting volume to 1 L.

Draw

Potassium pyrophosphate ($K_2P_5O_7$) is elected as osmotic agent for many reasons:

1) Low water activity in saturated solution;

2) Low cost;
3) Nontoxic.

Draw is prepared dissolving ~1280g/L of potassium pyrophosphate in distilled water and adjusting volume to 1 L.

4.1.2.2 Operational conditions

Carbon dioxide solubility test

CO2 solubility at saturation was measured in many draw ($K_5P_2O_7$ - water) and sucrose solution (sucrose - water), with the aim of quantifying the CO2 affinity with these solutions.

These values give informations about magnitude of the CO2 concentration gradient that takes place respectively between hot and cold water (MD process) and between draw and juice (combined OE+MD process).

Remembering that draw regeneration process is carried out by bubbling a combustion gas with high CO2 content, these solubility tests were carried out in samples at CO2 saturation condition, that means the worst possible condition of process.

Practically, a 150 mL liquid sample was collected in a beaker and kept at the temperature of 15 °C for 5 minutes using a thermostatic system, meanwhile feed CO2 was bubbling trough a sparger with the aim of improving the gas-liquid mass transfer. (Figure 4.4)

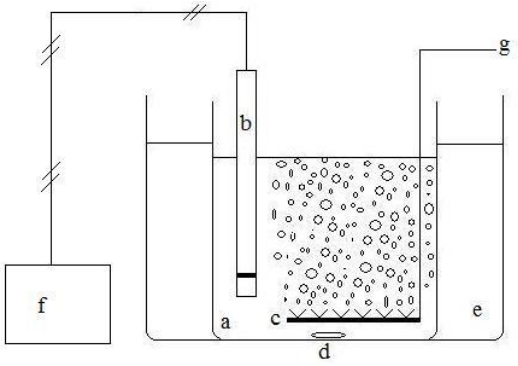

Figure 4.4 *Schematic representation of the CO2 testing system. a) Analized solution; b) CO2 sensor; c) CO2 sparger; d) mixer; e) thermostatic bath; f) transmissor; g) CO2 gas feed.*

After 5 minutes, CO2 concentration was measured reading the CO2 sensor value. Then, sample temperature was brought to the next desired value by acting on the thermostatic bath. After others 5 minutes of gas bubbling, CO2 concentration was measured reading the value shown by the sensor.

Operation was repeated until the higher temperature value selected was reached.

It was proven for all the selected temperatures that a duration of 5 minutes of gas bubbling was sufficient for the CO2 concentration signal to show an insignificant drifting. This could prove the condition of the CO2 saturation in the liquid sample.

MD process

- ***Test: Water (20°C) – Water (35°C)***

A first test using hot water (35°C) in tube side and cold water (20°C) in membrane shell side was carried out in duplicate with the aim of evaluating the CO2 flux through the membrane and the temperature gradient contribution to the mass flux.

Tests lasted 3 hours, permeated mass (excess draw) was quantified at the end of the process and this value enables the total permeate flux determination.

Permeated water was calculated by measuring the juice solution volume loss with a yardstick (0.001 m sensibility).

Knowing that membrane cross sectional flow area is 0.1 m^2 both in tubes and in shell side, flow rates were calculated using the tube and shell side rates.

In Table 4.2, operational conditions used in MD+OE process are schematized.

Table 4.2 *Operational conditions used in OE.*

	Hot wate		Cold water	
Configuration	Tube side		Shell side	
Temperature	C 35	°C	~ 20	°C
Flow rate	23.19	L/h	44.72	L/h
Rate	6.44	cm/s	12.42	cm/s
Time duration	3	h	3	h

Temperature of both solutions was determined at every 15 minutes, as well as hot water pH value.

Also, carbon dioxide concentration in sucrose solution, was measured at each time interval. Carbon dioxide concentration was measured using a InPro 5000 sensor (Mettler Toledo, Switzerland) which specifications are reported in Figure 4.3.

Table 4.3 *Sensor specifications.*

Variable	Value
Detection range:	10 to 1000 mbar
CO2 Lower detection limit:	10 mbar
Accuracy: ±10% (pCO2 10 to 900 mbar)	±15% (pCO2 > 900 mbar)
Response time:	90% of final value <120 sec at 25 °C

OE+MD process

- **Test: Draw (20°C) – Juice (35°C)**

OE+MD was carried out in duplicate by injecting draw at 20°C in membrane shell side and juice at 35°C in tube side.

Draw initial concentration is equal to osmotic agent saturation concentration, as previously mentioned. Sucrose concentration used for juice preparation is representative of common juices.

Tests lasted 3 hours, the permeated mass (excess draw) was quantified at the end of the process and this value enables the total permeate flux determination.

Permeated water was calculated by measuring juice solution volume loss with a yardstick (0.001 m sensibility).

No draw regeneration throughout the test was carried out, so hypertonic solution concentration decreased throughout the process.

Knowing that membrane cross sectional flow area is 0.1 m^2 both in tubes and in shell side, flow rates were calculated using tube and shell side rates.

In Table 4.4, operational conditions used in OE+MD process are schematized.

Table 4.4 *Operational conditions used in OE+MD.*

	Juice		Draw	
Configuration	Tube side		Shell side	
Concentration	160	g/L sucrose	1280	g/L $K_5P_2O_7$
Temperature	~ 35	°C	~ 20	°C
Flow rate	23.19	L/h	44.72	L/h
Rate	6.44	cm/s	12.42	cm/s

Both solutions conductivity and temperature were determined at every 15 minutes, as well as sucrose solution soluble solids and refractive index. Sucrose solution conductivity was monitored, in order to detect an eventual hypertonic solution passage through the membrane, if this occurred.

Solutions conductivity and temperature were determined trough conductivity meters model CON110 (Oakton, USA).

Refractive index was determined using two types of refractometers, portable model RHB-32 (Cole-Parmer, USA) and bench model Abbemat (Anton Paar, Austria).

Sucrose concentration (C, °Brix) was measured using a portable refractometer, and then related to refractive index (*RI*) as described by the following equation (AOAC, 1965 apud Ongaratto, 2012):

$$RI = 8 \times 10^{-6} \cdot C^2 + 0.0013 \cdot C + 1.3334 \quad (4.3)$$

Also, carbon dioxide concentration in sucrose solution was measured at each time interval. Carbon dioxide concentration was measured by using a InPro 5000 sensor (Mettler Toledo, Switzerland).

4.1.2.3 Cleaning procedure

Cleaning method starts after experimental solutions removal and consists of three steps:

1) Rinsing with filtered water;
2) Pre-washing with filtered water;
3) Washing with distilled water.

In first step, about 4 L of filtered water are added in draw and feed tanks, making them passing into the system without recirculation, thus after leaving the membrane module, water is discarded.

In second step, filtered water is added in tanks, making it circulate in the system for 20 minutes. After this time, wash water was drained and again filtered water was added to recirculation tank. Procedure is iterated until water electrical conductivity lies between 60 and 90 μS/cm.

Last cleaning step consists in adding distilled water to unit tanks, recirculating for 20 minutes and finally drained. This step is iterated until wash water conductivity lays between 5 and 10 μS/cm.

After washing, starts membrane drying procedure. Drying was performed in three steps, lasting 20 minutes each:

1) Passing compressed air inside the fibers;
2) Passing compressed air inside the carcass;
3) Passing compressed air across the membrane.

Drying efficiency test consists in circulating gaseous nitrogen at a pressure of 0.1 kg_f/cm^2 in order to verify that the permeated flow of gas keeps being the same as in the previous iteration. In practice, about 5 L of gas passing through the membrane are required.

Gas inlet is put in one of the fiber side entries and gas flowing across the membrane is determined with the aid of a gas tank connected to one of the shell side outputs. The remaining ends of the fiber and shell sides were kept closed.

4.2 DIRECT CONTACT EVAPORATION

Bench-scale unit used in membrane separation, solutions preparation criterion, cleaning procedure as well as experimental procedure followed for experiments are described in this section. Operational conditions adopted for DCE are presented.

4.2.1 Bench-scale unit

System was powered by compressed air and a rotameter was used to determine the flow rate. Air stream was heated in an electric furnace with a total power of 2000 W, in which the air flows in a coil of stainless steel AISI 316 with a nominal diameter of ¼ inch and a length of 23 m, and the heating element is located in the oven centre. The heating element has 10 shallow gutters uniformly distributed over the cross section, in which the electrical resistances are placed, being in direct contact with the air in the oven. Coil is insulated with ceramic wool and refractory bricks. A K type thermocouple measures the temperature of the furnace, which is maintained below the stainless steel AISI 316 (925 K) working temperature limit by a control system of type on-off voltage applied to the electric resistors. The line that connects the furnace to the evaporator is fully insulated with ceramic and glass wool. In order to minimize heat losses, electrical resistance with overall power equal 400 W was wound on that part of the line. Gas temperature is determined both at the furnace exit and at the entrance of the chamber below the gas distributor using K-type thermocouples. Such sensors are located in the middle of the pipe cross section, using T-form joints. After first thermocouple, there is a needle valve to control air flow in bypass line, used during the transient furnace heating. Above this, there is another needle valve that controls the gas flow fed to the equipment. Evaporator consists of a glass column with internal diameter of 7.3 cm and 1.34 m of height. On the column base, a gas distributor is mounted and column top is closed with a lid of stainless steel AISI 316 sealed with Viton O-rings.

A 1 m length resistance thermometer (Pt-100) is placed in this lid for measuring the temperature of the liquid inside the column (0.3 K accuracy). Gas stream coming from evaporator is sent to two Graham glass condensers, and then collected in a beaker positioned above a standard analytical balance.

Condensers are supplied with water at 278 K as cold fluid, coming from a circulation system provided cryostatic/thermal bath model DC30 (Haake, Austria).

Gas distribution system is composed by two sintered plates of AISI 316 stainless steel with a thickness of 3.24 and 2.19 mm, both with a diameter of 8.0 cm.

Thinner plate surface region has an average pore diameter of 12 ± 5 μ m. On porous plate top, a perforated alumina ceramic plate is used. This plate is 4.7 mm thick, 8 cm in diameter containing 89 holes with a diameter of 0.4 mm, arranged in a quadrangular pattern with a spacing of 6.3 mm. The desired plates set is fixed between two stainless steel flanged pieces, being glass column positioned above the metal piece, in which there is an outlet line to remove liquid. System is sealed with Viton O-rings and the column base is supported on insulating bricks, which are covered with ceramic fiber to increase the efficiency of the insulation.

Lateral evaporator (glass column) area is insulated with fiberglass, which is divided into two equal parts. One half is fixed to the column wall, as well as a graduated scale for measurement of the total height of the mixture in the column. The other half connected

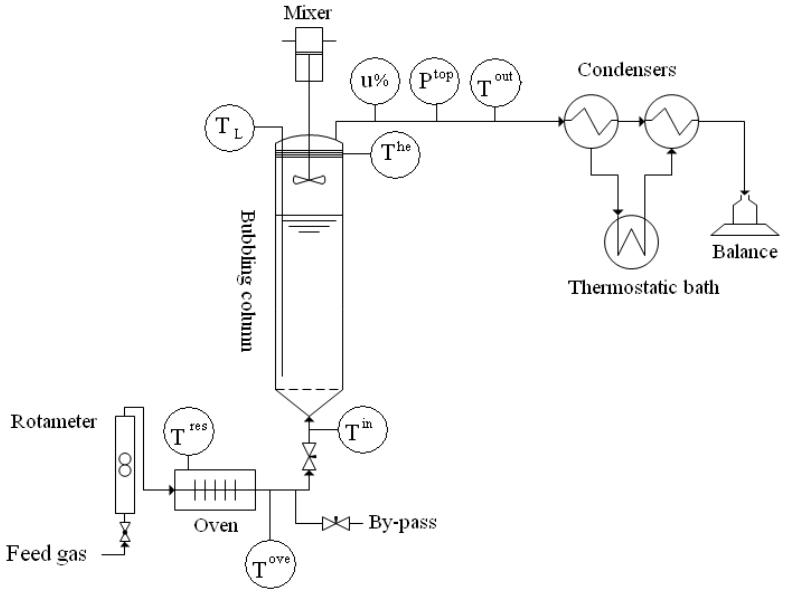

Figure 4.5 *Graphical representation of bench-scale DCE unit showing experimental measurement.*

to the first, can be moved to allow liquid height reading.

An electrical resistance generating 25W of power is wounded around the column top and settled to 100°C to prevent vapour condensation, because of the heat dispersions effect. DCE tests were performed in a unit as shown graphically in Figure 4.5.

4.2.2 Experimental procedure

4.2.2.1 Solution preparation

Solution was prepared at room temperature, by weighing ~323 g of NaCl in the semi-analytical balance (Gehaka, accuracy 0.001 g), adding distilled water and stirring until solute complete dissolution. Solution was then adjusted to volume in a calibrated flask.

Sodium chloride was chosen for many reasons:

1) Easier activity coefficient modelling in temperature and concentration range used in the process;

2) Low cost;

3) Nontoxic.

4.2.2.2 Operational conditions

DCE run was evaluated using a sodium chloride solution with a concentration equivalent to 90% of the saturation concentration (~323 g/L)

Also, run was conducted with distilled water to allow salt influence evaluation in the DCE result.

Hot air flow rotameter Index was settled at 20, equivalent to 9.855 L/min (Rotameter calibration curve, Appendix D) of entering total gas flow rate (G).

So, applying Gay Lussac law for taking in account gas expansion due to the temperature increase from T^{amb} to T^{L}, it was possible to calculate superficial velocity value in the column:

$$v_{gas} = \frac{G}{\frac{\pi D^2}{4}} \frac{T^L}{T^{amb}} \tag{4.4}$$

At the beginning of each run, column feed valve was closed and bypass valve was opened. Electric oven was turned on and 2 liters of solution to be concentrated were added to the column. Then, heating lines at the top of the column and between the column and the oven were switched on. Bypass valve was closed and evaporator valve was immediately opened for letting air to flow and starting bubbling.

Total blend height was read and insulation of fiberglass applied. Every 15 minutes were collected the values of: T^{res} : Oven resistance temperature (Thermocouple); T^{ove} : Temperature of gas coming from oven (Thermocouple); T^{in} : Temperature of gas entering the column (Thermocouple); T^{L}: Temperature of the liquid in the column (Thermocouple); T^{out} : Temperature of gas coming out from the top of the column (Hygrometer Hygropalm Rotronic); $u\%$: Relative humidity of gas flux coming out from the top of the column (Hygrometer Hygropalm Rotronic); m_w: mass of condensated water (Balance Marte, sensitivity 0.01 g); At the end of process was ridden the pressure at the top of the column (P^{top}) using a U manometer.

Every 30 minutes and only in the case of NaCl, solution refraction index (RI) was read by spilling a little liquid amount from the column bottom, that then is added from the column top. Each run lasted 5 hours, and total blend height was read at the end of the process. Test was conducted until quasi-stationary state was reached, where liquid temperature and evaporation rate become almost constant.

In Table 4.5, values range of the principal operating variables monitored during the processes is reported.

Table 4.5 *Range of values adopted for principal operating variables monitored in DCE process.*

Varable		Distilled water	Salt solution
v_{gas}	cm/s	4.32	4.32
T^{res}	C	520-526	501-526
T^{ove}	°C	530-566	418-537
T^{in}	°C	274-284	150-261

4.2.2.3 Cleaning procedure

Cleaning method follows the end of each experiment and consists of three steps:

1) Draining of column solution;
2) Rinsing with filtered water;
3) Pre-washing with filtered water;
4) Washing with distilled water.

For first, resistance furnace is turned off and the solution contained in the column was drained.

Then, a first wash step (pre-wash) was performed adding water in continuous flow to remove excess salt. Primary wash continues until the water conductivity from the column outlet arrives next to inlet water conductivity value (between 70 and 100 μS/cm).

After prewashing, distilled water is added in the column (about 3.5 L) and remains for 20 minutes without interrupting gas injection. Wash water is drained and again 3.5 L of distilled water were added. This procedure was repeated until wash water conductivity brings close to distilled water conductivity (between 3 and 15 μm /cm). Then, 90 °C heated air is injected to dry the column.

Chapter 5

Experimental results and modeling of OE and MD

In this section, experimental results obtained in tests of water MD and combined OE+MD concentration of sucrose solution are presented, compared and analyzed with a simplified mathematical model.

5.1 MD AND COMBINED OE+MD EXPERIMENTAL RESULTS

Experimental data obtained in tests of water MD and combined OE+MD concentration of sucrose solution using a pyrophosphate solution are presented in this section. In MD and combined MD+OE, water and CO2 fluxes were compared.

5.1.1 Carbon dioxide solubility test results

In this section are reported CO2 solubility tests experimental results, involving sucrose solution and draw at two concentrations. Tests were conducted with the aim of obtaining informations used to prove MD and OE experimental data reliability and to estimate CO2 concentration values used later in mass transfer models.
Experimental data, reported in Table 5.1, show clearly that sucrose solutions can dissolve a smaller amount of CO2 than water, and this effect is more relevant as sucrose concentration grows.

Table 5.1 *Experimental values of CO2 saturation concentration by varying temperature of sucrose and pyrophosphate solutions at many concentrations.*

Temperature	**Sucros5°B**	**Sucrose 57°B**	**Pirofosphate 640 g/L**	**Pirofosphate 1280 g/L**	**Water**
T	***[CO2]***	***[CO2]***	***[CO2]***	***[CO2]***	***[CO2]***
°C	**mg/L**	**mg/L**	**mg/L**	**mg/L**	**mg/L**
15	1740	1460	238	99	1903
25	1184	956	167	67	1398
35	902	702	122	43	1032
45	709	551	74	25	795

CO2 concentration in pyrophosphate solutions keeps very low, and even in this case this effect is more relevant as salt concentration grows. Figure 5.1 shows CO2 saturation

concentration trend by varying sucrose and pyrophosphate solutions temperature at many concentrations.

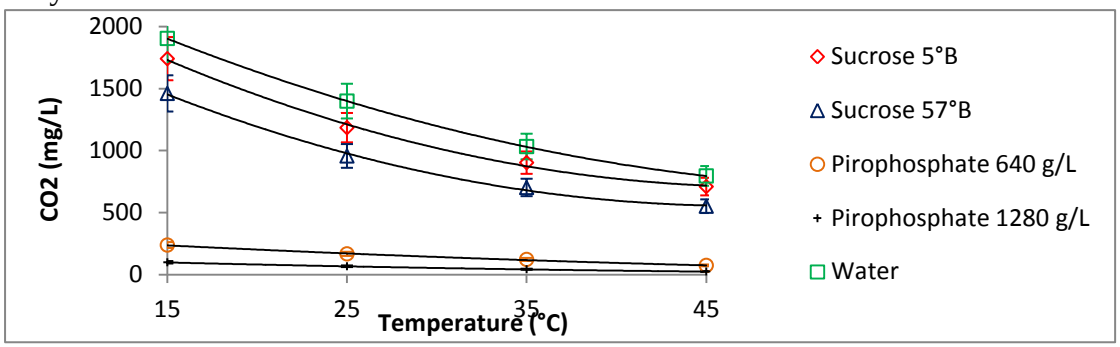

Figure 5.1 *CO2 saturation concentration trend by varying temperature of sucrose and pyrophosphate solutions at many concentrations.*

Figure 5.2 shows pH trend by varying temperature of CO_2 saturated sucrose and pyrophosphate solutions at many concentrations. As expected, pH grows in both sucrose solutions, as temperature increase. This effect reflects the CO_2 concentration decrease as long as the temperature increases.

As regard both pyrophosphate solutions, pH shows an opposite trend in respect of sucrose solutions; this could be due to pyrophosphate hydrolyse constant variation in function of temperature. Anyway, low phenomenon magnitude ensures that no relevant reaction happens between salt and CO_2.

Anyway, pH of all solutions does not show wide variation for the range of temperature analyzed.

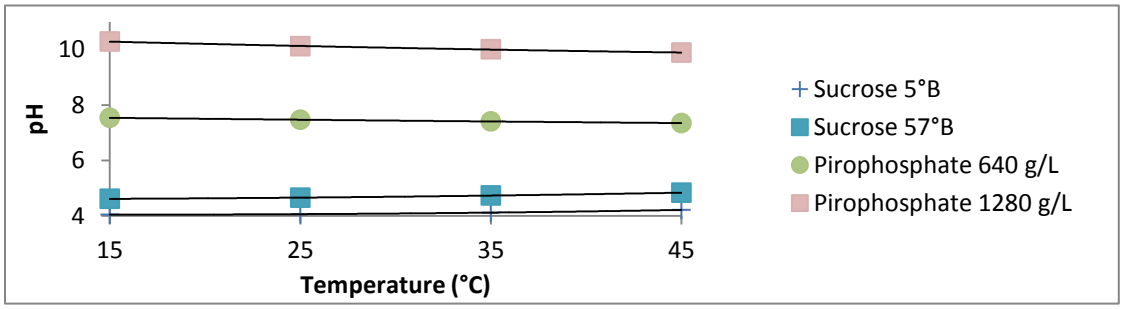

Figure 5.2 *pH trend by varying temperature of CO2 saturated sucrose and pyrophosphate solution at many concentrations.*

5.1.2 OE and MD process results

5.1.2.1 MD Test: water – water

In this section, CO2 concentration experimental result of MD process involving hot (35°C) and cold CO2 saturated (20°C) water, for test 1 (Table 5.2) and for test 2 (Table 14) is reported.

Table 5.2 *Operational conditions and experimental results in MD process: CO2 saturated water (20°C) – Water (35°C) (Test n°1).*

	CO2 saturated cold water	**Hot water**	
Time	T_{cold}	T_{hot}	$[CO2]_{hot\ water}$
min	**°C**	**°C**	**mg/L**
0	19	35	6
15	21	35	316
30	21	35	408
45	21	35	436
60	20	35	462
75	20	35	481
90	20	35	500
105	20	35	504
120	20	35	504
135	20	35	502
150	20	35	499
165	20	35	498
180	20	35	496

Table 5.3 *Operational conditions and experimental results in MD process: CO2 saturated water (20°C) – Water (35°C) (Test n°2).*

	CO2 saturated cold water	**Hot water**	
Time	T_{cold}	T_{hot}	$[CO2]_{hot\ water}$
min	**°C**	**°C**	**mg/L**
0	18	37	3
15	21	36	240
30	20	36	366
45	20	35	428
60	20	35	453
75	20	35	468
90	20	35	481
105	20	35	481
120	20	35	482
135	20	35	482
150	20	35	481
165	20	35	479
180	20	35	476

Tables 5.2 and 5.3 show that after 90 min of process duration, hot water CO2 concentration in test n°1 and test n°2 arrived at a stationary value.

In particular, temperature range chosen for stationary state definition is based on last CO_2 concentration value measured in hot water $[CO2]_{hot\ water}^{180\ min}$ ± 10 mg/L; Then, stationary state includes the last 7 values for Test 1 and the last 8 values for Test 2. In

Table 5.4, ratio between average experimental CO2 stationary state concentration value in hot water and cold water CO2 saturation concentration (obtained interpolating Table 5.2 and 5.3 experimental data at a temperature value of 20°C, Annex H) was calculated. Observing high CO2 percentage passed between the liquids, it is clear that its flux is only lightly obstacled by the PP membrane layer.

Table 5.4 *Comparison between stationary state experimental value of CO2 concentration in hot water and CO2 saturated cold water, for Test 1 and Test 2.*

	Unit	**Test 1**	**Test 2**
$[CO2]_{hot\ water}^{mean}$	mg/L	500	479
$[CO2]_{cold\ water}^{saturation}$	mg/L	1634	1634
CO2 passed	%	30.6	29.3

Knowing MD process mass permeate experimental result and that membrane area is 0.1 m^2, permeate flux was calculated considering 3 hours of process duration.
Mathematic relation used for permeate flux calculation is:

$$J_w = \frac{M_p}{A_m t} \tag{5.1}$$

Experimental result of MD process mass permeate and permeate flux are reported in Table 5.5.

Table 5.5 *Experimental results of mass permeate in MD process: CO2 saturated water (20°C) – Water (35°C).*

Test n°	M_p	J_w
	g	**Kg/h m²**
1	164	0.548
2	190	0.635

So, for test 1 and 2, water flux average value is: 0.592 Kg/h K m^2. This value is included in the average values range observed in literature (Table 3.1).

5.1.2.2 Combined OE+MD Test: Pyrophosphate draw – Sucrose solution

In this section, experimental result of OE+MD process involving sucrose solution and draw are reported. Sugar content values in sucrose solution ($[sucrose]^{RI}$) are calculated from experimentally determined refraction index (equation 4.3).
During OE+MD process, temperature profiles of sucrose solution and draw are plotted in Figure 5.3, with the aim to point out that temperature gradient contribution was almost constant during the whole process, except a little variation during the first half of the operation.

Tables 5.6 and 5.7 report, respectively for Test n°1 and n°2, operational conditions and experimental results in OE+MD process: CO2 saturated pyrophosphate draw (20°C) – Sucrose solution (35°C).

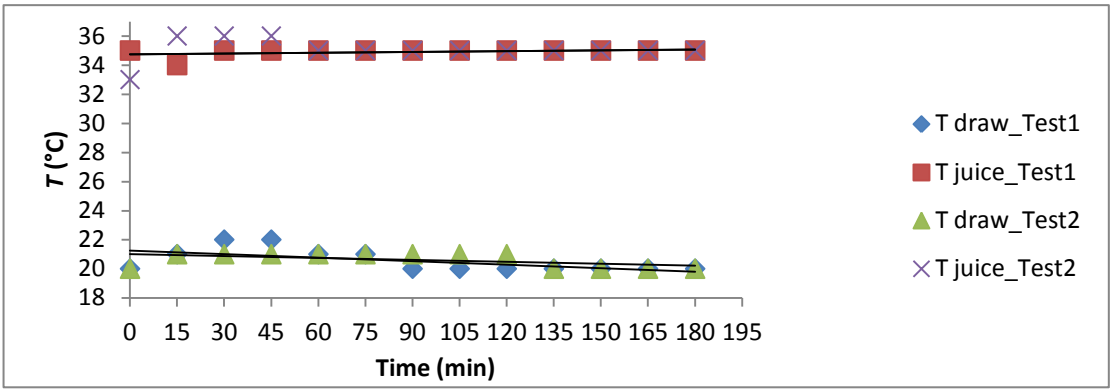

Figure 5.3 *Profiles of temperature for sucrose solution and draw during OE+MD process: CO2 saturated pyrophosphate draw (20°C) – Sucrose solution (35°C) (for test n°1 and n°2).*

Observing Tables 5.6 and 5.7, it is clear that stationary state was achieved: CO2 concentration in sucrose solution remained constant for the whole process duration, at a very low average value of ~7 mg/L (Test 1) and ~3 mg/L (Test 2); that means that practically no CO2 passed through the membrane.

Table 5.6 *Operational conditions and experimental results in OE+MD process: CO2 saturated pyrophosphate draw (20°C) – Sucrose solution (35°C) (Test n°1).*

	CO2 saturated pyrophosphate draw		**Sucrose solution**					
Time	T_{draw}	σ_{draw}	T_{sucr}	σ_{sucr}	***RI***	$[sucrose]^{RI}$	$[sucrose]^{meas}$	$[CO2]_{sucr}$
min	**°C**	**mS/cm**	**°C**	**µS/cm**	**-**	**° B**	**° B**	**mg/L**
0	20	30.2	35	25.6	1.355112	15.27	14.9	7
15	21	42.8	34	29.3	1.356544	16.19	15.7	7
30	22	48.5	35	30.7	1.357592	16.86	16.3	7
45	22	53.2	35	31.1	1.358711	17.57	17.3	7
60	21	60.9	35	32.5	1.360604	18.76	18.2	7
75	21	67.2	35	33.8	1.362260	19.79	19.4	7
90	20	73.4	35	34.4	1.363705	20.68	20.2	7
105	20	79.0	35	35.2	1.364982	21.46	21.1	7
120	20	85.1	35	36.6	1.367469	22.96	22.4	7
135	20	90.9	35	37.1	1.369259	24.03	23.5	7
150	20	95.8	35	38.6	1.370170	24.57	24.3	7
165	20	100.8	35	39.9	1.371615	25.42	25.2	7
180	20	105.8	35	40.2	1.372574	25.98	25.7	7

Table 5.7 *Operational conditions and experimental results in OE+MD process: CO2 saturated pyrophosphate draw (20°C) – Sucrose solution (35°C) (Test n°2).*

	CO2 saturated pyrophosphate draw		**Sucrose solution**					
Time	T_{draw}	σ_{draw}	T_{sucr}	σ_{sucr}	***RI***	$[sucrose]^{RI}$	$[sucrose]^{meas}$	$[CO2]_{sucr}$
min	**C**	**mS/cm**	**C**	**µS/cm**	**-**	**° B**	**° B**	**mg/L**
0	20	29.5	33	26.8	1.355055	15.23	14.7	3
15	21	41.9	36	27.7	1.356419	16.11	15.6	5
30	21	48.3	36	28.4	1.357231	16.63	16.1	5
45	21	57.1	36	29.2	1.358726	17.58	17.0	4
60	21	65.2	35	30.3	1.359981	18.37	17.8	3
75	21	71.7	35	31.9	1.361181	19.12	18.6	3
90	21	77.8	35	32.6	1.362082	19.68	19.1	3
105	21	85.3	35	33.3	1.363624	20.63	20.1	3
120	21	92.4	35	34.6	1.364572	21.21	20.6	3
135	20	98.8	5	35.1	1.366484	22.37	21.7	3
150	20	103.6	35	.7	1.367232	22.82	22.2	3
165	20	108.9	35	36.2	1.368552	23.61	23.2	3
180	20	116.0	35	37.0	1.369495	4.17	23.5	3

In Table 5.8, ratio between average experimental CO2 stationary state concentration value in hot sucrose solution and CO2 saturation concentration in cold pyrophosphate draw (obtained interpolating Table 12 experimental data at a temperature value of 20°C, Annex H) was calculated.

As regards MD+OE, CO2 saturation concentration in cold pyrophosphate draw is very much lower than in cold water used in MD process and this is probably due to salting out effect produced by salt presence. Comparing CO2 percentage passed between the liquids in the cases of MD (Table 5.4) and combined MD+OE (Table 5.8) and remembering that membrane and operational conditions were the same, it is clear that in the second case CO2 flux is obstacled by the presence of salt. This phenomenon could be attributed to the boundary layer that originates in draw solution region, very next to the membrane (Figure 3.2). In fact, higher salt concentration implies lower CO2 concentrations and so, CO2 concentration is lower in the boundary layer than in the bulk, with the effect that actual CO2 concentration gradient is lower than the apparent.

Table 5.8 *Comparison between stationary state experimental value of CO2 concentration in hot sucrose solution and CO2 saturated cold draw, for Test 1 and Test 2.*

	Unit	**Test 1**	**Test 2**
$[CO2]_{hot\ sucrose\ solution}^{mean}$	mg/L	7	3
$[CO2]_{cold\ draw}^{saturation}$	mg/L	82	82
CO2 passed	%	8.5	4.1

Using equation (1) experimental results of mass permeate in OE+MD process and permeate flux are reported in Table 20.

Table 5.9 *Experimental results of mass permeate in OE+MD process: CO2 saturated pyrophosphate draw (20°C) – Sucrose solution (35°C) (for test n°1 and n°2).*

Test n	M_p	J_w
	g	Kg/hm^2
1	519	2.019
2	441	1.471

So, for test 1 and 2, water flux average value is: 1.718 Kg/h K m^2. This value is greater than the average values observed in literature (Table 3.1). Concentration effect can be seen plotting sucrose solution refraction index, conductivity and sugar content data versus time duration (respectively Figures 5.5, 5.6 and 5.7).

Variables represented in these plots are lower for test 2 because of the lower permeated water flux. In Figure 5.4, CO2 concentrations measured respectively in water (35°C) used in MD tests and in sucrose solution (35°C) used in combined MD+OE tests indicate that a lower CO2 flux took place in the second case. Error bars related to CO2 sensor accuracy are reported for one data each test, although only values in MD are

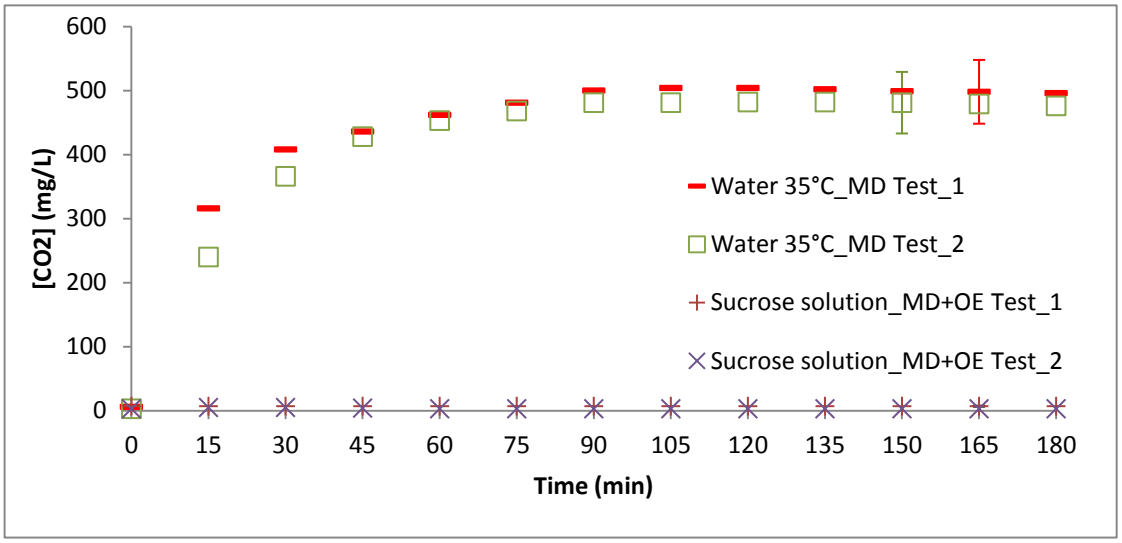

Figure 5.4 *Experimental values of CO2 concentration measured respectively in water at 35°C (MD tests) and in sucrose solution at 35°C (MD+OE tests).*

significant. Figure 5.3 shows that temperature gradient between the solutions was almost constant during the whole process, while experimental sugar content values in sucrose solution showed a linear trend; this could mean that solutions concentration variation during process did not influence water flux through the membrane, that was kept constant. This could mean that mass transport through the membrane was the main contribution to overall mass transfer resistance. All plots were showed a linear trend, that could mean that permeate flux was almost constant during the whole process.

In Figure 5.5, different slope between test n°1 and n°2 experimental sucrose solution refraction index values in OE+MD process is due to different water flux that took place.

In Figure 5.7 can be observed a divergence between sugar content data determined trough the two methods; this could be produced by a systematic instrumental or human error, by the way error magnitude could be overlooked. Draw conductivity data is represented in Figure 5.8, showing that values were higher for test 1 because the higher permeated water flux produce a more diluted solution.

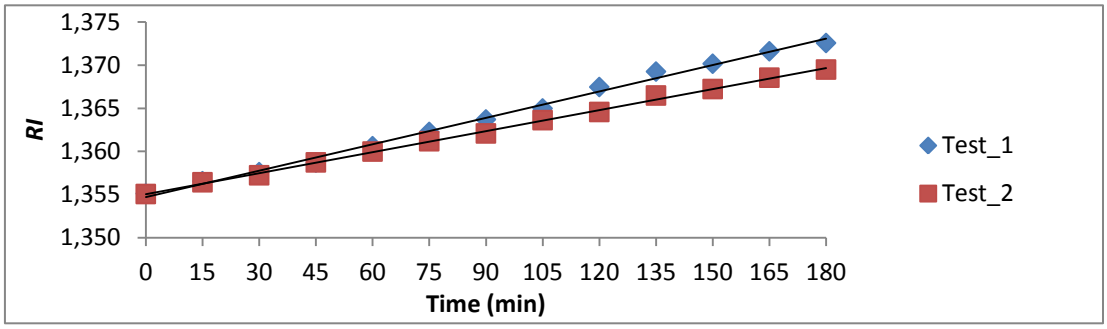

Figure 5.5 *Experimental values of sucrose solution refraction index in OE+MD process: CO2 saturated pyrophosphate draw (20°C) – Sucrose solution (35°C) (for test n°1 and n°2).*

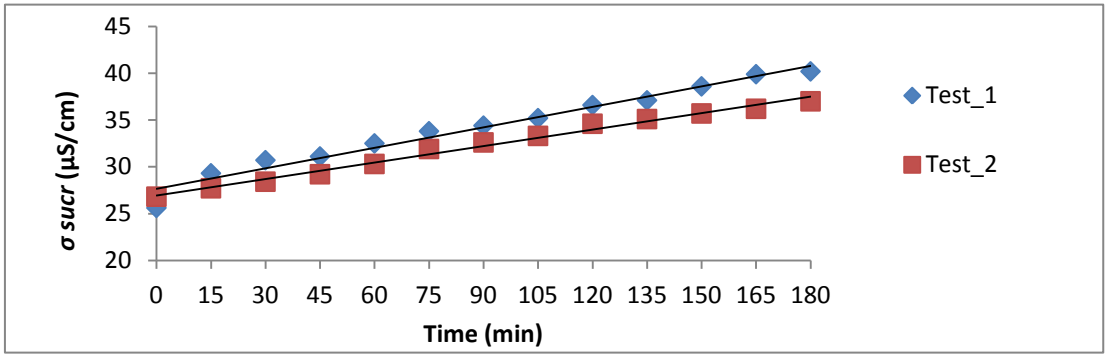

Figure 5.6 *Experimental values of sucrose solution conductivity in OE+MD process: CO2 pyrophosphate draw (20°C) – Sucrose solution (35°C) (for test n°1 and n°2).*

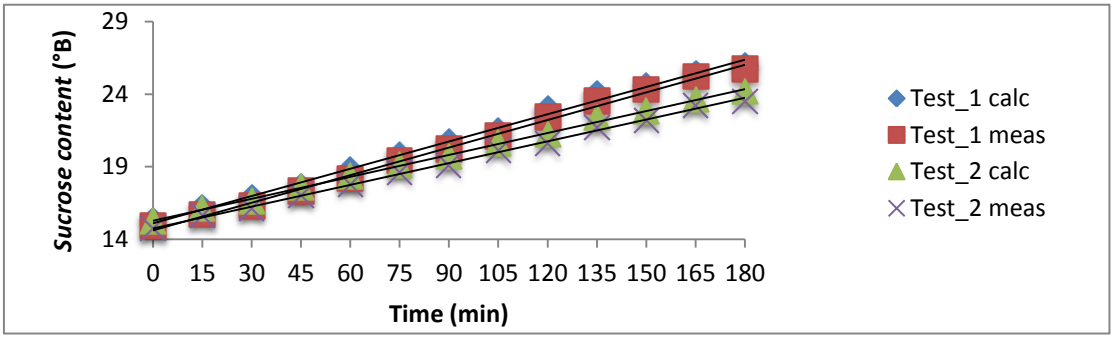

Figure 5.7 *Experimental values of sucrose solution sugar content in OE+MD process: CO2 pyrophosphate draw (20°C) – Sucrose solution (35°C) (for test n°1 and n°2).*

In Figure 5.8, a different slope in draw conductivity experimental values in OE+MD process proof the difference in water flux that took place in test n°1 and n°2.

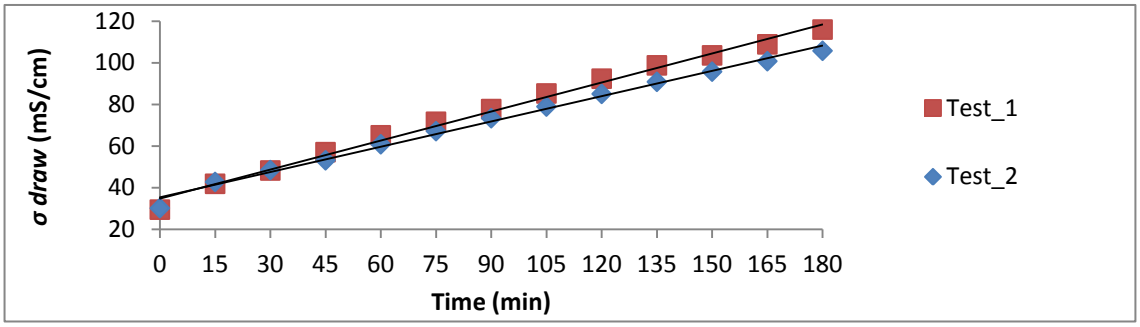

Figure 5.8 *Experimental values of draw conductivity in OE+MD process: CO2 saturated pyrophosphate draw (20°C) – Sucrose solution (35°C) (for test n°1 and n°2).*

5.2 MATHEMATIC MODELING OF OE AND MD PROCESS

In this section, experimental results of water MD and combined OE+MD concentration of sucrose solution using a pyrophosphate draw solution were analyzed using a simplified mathematical model which splits the temperature gradient and the osmotic pressure gradient contributions to water flux.

5.2.1 MD Test: water – water

Mass transfer model was applied to MD experimental results with the aim of evaluating temperature gradient effect on water and CO2 fluxes.

5.2.1.1 Mass transfer model

In MD, mass transfer between hot and cold water is due totally to temperature gradient. Then, diffusion coefficient was calculated applying the Fick's law and consideration that the only driving force is the temperature gradient. In Table 5.10, calculation of ΔT_a, carried out determining the time averaged value of ΔT between hot and cold water (Tables 5.2 and 5.3) is reported:

$$k_{m,t} = \frac{J_w}{\Delta T_a} \tag{5.2}$$

Where, ΔT_a and J_w are respectively average hot and cold water temperature gradient and permeate flux, while mass transfer coefficient relative to temperature gradient is represented by $k_{m,t}$.

Table 5.10 *Values of ΔT_a and $k_{m,t}$ calculated for MD process (Test 1 and test 2).*

Test n°	ΔT_a	$k_{m,t}$
	°C	Kg/h K m^2
1	14.9	0.0365
2	15.4	0.0423

So, for test 1 and 2, the average mass transfer coefficient value relative to the temperature gradient is: 0.0394 Kg/h K m^2

5.2.2 Combined OE+MD Test: pyrophosphate draw – Sucrose solution

Mass transfer model was applied to combined MD+OE experimental results with the aim of evaluating both temperature gradient and osmotic pressure gradient effects on water and CO2 fluxes.

Osmotic pressure gradients for sucrose and draw solutions were estimated to be subsequently employed in mass transfer model.

5.2.2.1 Sucrose solution mass balance and osmotic pressure drop

Using equation 5.3, sucrose concentration in sucrose solution at the start of process was calculated knowing experimental mass values of sucrose and water used for sucrose solution preparation. Results were reported in Table 5.11.

Introducing in sucrose mass conservation equation the experimental permeated water mass value and experimental sucrose and water mass values used for sucrose solution preparation, enables to calculate sucrose concentration in sucrose solution at the end of process.

Just to give an example, for °B concentration calculation, the equation used is:

$$C_{solute}^{calc}(°B) = \frac{Weighed\ mass\ of\ solute\ (g)}{Water\ in\ solution\ (g) + weighed\ mass\ of\ solute\ (g)}\ 100 \qquad (5.3)$$

Where, for process start concentration calculation, water in solution (g) is the weighed initial water in solution preparation. For process end concentration calculation, water in solution (g) is the difference between weighed initial water in solution preparation and permeated water. For sucrose final concentration calculation (g/L) a diluted solution hypothesis was considered. So, excess volume difference due to end of process greater concentration was not taken in account.

Also, relative error between experimental and calculated concentration values (Table 5.11) can be determined using equation 5.4.

This error is probably correlated to sucrose solution passage through the membrane, which affected sucrose conservation mass balance in the solution.

$$Relative\ error\ (\%) = \frac{C_{sucrose}^{calc} - C_{sucrose}^{Exp}}{C_{sucrose}^{calc}}\ 100 \qquad (5.4)$$

Sucrose concentration values at the start and at the end of the process were used for mean concentration calculation. Results are reported in Table 5.11.

$$\Pi_a^{sucr} = \frac{\Pi\ _{t=o}^{sucr} + \Pi\ _{t=18o}^{sucr}}{2} \quad (5.5)$$

Sucrose osmotic pressure was calculated using Van t'Hoff equation, corrected with sucrose osmotic coefficient:

$$\Pi_a^{sucr} = \Phi\ iMRT \quad (5.6)$$

Where, Π_a^{sucr} and Φ are respectively average sucrose osmotic pressure and sucrose osmotic coefficient (From data regression in Annex A); Mean molarity and gas universal constant (L atm $K^{-1}mol^{-1}$) are represented respectively by M and R, while i and *T* are respectively Van't Hoff factor (1 for sucrose) and temperature (K).
Results are reported in Table 5.11.

Table 5.11 Data used for sucrose osmotic pressure calculation in OE+MD: CO2 pyrophosphate draw (20°C) – Sucrose *solution (35°C) (Test n°1 and n°2).*

Sucrose solution	**Test 1**		**Test 2**	
Experimental initial concentration	15.27	mol/kg $_{water}$	15.23	mol/kg $_{water}$
Experimental final concentration	25.98	mol/kg $_{water}$	24.17	mol/kg $_{water}$
Sucrose for solution preparation	160.0	g	160.0	g
Water for solution preparation	900.5	g	901.2	g
Permeated water	606	g	441	g
Calculated Initial concentration	15.08	°B	15.07	°B
	160.0	g/L	160.0	g/L
	0.519	mol/kg $_{water}$	0.518	mol/kg $_{water}$
Calculated Final concentration	35.2	°B	25.8	°B
	406	g/L	286	g/L
	1.59	mol/kg $_{water}$	1.02	mol/kg $_{water}$
Calculated mean concentration	1.05	mol/kg $_{water}$	0.77	mol/kg $_{water}$
	283	g/L	223	g/L
	0.827	mol/L	0.652	mol/L
Relative error between calculated and experimental initial concentration	-1	%	-1	%
Relative error between calculated and experimental final concentration	26	%	6	%
i	1	-	1	-
Φ	1.146	-	1.099	-
R	0.0821	L atm/K mol	0.0821	L atm/K mol
T^{mean}	307.9	K	293.5	K
M^{mean}	0.827	mol/L	0.652	mol/L
$\Pi\ _{t=0}^{sucr}$	15.0	atm	13.7	atm
$\Pi\ _{t=180}^{sucr}$	45.9	atm	26.9	atm
Π_a^{sucr}	30.4	atm	20.3	atm

Relative error between calculated and experimental initial concentration is very low and equal for test n°1 and test n°2, this could suggest a systematic error in measurement that anyway is negligible. Relative error between calculated and experimental final concentration is low for test n°2 but in test n°1 is not negligible because experimental sucrose solution was more diluted than the expected.

This could find an explication by considering the occurrence of sucrose passage to draw solution, across the membrane. This could be generated likely by a instantaneous pressure pulsation.

5.2.2.2 Draw solution mass balance and osmotic pressure drop

Using equation 5.3, draw pyrophosphate concentration at the start of process is calculated knowing experimental pyrophosphate and water mass values used for draw preparation. Results are reported in Table 5.12. Using equation 5.3 and considering permeated water experimental mass value and experimental pyrophosphate and water mass values used for draw preparation, enable to calculate pyrophosphate concentration in draw at the end of the process. Then, pyrophosphate osmotic pressure corresponding to initial and final draw concentration were calculated, using data regression (Annex B). Results are reported in Table 5.12.

Concentration values of pyrophosphate draw at the start (t=0 min) and at the end (t=180 min) of process were used for mean concentration calculation. Results are reported in Table 5.12.

$$\Pi_a^{draw} = \frac{\Pi\ {}^{draw}_{t=0} + \Pi\ {}^{draw}_{t=180}}{2} \quad (5.7)$$

Table 5.12 *Data used for pyrophosphate osmotic pressure calculation in OE+MD: CO2 pyrophosphate draw (20°C) – Sucrose solution (35°C) (Test n°1 and n°2).*

Draw solution	**Test 1**		**Test 2**	
Pyrophosphate for solution preparation	1280.0	g	1280.0	g
Water for solution preparation	572.1	g	572.0	g
Calculated Initial concentration	6.78	mol/kg $_{water}$	6.78	mol/kg $_{water}$
Permeated water	606.0	g	441.0	g
Calculated Final concentration	3.29	mol/kg $_{water}$	3.83	mol/kg $_{water}$
Calculated mean concentration	5.03	mol/kg $_{water}$	5.30	mol/kg $_{water}$
Π_a^{draw}	796.2	atm	796.3	atm
$\Pi\ {}^{draw}_{t=0}$	465.5	atm	531.7	atm
$\Pi\ {}^{draw}_{t=180}$	630.9	atm	664.1	atm

5.2.2.3 Mass transfer model

In combined OE+MD, mass transfer between draw and sucrose solution is due partially to temperature gradient and partially to osmotic pressure gradient. A simple two parameters model (equation 5.9) was developed for the case.

The mass transfer coefficient value relative to temperature gradient ($k_{m,t}$) is taken from the water-water MD calculation. (equation 5.10)

Mass transfer coefficient relative to osmotic pressure gradient is calculated applying equation 5.10 that is based on Fick's law and considers the driving force effect of both temperature and concentration gradients. Results are reported in Table 24.

$$J_w = J_{w,T} + J_{w,\Pi} \quad (5.8)$$

$$= k_{m,t}\,\Delta T_a + k_{m,\Pi}\,\Delta \Pi_a \quad (5.9)$$

Reorganizing, calculation of $k_{m,\Pi}$ is allowed:

$$k_{m,\Pi} = \frac{J_w - k_{m,t}\,\Delta T_a}{\Delta \Pi_a} \quad (5.10)$$

Where, ΔT_a and $\Delta \Pi_a$ are respectively average temperature and concentration gradients between draw and sucrose solution. Permeate flux due respectively to temperature gradient and osmotic pressure gradient are represented by $J_{w,T}$ and $J_{w,\pi}$. Mass transfer coefficient relative respectively to temperature gradient and osmotic pressure gradient are represented by $k_{m,t}$ and $k_{m,\Pi}$.

Calculation of ΔT_a is carried out determining the time averaged value of ΔT between draw and sucrose solutions (Tables 16 and 17)

$$\Delta T_a = \frac{\sum_{i=1}^{13} \Delta T}{13} \quad (5.11)$$

Table 5.13 reports values of osmotic pressure gradient ($\Delta \Pi_a$) between draw and sucrose solutions, calculated as:

$$\Delta \Pi_a = \Pi_a^{draw} - \Pi_a^{sucr} \quad (5.12)$$

Table 5.13 *Variables and parameters involved in combined OE+MD process model for CO2 pyrophosphate draw (20°C) – Sucrose solution (35°C) (Test n°1 and n°2).*

	Temperature contribution				**Osmotic pressure contribution**			
Test n°	ΔT_a	$k_{m,T}$	$J_{w,T}$	$\frac{J_{w,T}}{J_w}$	$\Delta \Pi_a$	$k_{m,\Pi}$	$J_{w,\Pi}$	$\frac{J_{w,\Pi}}{J_w}$
	°C	**kg/h K m²**	**kg/hm²**	**%**	**atm**	**kg/h atm m²**	**kg/hm²**	**%**
1	14.4	0.0370	0.532	26	600.4	0.0025	1.487	74
2	14.5	0.0370	0.535	36	643.7	0.0015	0.936	64

Then, the average mass transfer coefficient value relative to osmotic pressure gradient is: 0.001566 Kg/h atm m^2 .

Figure 5.9 shows, in operational conditions adopted for combined OE+MD process, a greater temperature gradient contribution in respect to osmotic pressure gradient.

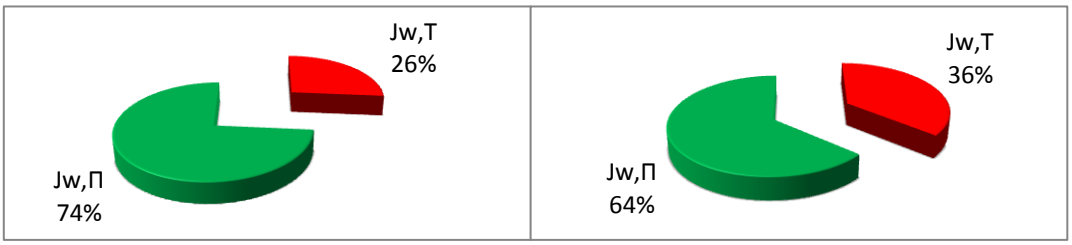

Figure 5.9 *Temperature gradient and osmotic pressure gradient contribution on total permeate flux: comparison between test n°1and test n°2 in combined OE+MD process, CO2 pyrophosphate draw (20°C) – Sucrose solution (35°C).*

Chapter 6

Experimental results and mathematic modelling of DCE process

In this section, experimental results obtained in tests of water and draw (NaCl solution) DCE are presented and compared with a simplified mathematical predictive model.

6.1 Experimental data of DCE

Experimental results obtained in water and draw DCE tests are presented in this section. Water and draw DCE mass transport efficiencies were compared.

DCE tests showed a heterogeneous bubbling regime in both water and salt solution cases.

In Table 6.1, measured at 15 minutes intervals, experimental results of water tests 1 and 2 are shown for the following variables: T^L and T^{out}, which represent temperatures of respectively liquid in the column and gas coming out from column top; M_w^c (i) and $u\%$ which represent respectively condensed water mass amount during a 15 minutes generic interval (i) and relative humidity of gas flux coming out from column top.

As regard NaCl solution test, results are reported in Table 6.2. As well as the variables above, are shown also experimental results of:

RI and γ_w , which are respectively refraction index and water activity coefficient, calculated as explained in model section 6.2.13; x_{water} and x_{NaCl} which represent water molar fraction in column liquid and NaCl molar fraction in column liquid.

With the aim of limiting analyses invasiveness (liquid samples spilling), *RI* values was measured only at 30 minutes intervals.

Then, in order to provide *RI* values at every 15 minutes and allowing a more complete comparison with thermo hygrometer data, a data regression was adopted (Annex C).

Tables 6.1 and 6.2 show that, after an initial transient state when system temperature and water evaporated mass increase, a stationary state is observed in both water and NaCl solution cases.

This transition takes place at about half time duration and for stationary state definition, the temperature range T^L (°C) ± ~1 (°C) was chosen. Where T^L is the liquid temperature at DCE process end.

For both water tests, stationary state goes from interval nº13 to interval nº21.
For NaCl solution test, stationary state goes only from interval 19 to 21. This difference could be also due to ebullioscopic increase.

Table 6.1 *Experimental results, measured at 15 minutes intervals, are reported for water tests.*

		Water							
		Test n°1				**Test n°2**			
Interval	***t***	T^L	T^{out}	M_w^c	***u relative***	T^L	T^{out}	M_w^c	***u relative***
i	**min**	**°C**	**°C**	**g**	**%**	**°C**	**°C**	**g**	**%**
1	0	32.2	42.1	0.00	94.3	36.8	46.2	0.00	95.6
2	15	43.0	75.9	7.22	20.4	48.3	74.6	8.43	21.7
3	30	50.1	93.3	12.61	22.4	52.1	92.3	11.64	20.6
4	45	54.6	93.1	17.36	19.3	53.5	94.9	15.88	19.4
5	60	56.4	101.3	22.83	16.8	54.7	100.3	24.95	17.1
6	75	59.5	106.8	27.78	15.2	56.8	103.9	28.64	16.2
7	90	60.3	110.5	29.66	14.5	58.4	107.8	30.44	14.2
8	105	61.8	113.1	32.22	14.1	59.9	111.4	31.78	13.8
9	120	62.3	115.5	31.57	13.6	61.3	113.9	31.95	13.1
10	135	62.9	116.9	31.43	13.3	62.3	115.2	31.03	13.2
11	150	63.2	117.7	31.18	13.1	62.8	116.1	31.65	13.1
12	165	63.4	118.8	32.64	12.9	63.0	117.3	31.78	12.9
13	180	63.9	119.0	32.76	12.9	63.8	118.5	32.03	12.8
14	195	64.1	119.6	31.90	12.6	64.1	119.2	32.61	12.6
15	210	64.2	120.1	31.29	12.5	64.1	119.9	31.19	12.5
16	225	64.3	120.4	29.68	12.5	64.3	120.1	31.08	12.5
17	240	64.4	120.5	29.98	12.5	64.4	120.6	31.56	12.6
18	255	64.5	120.8	30.03	12.2	64.5	120.9	31.87	12.4
19	270	64.6	121.2	29.71	12.1	64.7	120.8	30.97	12.2
20	285	64.7	120.9	28.36	12.4	64.6	120.9	31.51	12.3
21	300	64.9	121.1	29.04	12.3	64.8	121.0	31.76	12.5

Figure 6.1 shows that operational temperature were the same for water test 1 and 2, but for NaCl solution test, the gas coming from oven and so the gas entering the column were colder at the start: this could explain why salt solution pseudo stationary state was achieved later.
Figure 6.2 shows that temperature values of the liquid and the gas leaving the column are reproducible for water test 1 and 2.
In the case of NaCl solution, gas leaving the column is colder than for water cases and, as shown in Tables 6.1 and 6.2; this could be caused by a problem with the electrical resistance on the column top.

Table 6.2 *Experimental results and calculated variables used in model, are reported at 15 minutes intervals, are shown for NaCl solution test.*

NaCl solution									
Interval	***t***	T^L	T^{out}	***u relative***	***RI***	x_{NaCl}	x_w	m_{NaCl}	γ_w
i	**min**	**°C**	**°C**	**%**	**-**		**-**		**-**
1	0	32.7	39.5	97.1	1.33561	0.0029	0.9971	0.1640	0.7423
2	15	39.6	60.0	25.2	1.33542	0.0024	0.9976	0.1352	0.7523
3	30	42.5	70.4	19.8	1.33550	0.0027	0.9973	0.1477	0.7440
4	45	44.7	76.1	21.5	1.33501	0.0014	0.9986	0.0755	0.7887
5	60	49.4	80.2	22.9	1.33508	0.0015	0.9985	0.0859	0.7781
6	75	56.4	84.1	23.8	1.33503	0.0014	0.9986	0.0777	0.7823
7	90	61.4	86.3	25.1	1.33523	0.0019	0.9981	0.1070	0.7565
8	105	62.9	88.4	26.2	1.33538	0.0023	0.9977	0.1297	0.7448
9	120	64.2	90.3	26.5	1.33584	0.0036	0.9964	0.1983	0.7152
10	135	63.7	90.9	27.6	1.33599	0.0039	0.9961	0.2200	0.7092
11	150	65.0	91.5	27.9	1.33631	0.0048	0.9952	0.2679	0.6957
12	165	66.2	92.2	29.4	1.33677	0.0060	0.9940	0.3366	0.6920
13	180	66.2	91.1	28.6	1.33737	0.0076	0.9924	0.4259	0.6692
14	195	66.8	91.7	29.0	1.33765	0.0084	0.9916	0.4680	0.6647
15	210	67.1	91.9	29.8	1.33844	0.0104	0.9896	0.5860	0.6551
16	225	67.5	92.1	29.9	1.33854	0.0107	0.9893	0.6019	0.6541
17	240	67.8	92.2	29.4	1.33913	0.0123	0.9877	0.6906	0.6496
18	255	68.1	92.4	29.6	1.33937	0.0129	0.9871	0.7263	0.6482
19	270	68.6	92.6	29.8	1.33982	0.0141	0.9859	0.7949	0.6462
20	285	69.2	92.7	29.6	1.34004	0.0147	0.9853	0.8288	0.6448
21	300	69.7	92.8	29.6	1.34032	0.0155	0.9845	0.8713	0.6449

Also in salt solution test, a leak affected the condensing system and for this, balance measurement weight data cannot be trusted.

Observing liquid temperature trend is clear that in salt solution case, value keeps a few degrees higher and this, considering the high salinity of the solution, could be due to the ebullioscopic increase.

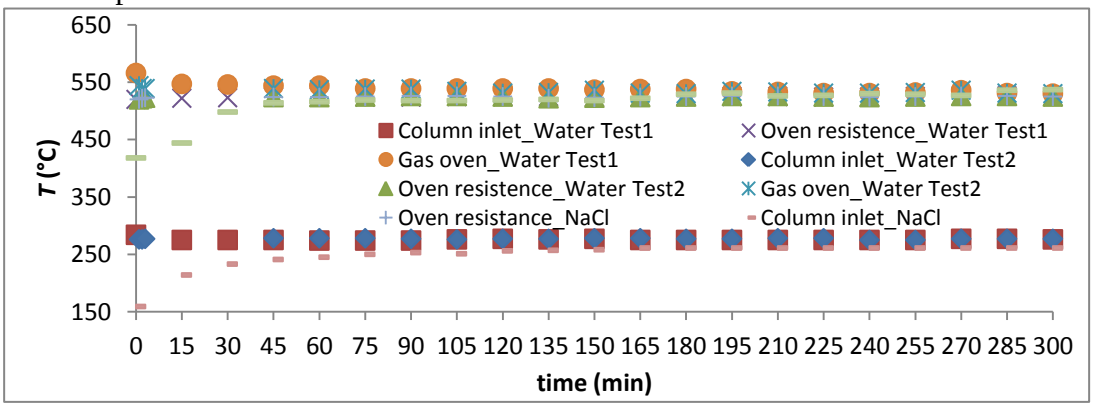

Figure 6.1 *Experimental values of operational temperatures for water and NaCl solution tests are reported at 15 minutes intervals.*

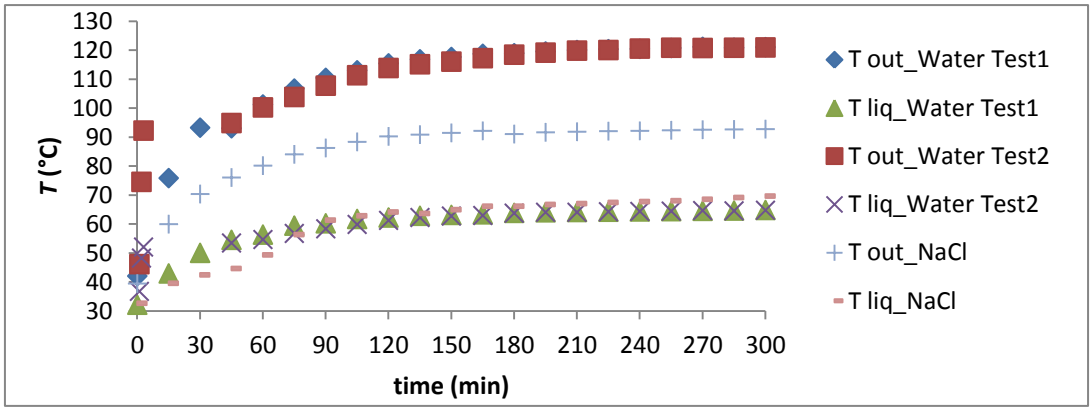

Figure 6.2 *Experimental data of temperatures measured in water and NaCl solution tests.*

Figure 6.3 shows that after an unexpected initial phase (from 1st to 6th intervals) probably due to a spilling system solution stagnation, water concentration in NaCl solution decreases showing a linear trend, proving that evaporated flow rate is constant.

Figure 6.4 reports water activity coefficient in NaCl solution that, being calculated using water molar fraction, cannot be trusted in intervals from 1st to 6th because of the reason explained above.

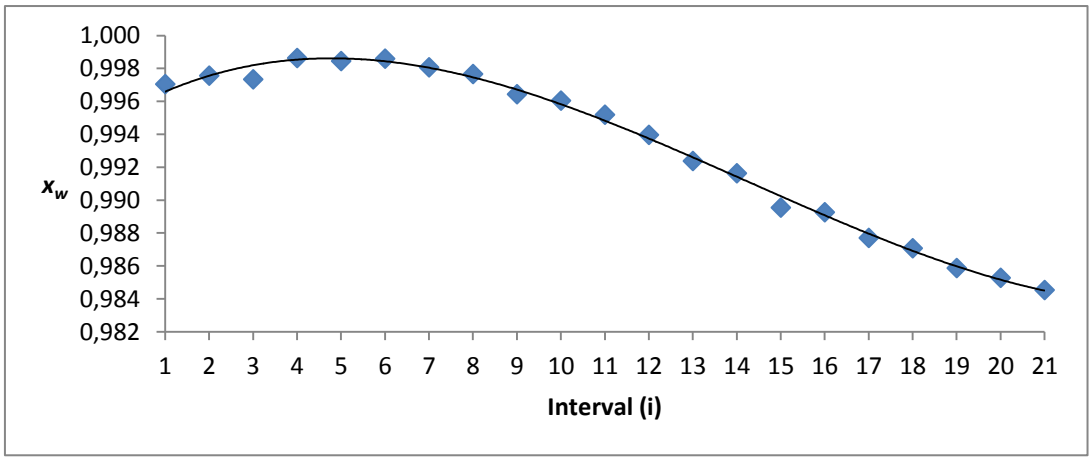

Figure 6.3 *Water molar fraction trend during NaCl solution DCE process.*

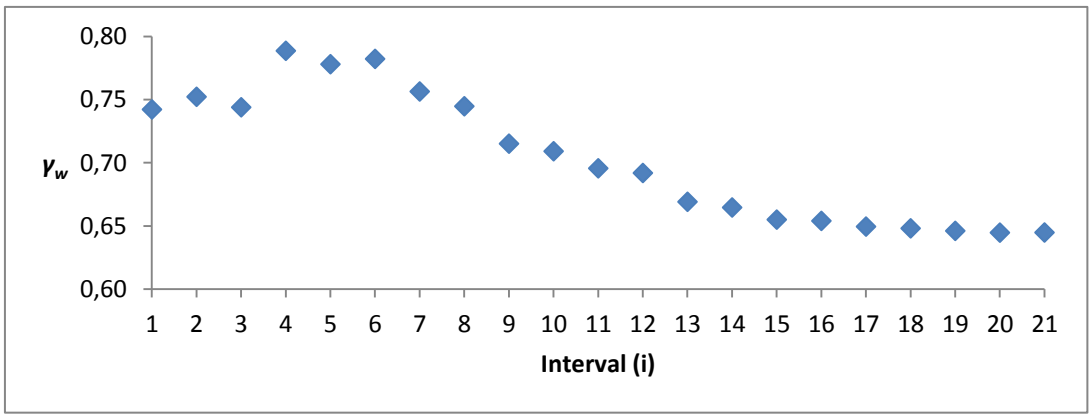

Figure 6.4 *Water activity coefficient trend during NaCl solution DCE process.*

6.2 MATHEMATIC MODELING OF DCE PROCESS

In this section, with the aim of predicting process efficiency in the cases of water and draw (NaCl solution) DCE processes, a simplified predictive model was built to simulate mass and energy balances. Then, models and experimental results were compared.

6.2.1 Process mass balance

Figure 6.5 represents air and water flow rates and variables used in mass and energy balances.

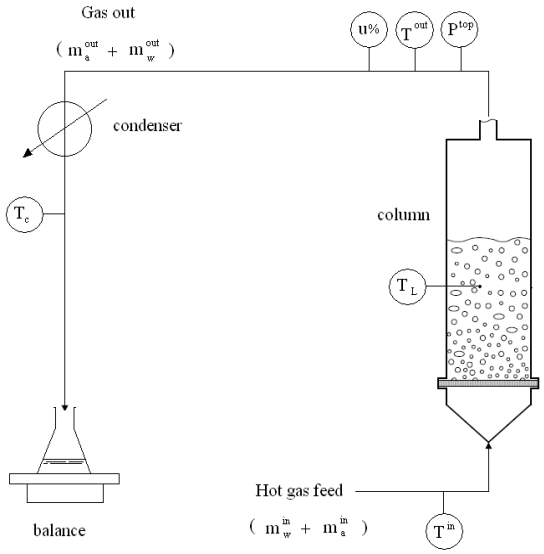

Figure 6.5 *Scheme representing air and water flow rates and variables used in mass and energy balances.*

In stationary state, air flow rate mass conservation principle is:

$$m_a^{in} = m_a^{out} \tag{6.1}$$

In water case, evaporation contribution is taken into account for mass flow rate balance:

$$m_w^{in} + m_w^{ev} = m_w^{out} \tag{6.2}$$

But rembering:

$$m_w^{out} = \frac{m_a^{out}}{(1-z_w^{out})} z_w^{out} = \frac{m_a^{in}}{(1-z_w^{out})} z_w^{out} \tag{6.3}$$

$$m_w^{in} = \frac{m_a^{in}}{(1-z_w^{in})} z_w^{in} \tag{6.4}$$

Then, rearranging (6.2) and substituting (6.3), (6.4):

$$m_w^{ev} = m_w^{out} - m_w^{in} \tag{6.5}$$

$$= m_a^{in} \left[\frac{z_w^{out}}{(1-z_w^{out})} - \frac{z_w^{in}}{(1-z_w^{in})}\right] \tag{6.6}$$

Now, integrating (6.5) in a time interval of 15 minutes it is possible to calculate evaporated water amount in each time interval ($M_w^{ev}(i)$).

$$M_w^{ev}(i) = M_w^{out}(i) - M_w^{in}(i) \tag{6.7}$$

$$= M_a^{in}(i) \left[\frac{z_w^{out}}{(1-z_w^{out})} - \frac{z_w^{in}}{(1-z_w^{in})}\right] \tag{6.8}$$

With the aim of expliciting z_w in function of y_w , it is used the relation:

$$z_w = \frac{y_w\ MW_w}{y_w\ MW_w + (1-y_w) MW_a} \tag{6.9}$$

Now, using (6.9) it is possible the substitution of (6.11) in (6.8):

$$y_w^{in} = \frac{p_w}{P^{top}} \tag{6.10}$$

$$= \frac{P_w^{sat}(T^{amb})}{P^{atm}} \times \frac{u\%}{100} \tag{6.11}$$

Where, Antoine equation is used for P_w^{sat} calculation (Annex E).

Now, the unique unknown variables are y_w^{out} (which is used in equations (6.8) and (6.9) combined) or $M_w^{out}(i)$ (which is used in equation 6.7); these values can be calculated respectively by thermo hygrometer experimental data and weight experimental data.

6.2.1.1 Evaporation rate calculation using thermo hygrometer experimental data

Using (6.9), (6.13) can be substituted in (6.8) and experimental water percentage values in gas leaving the top column ($u\%$) enable to calculate $M_w^{ev}(i)$ in a direct way.

$$y_w^{out} = \frac{p_w}{P^{top}} \tag{6.12}$$

$$= \frac{P_w^{sat}(T^{out})}{P^{top}} \times \frac{u\%}{100} \tag{6.13}$$

Where, Antoine equation is used for P_w^{sat} calculation (Annex E)

6.2.1.2 Evaporation rate calculation using weight experimental data

Assuming thermodynamic equilibrium between gas and liquid leaving the condenser, equations (6.14), (6.15) can be written:

$$y_w^{inc} = \frac{p_w^{inc}}{P^{atm}} \tag{6.14}$$

$$= \frac{P_w^{sat}(T^{cold})}{P^{atm}} \times \frac{u\%}{100} \tag{6.15}$$

Where, T^{cold} indicates the gas temperature of gas leaving the condenser and it was proof experimentally that is practically equal to cryostatic bath temperature (5°C).

Using weight (balance measurement) experimental values of condensed water vapor (M_w^c) it is true the relation:

$$M_w^{out}(i) = M_w^c(i) + M_w^{inc}(i) \tag{6.16}$$

$$= M_w^c(i) + M_a^{in}(i)\ \frac{z_w^{inc}}{1-z_w^{inc}} \tag{6.17}$$

Now, substituting in (6.17) the equations (6.9), (6.15), $M_w^{out}\ (i)$ can be calculated.

Where, Antoine equation is used for P_w^{sat} calculation (Annex E) and $u\% = 1$, for hypothesis of condensing system saturation.

Now, by substituting $M_w^{out}(i)$ value in (6.7) is possible to calculate $M_w^{ev}(i)$.

This value is calculated in a quasi direct way, because of the hypothesis (6.14), (6.15).

6.2.1.3 Evaporation rate prediction using mass balance model

A simple model was built by assuming three hypotheses:

- Perfect mixing of liquid in the column;
- Thermodynamic equilibrium between liquid in the column and gas leaving it after bubbling;
- Temperature of gas leaving the liquid keeps constantly higher than liquid temperature.

First hypothesis allows to state that liquid temperature is homogeneous.

Second one allows to predict water molar fraction in gas flow rate leaving the liquid (y_w^{out}) only by knowing liquid temperature.

Third hypothesis ensures that no water vapor condensation takes place in the way of gas from liquid surface to column outlet. This means that water molar fraction in the gas leaving the column is the same of the gas leaving the liquid surface.

For this purpose, modified Raoult equation was applied to water:

$$p_w \emptyset_w = \gamma_w x_w f_w^0 \tag{6.18}$$

But knowing,

$$p_w = y_w^{out} P^{top} \tag{6.19}$$

it becomes:

$$y_w^{out} = \frac{\gamma_w \, x_w f_w^0}{\emptyset_w P^{top}} \tag{6.20}$$

To obtain the averaged variable value during each interval (i), mean value between measurements at the start and at the end of each interval was calculated. This calculation was done for both T_L and x_w.

Then, using T_L and x_{NaCl} for each interval, $\gamma_w\left(T_L, x_w\right)$ was calculated as explained in Annex G. In the case of distilled water γ_w is assumed unitary.

The same operation was used to calculate $f_w^0(T_L)$ value for each interval. As operational pressure is close to atmospheric pressure, a unitary value for $\emptyset_w$ was assumed.

Then, combining (6.8) with (6.9), (6.11) and (6.20) evaporated water amount in each time interval ($M_{VLE}^{ev}(i)$) was predicted.

6.2.2 Evaporation rate results comparison

In this section, evaporation rates calculated from weight experimental data (Section 6.2.1.2) and predictive model (Section 6.2.1.3) are compared with evaporation rate, calculated using thermo hygrometer experimental data (Section 6.2.1.1).

6.2.2.1 Thermo hygrometer and weight experimental data comparison:

Then for each interval (i), the relative error between the value measured by weighting ($M_{wei}^{ev}(i)$) and the value calculated using thermo hygrometer experimental data ($M_{VLE}^{ev}(i)$) is calculated:

$$e_{wei}^{ev}(i) = \frac{M_{the}^{ev}(i) - M_{wei}^{ev}(i)}{M_{the}^{ev}(i)} 100 \qquad (6.21)$$

Results are reported in Table 6.4.

6.2.2.2 Thermo hygrometer experimental data and model comparison:

In Figures 6.6 and 6.7, evaporated water mass values calculated from weight and thermo hygrometer data and from predictive model were compared, respectively for water test 1 and 2. For both tests, a good similarity is shown between thermo hygrometer and predictive model values. Weight data keeps initially below the others

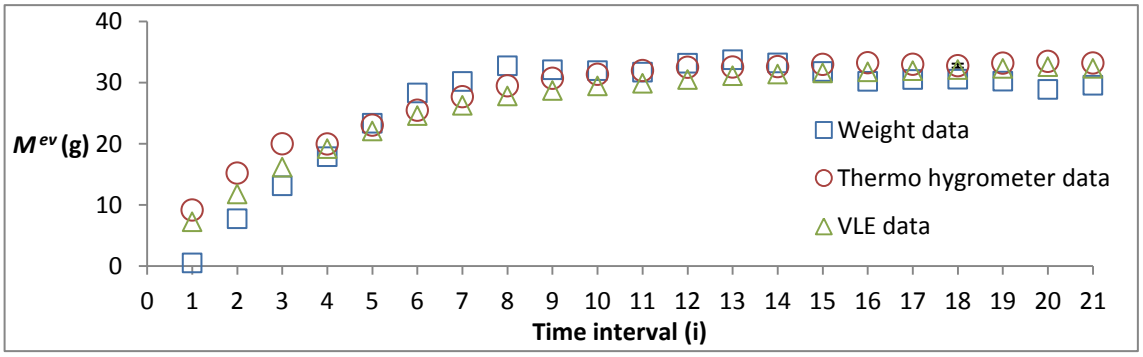

Figure 6.6 *Experimental of evaporated water mass calculated using weight and thermo hygrometer data values and predictive model, for Test n°1.*

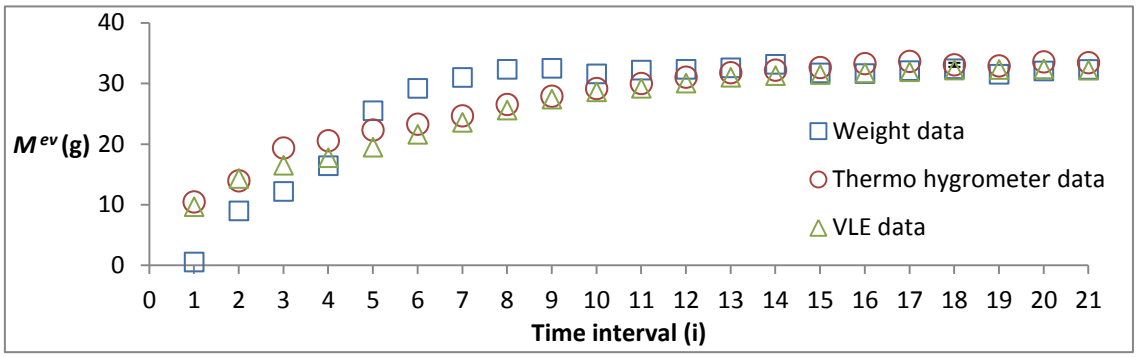

Figure 6.7 *Experimental of evaporated water mass calculated using weight and thermo hygrometer data values and predictive model, for Test n°2.*

two curves; this can be explained because, as said before, condenser is accumulating condensed water until stationary state is reached.

Figure 6.8 underlines evaporated water mass value reproducibility between weight data, in water test 1 and 2. Figure 6.9 shows NaCl solution case where, pseudo stationary state experimental values of evaporated water mass calculated using thermo hygrometer data, keeps very low in respect to predictive model values.

As said before, this effect is probably due to the problem on the column top resistance, that did not ensured at least 100 °C. In fact, thermo hygrometer data interpretation is more complicated because there is water vapor condensation in the column freeboard. In this case, gas reaching the thermo hygrometer has not the water vapor fraction in solution equilibrium condition, but is instead in a intermediate condition between this and pure condensed water equilibrium condition. It is to avoid this that the column needs to operate with heating turned on.

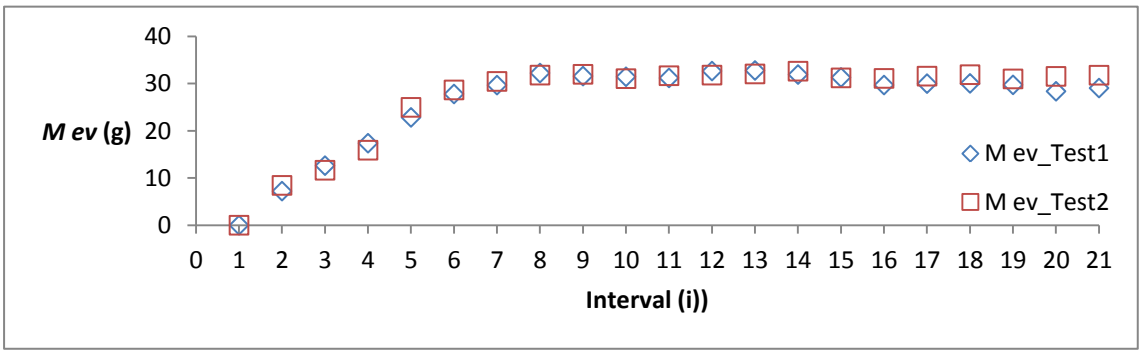

Figure 6.8 *Experimental values of evaporated water mass calculated using weight data values, for water Test n°1 and Test n°2.*

Probably, there is VLE between gas and liquid coming out of it, but constant water molar fraction hypothesis between the liquid surface and the column top is no longer valid. For this reason, only thermo hygrometer data can be used.

In Figures 6.6-6.9, error bar relative to thermo hygrometer case was calculated for interval n°18 considering relative humidity accuracy (±1%) as the one and only influencing factor, while error bar for weight data was calculated using a balance

accuracy of ±0.1 g and resulted insignificant. Model error bar was related to liquid temperature measurement accuracy (±0.2 K) and even in this case resulted insignificant.

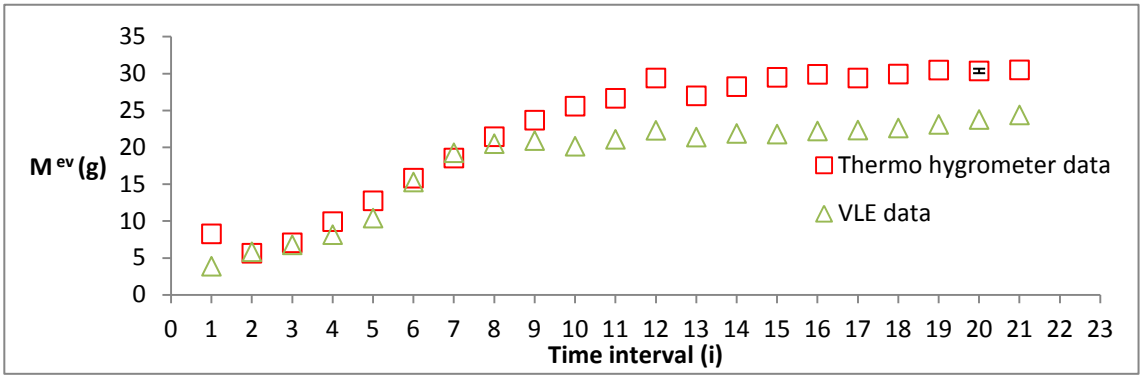

Figure 6.9 *Experimental values evaporated of water mass calculated using thermo hygrometer data and predictive model values, for NaCl solution.*

With the aim of comparing experimental data and model values, relative error between $M^{ev}(i)$ value from model prediction ($M^{ev}_{VLE}(i)$) and value calculated using thermo hygrometer experimental data ($M^{ev}_{VLE}(i)$) was calculated for each interval:

$$e^{ev}_{VLE}(i) = \frac{M^{ev}_{the}(i) - M^{ev}_{VLE}(i)}{M^{ev}_{the}(i)} \; 100 \qquad (6.22)$$

Results are reported in Table 6.3, where in NaCl solution case, e^{ev}_{wei} is not reported because of condensing system problem. Value of e^{ev}_{wei} in water tests is very low, but for NaCl solution test its value is very high and the column top electrical resistance problem could be decisive.

In fact, in NaCl solution case, gas leaving the column is colder than for water cases and as shown in Table 6.2, it stayed below of water boiling temperature; in this conditions, some of evaporated water condensed before leaving the column because of heat dispersions, making hypothesis number 3 not more valid.

In Table 6.4, thermo hygrometer data of evaporated water mass value, for water and NaCl solution are reported.

Table 6.3 *Pseudo stationary state mean relative error between evaporation rates calculated using thermo hygrometer experimental data in respect to evaporation rates calculated using weight experimental data and predictive model.*

	Water		NaCl solution
	Test 1	**Test 2**	**Test 1**
e^{ev}_{wei}	7.3	3.5	-
e^{ev}_{VLE}	3.3	3.3	24.4

Table 6.4 *Evaporated water mass value calculated using thermo hygrometer data for water and NaCl solution.*

Interval	Water		NaCl solution
	Test 1	Test 2	Test 1
i	g	g	g
1	9.2	10.4	8.3
2	15.2	13.9	5.6
3	20.0	19.3	7.0
4	20.0	20.5	9.9
5	23.0	22.3	12.7
6	25.5	23.3	15.8
7	27.7	24.6	18.5
8	29.5	26.5	21.4
9	30.7	27.9	23.7
10	31.4	29.1	25.6
11	32.0	30.0	26.6
12	32.5	31.0	29.4
13	32.5	31.8	27.0
14	32.6	32.2	28.2
15	33.0	32.6	29.5
16	33.3	33.3	29.9
17	33.0	33.6	29.4
18	32.8	33.1	29.9
19	33.2	32.9	30.5
20	33.5	33.5	30.3
21	33.2	33.4	30.5
Pseudo stationary state mean value	33.0	32.9	30.4

Water stationary state values are reproducible and are a bit greater (~9%) than pseudo stationary state salt solution values. This is probably due to salt solution lower water activity and consequently reduced water vapour pressure at a similar temperature.

6.2.3 Process energy balance

Latent heat is provided both by gas entering the column as by sparger conduction, so energy conservation principle at stationary state is true:

$$q^{ev} = q_G + q_{conduct} \tag{6.23}$$

Then, using equation (6.9) and λ_m calculated at T^L, q^{ev} can be calculated:

$$q^{ev} = m_a^{in}\lambda_m \left[\frac{z_w^{out}}{(1-z_w^{out})} - \frac{z_w^{in}}{(1-z_w^{in})}\right] \tag{6.24}$$

Then, q_G can be calculated, using equation (6.9):

$$q_G = q_a + q_w \tag{6.25}$$

$$= m_a^{in}\left[C_{p,a}^m\left(T^{in} - T^L\right) + C_{p,w}^m\left(T^{in} - T^L\right)\frac{z_w^{in}}{(1-z_w^{in})}\right] \tag{6.26}$$

6.2.3.1 Evaporation heat calculation using thermo hygrometer experimental data

In a generic 15 minutes interval (i), heat amount leaving the whole system $Q_{wei}^{ev}(i)$ is calculated using integrated equation (6.24), (6.9) and y_w^{out} from thermo hygromether data (equation 6.13).

6.2.3.2 Evaporation heat flux calculation using weight experimental data

In a generic 15 minutes interval (i), heat amount leaving the whole system is:

$$Q_{wei}^{ev}(i) = \lambda_m M_w^{ev}(i) \tag{6.27}$$

Where $M_w^{ev}(i)$ is calculated as explicated in section 6.2.1.2.

6.2.3.3 Evaporation heat prediction using mass balance model

In a generic 15 minutes interval (i), heat amount leaving the whole system $Q_{wei}^{ev}(i)$ is calculated using integrated equation (6.24), (6.9) and y_w^{out} from predictive model (6.20).

6.2.4 Evaporation heat results comparison

In this section, percentage of evaporation heat provided by biphasic exchange was calculated basing on thermo hygrometer experimental data (Section 6.2.3.1), weight experimental data (Section 6.2.3.2) and predictive model (Section 6.2.3.3).
For q_G calculation, y_w^{out} from thermo hygromether data (equation 6.13) was used, because as said before, this value is the unique obtained in a direct way.
Results are reported in Table 6.5.

6.2.4.1 Biphasic exchanged heat from thermo hygrometer experimental data:

For each interval(i), ratio between $Q_G\,(i)$ from equation (6.26) integration and Q_{the}^{ev} from equation (6.24) integration, is calculated using y_w^{out} from (28):

$$\eta_{biphasic_{the}}(i) = \frac{Q_G\,(i)}{Q_{the}^{ev}} 100 \tag{6.28}$$

6.2.4.2 Biphasic exchanged heat from predictive model:

For each interval(i), ratio between $Q_G\,(i)$ from equation (6.26) integration and Q_{VLE}^{ev} from equation (6.24) integration, is calculated using y_w^{out} from (6.20):

$$\eta_{biphasic_{VLE}}(i) = \frac{Q_G\,(i)}{Q_{VLE}^{ev}} 100 \tag{6.29}$$

6.2.4.3 Biphasic exchanged heat from weight experimental data:

For each interval(i), ratio between $Q_G\ (i)$ from integrated equation (6.26) and $Q_{wei}^{ev}(i)$ from equation (6.31) is calculated using $M_w^{out}(i)$ from (6.17):

$$\eta_{biphasic_{wei}}(i) = \frac{Q_G\ (i)}{Q_{wei}^{ev}(i)}\,100 \tag{6.30}$$

$$Q_{wei}^{ev}(i) = \lambda_m M_w^{ev}(i) \tag{6.31}$$

Table 6.5 *Pseudo stationary state mean percentages of latent heat provided by biphasic exchange in respect to total latent heat provided. Values obtained using predictive model calculation and thermo hygrometer and weight experimental data.*

	Water		NaCl solution
	Test 1	**Test 2**	**Test 1**
$\eta_{biphasic_{the}}(i)$	66.2	66.9	64.4
$\eta_{biphasic_{wei}}(i)$	58.6	56.7	-
$\eta_{biphasic_{VLE}}(i)$	68.2	68.8	-

In water the case, $\eta_{biphasic}$ values obtained in all three cases are reproducible and there is a values correspondence between weight and thermo hygrometer data.

In salt solution case, heat provided by biphasic exchange is a little less than in water case and this can be explained considering the higher salt solution heat conductivity in respect of pure water. In fact, a liquid with higher heat conductivity can exchange a larger heat amount with the sparger.

Chapter 7

Conclusions

The aim of this thesis is to complement works developed by Ribeiro Jr. (2005) and Ongaratto (2012) analyzing the viability of a new process, made-up by a combined OE+MD process and DCE for draw regeneration, allowing production of superior quality concentrated fruit juice.

In fact, in combined OE+MD process, process driving force is the sum of the effects of osmotic pressure gradient and temperature gradient between the two streams (feed and draw) and being a membrane separation process, allow solutions concentration without needing high temperature; For this reason, this combined process improves traditional process of vacuum evaporation of thermo labile solutions concentration, preserving flavours, vitamins and colour, without leading to a "cooked" featured final product.

Regeneration of diluted draw solution coming from membrane process, needs the use of a process suitable for fouling and corrosive solutions such as solutions with high salt concentrations; DCE process, due to the absence of walls separating fluids and the chance to use low cost exhaust combustion gas, it seems to be the ideal answer to this demand. In DCE, instead of potassium pyrophosphate, sodium chloride was used for draw preparation, in order to its easier availability of water activity coefficient used in models.

7.1 RESULTS OF MEMBRANE PROCESSES

Before being processed by membrane separation, juice needs to be clarified and filtered; As the goal of this work does not include flavours analysis, sucrose solution was used instead of fruit juice, with the aim of simplifying operations.

For first, pH and CO2 solubility against temperature essays were carried out at many concentrations for water, pyrophosphate solution and sucrose solution; this informations are then used for MD and OE results comparison and to estimate CO2 concentration values used in mass transfer model models.

Experimental data show clearly that sucrose solutions can dissolve a smaller amount of CO2 than water, and this effect is more relevant as sucrose concentration grows: this is a positive factor because it opposes to CO2 enrichment of juice.

In pyrophosphate solutions, CO2 concentration keeps very low and, even in this case, effect is more relevant as salt concentration grows. As for sucrose solution, this is a favourable aspect because it means that pyrophosphate solution coming from draw regeneration is low in CO2 concentration; As a consequence, a low CO2 concentration gradient between draw and sucrose solution that takes place in membrane separation process, limiting CO2 flux from pyrophosphate to sucrose solution.

As temperature increases, CO2 concentration reduces, so pH of draw solution decreases slightly but keeps constantly in basic range, for the reason explained before: this ensures that no reaction take place between pyrophosphate and CO2.

As a second step, membrane separations were performed using hollow fibers of polypropylene both for MD and OE+MD.

MD process was carried out using hot and cold water and tests suggested that after 90 min of duration, the system arrived at a stationary state reaching a constant value of CO2 concentration in hot water and a constant water flux. This means that CO2 flux at stationary state is almost null.

Water flux was calculated using experimental data of the whole process, shown a value of 0.592 Kg/h K m^2, that is totally standing in the range of values observed in literature.

A comparison between average experimental value of CO2 stationary state concentration in hot water and CO2 saturation concentration in cold water shows that at stationary state, sucrose solution contained almost 30% of CO2 draw concentration (Table 5.4).

Observing high percentage of CO2 passed between the liquids, it is clear that PP membrane layer offers only a lightly resistance to CO2 flux and for this reason MD process adopted alone is not competitive for the purpose of the thesis.

Then, combined OE+MD process was carried out using hot sucrose solution and cold pyrophosphate draw solution.

Tests suggested that, after 15 minutes, systems achieved stationary state, in fact first measurement of CO2 concentration in sucrose solution remained constant for the all the process duration at a very low average value of ~5 mg/L: that means that practically no CO2 passed through the membrane.

Experimental data obtained of the whole process allowed calculation of water flux, that shown a greater value than the average values observed in literature (1.718 Kg/h K m^2).

Regarding combined MD+OE, CO2 saturation concentration in cold pyrophosphate draw is very much lower than in cold water used in MD process: this is probably caused by salting out effect, due to high pyrophosphate concentration.

Comparing percentage of CO2 passed between the liquids in MD (Table5.4) and combined MD+OE (Table 5.8) cases, and remembering that membrane and operational conditions were the same, it is clear that in the second case CO2 flux is obstacled by the

presence of salt. This phenomenon could be attributed to the boundary layer that originates in the region of draw solution, very next to the membrane (Figure 3.2). In fact, higher salt concentration implies a greater salting out effect in respect to CO2, so CO2 concentration is lower in the boundary layer than in the bulk. Then, being actual CO2 concentration gradient lower than the apparent, a reduced CO2 flux takes place.
With the aim of evaluating the respective contribution of temperature (MD process) and osmotic pressure gradient (OE) to water flux, two simples models were used.
As regard MD, mass transfer constant was calculated knowing experimental values of water flux and temperature gradient between hot and cold water.
Comparing averaged water fluxes of MD and combined OE+MD, results that temperature gradient contribute only for an almost 31% at the total water flux, so the remaining 69% is due to osmotic pressure gradient.
Resuming, CO2 does not represent a serious contamination problem if potassium pyrophosphate is used in combined OE+MD. In the case of water, values obtained in all the three cases are reproducible.

7.2 RESULTS OF DCE

DCE tests were performed using water and a concentrated NaCl solution (draw).
The same hot CO2 rich air flow rate was used and a heterogeneous bubbling regime established in both cases.
In both water tests, stationary state goes from interval nº13 to interval nº21.
In draw test, stationary state goes only from interval 19 to 21. This difference could be due to ebullioscopic increase, as well as different gas inlet temperature.
Observing the liquid temperature trend is clear that in the draw case, the value keeps a few degrees higher and this, considering the high salinity of the solution, could be due to the ebullioscopic increase.
Using respectively weight (balance measurement) and thermo hygrometer experimental values of condensed water vapour, evaporated water mass in both cases was calculated.
Then, a simple model based on modified Raoult law allowed to predict evaporated water mass; for both water tests, a good similarity is shown between evaporated water mass values calculated using thermo hygrometer and predictive model. Weight data keeps initially below the others two curves, this can be explained because, during this phase, the condenser is accumulating condensed water until stationary state is reached.
As experimental values of evaporated water mass calculated using thermo hygrometer data are the most reliable data because are coming from a direct calculation, they were chosen as a true value for error calculation of stationary state evaporated water mass using respectively predictive model (~3%) and weight measurement case (~5%).

In the case of NaCl solution, pseudo stationary state experimental values of evaporated water mass, calculated using thermo hygrometer data, keeps very low in respect to predictive model values (~24% of error). This effect is probably due to the problem on the top of the column resistance, that did not ensured at least 100 °C. In fact, the interpretation of the measured thermo hygrometer data is more complicated because there is condensation of water vapor in the column freeboard. For this reason, in NaCl solution test, only data from thermo hygrometer can be used.

Percentage of evaporation heat provided by biphasic exchange was calculated basing on thermo hygrometer experimental data (~67% for water tests, ~64% for NaCl solution test), weight experimental data (~58% for water tests) and predictive model (~69% for water tests). The last value for NaCl solution case was not calculated because of the unreliability of available data.

In the case of water, values obtained in all the three cases are reproducible. In salt solution case, the heat provided for biphasic exchange is almost the same of water case.

7.3 FUTURE WORKS AND RECOMMENDATIONS

In combined OE+MD process, experimental values of sugar content in sucrose solution versus duration of process shown a linear trend; this could mean that the solutions concentration variation during the process did not influence the water flux through the membrane that was kept at a constant value. This induces to think that mass transport through the membrane was the main contribution to overall mass transfer resistance and so represents the limiting factor. For this reason, process performance can be enhanced by membrane thickness reduction or increase in the surface porosity keeping a great selectiveness. This improvement would lead to higher specific fluxes, which means lower plant costs.

For sure, Reynolds number play an important role on process performance and so, adopting a less viscous draw solution, improving the geometrical configuration of membrane and increasing the velocity of flowing solutions, a reduced boundary layer mass transfer resistance: this means higher specific fluxes.

A further step is to continue the process for a larger duration, so a more industrially interesting degree of concentration would be achieved.

As regard DCE, the predictive model developed is a useful tool because it allows calculating the evaporated water amount, in function of kind and concentration of salt chosen. So, further tests using NaCl solution could allow a better evaluation of predictive model reliability.

As a complementary step to membrane concentration process analysed, using a potassium pyrophosphate based draw in DCE process would be interesting, allowing evaluation of high viscosity effect in mass and heat transfer.

A stride could be achieved adopting a different draw solution which allows cost optimization of combined concentration and regeneration processes; a starting point could be to analyze different saline solutions, comparing specific costs per liter of permeate, like Achilli et al. (2010) did for a large range of salts.

The possibility that some hazardous combustion by product could be contained in exhaust gas and may cause a juice contamination, is another issue which needs to be analyzed.

Capitolo 8

Appendices

ANNEX A:

Sucrose osmotic coefficient data regression

A regression using Excel^{TM} was carried out using isothermal data at 20°C from Burlyn et al (Table 8.1, Figure 8.1) to allow the determination of the relation sucrose osmotic coefficient Vs molality. Then, just substituting the desired value of molality it was possible the calculation of the values of osmotic coefficient required by the models.

Table 8.1 *Sucrose osmotic coefficient isothermal data at 20°C in function of molality (Burlyn et al).*

m	**Φ**
mol/kg water	-
0.2	1.009
0.4	1.036
0.5	1.059

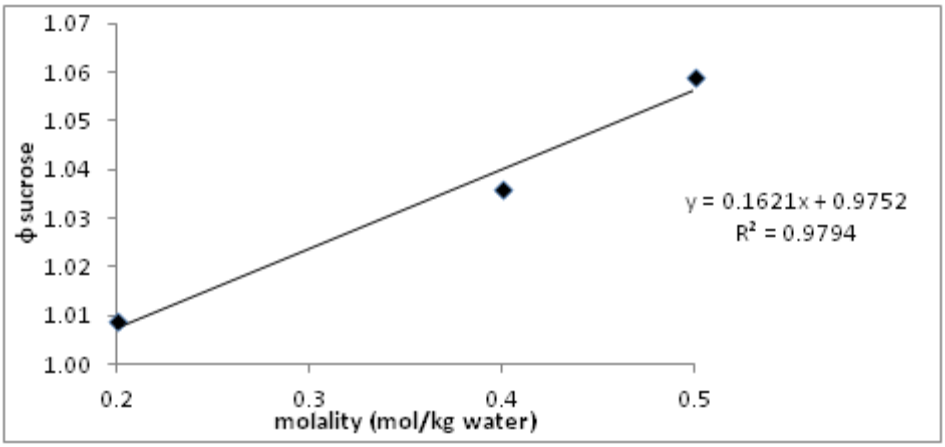

Figure 8.1 *Sucrose osmotic coefficient experimental data (20°C) and data regression.*

ANNEX B:

Potassium pyrophosphate osmotic pressure data regression

A regression using Excel™ was carried out using isothermal data at 25°C from Michaels et al to allow the determination of the relation sucrose osmotic pressure Vs molality (Figure 8.2). Then, just substituting the desired value of molality it was possible the calculation of the values of osmotic pressure required by the models.

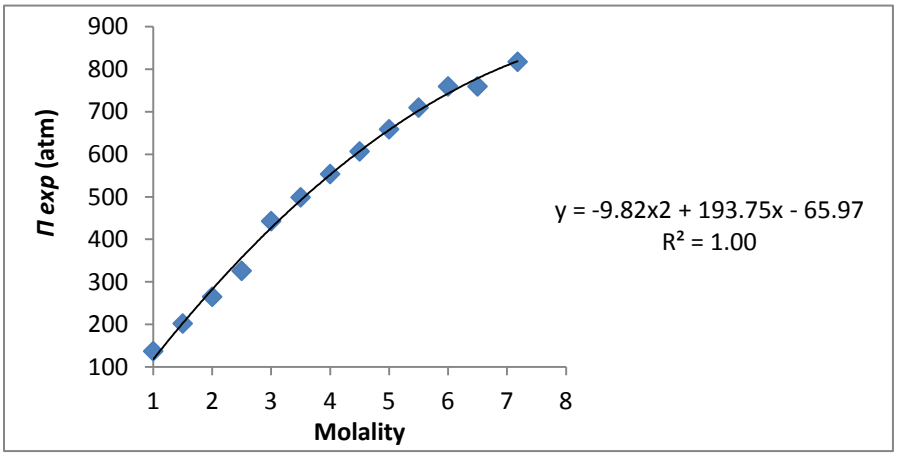

Figure 8.2 *Pyrophosphate osmotic pressure isothermal experimental data (25°C) data and data regression.*

Table 8.2 *Potassium pyrophosphate osmotic pressure isothermal experimental data (25°C) in function of molality (Michaels et al).*

m	Π^{exp}
mol/kg water	atm
1.00	137.00
1.50	202.07
2.00	265.01
2.50	326.02
3.00	442.87
3.50	498.93
4.00	553.58
4.50	606.90
5.00	658.97
5.50	709.88
6.00	759.71
6.50	759.71
7.18	817.64

ANNEX C:

RI data regression

Using data collected at 30 minutes interval, a regression (Excel™) was carried out to allow the determination of missing *RI* values at every 15 minutes (Figure 8.3).

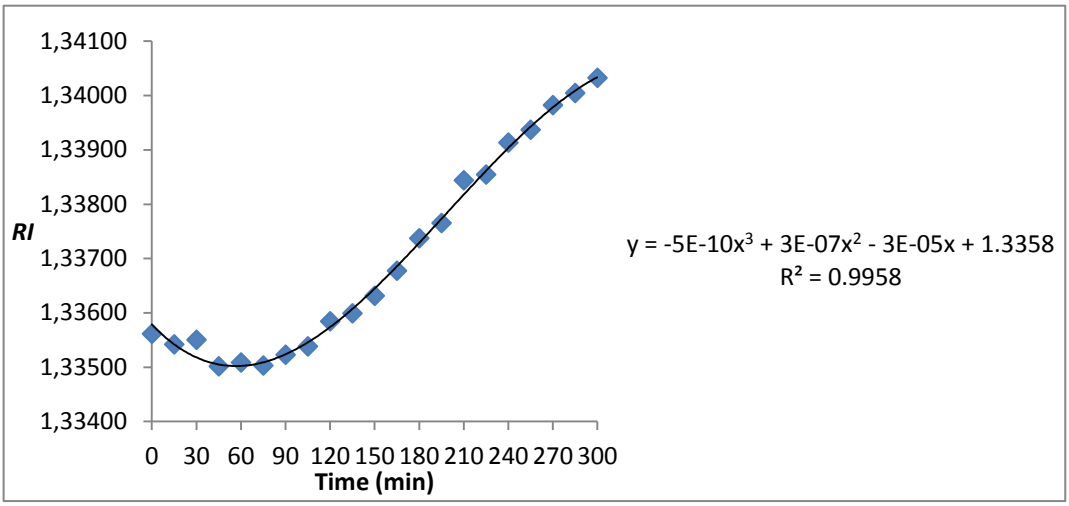

Figure 8.3 *Plot showing alternatively RI experimental and calculated values.*

ANNEX D:

Rotameter calibration

Experimental data of gas volumetric flow rate (G) at 25°C were measured at many values of rotameter index (I_{rot}). Then, a regression using Excel™ was used to allow the determination of the relation G and I_{rot} (Figure 8.4).

Table 8.3 *Gas volumetric flow rate (G) experimental data at 25°C, measured at many rotameter index (I_{rot}) values.*

I_{rot}	G (L/s)
10	3.3
20	10.0
30	17.2
40	26.0

So, just substituting the desired value of I_{rot} it was possible the calculation of the value of G (L/s) equivalent.

So, for G (L/s) calculation from I_{rot} value is used the relation:

$$x_{NaCl} = a \cdot I_{rot}^2 + b \cdot I_{rot} + c$$

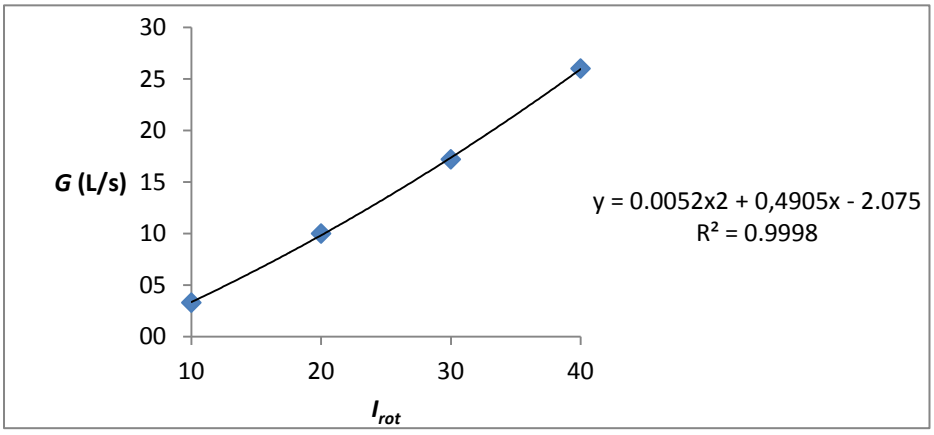

Figure 8.4 *Data regression of the relation G in function of I_{rot}.*

ANNEX E:

Antoine equation for water vapour pressure calculation

$$P_w^{sat}(T) = 10^{\left(A-\frac{B}{T+C}\right)}$$

Parameters from literature (Yaws, 1989):

For temperature range (1-100°C) were used parameters:

Table 8.4 *Antoine equation parameters, temperature range (1-100°C) (Yaws, 1989).*

A	8.07131
B	1730.63
C	233.426

For temperature range (99-374°C) were used parameters:

Table 8.5 *Antoine equation parameters, temperature range (99-374°C) (Yaws, 1989).*

A	8.14019
B	1810.94
C	244.485

ANNEX F:

Relation between refraction index and NaCl molar fraction in NaCl solution

Experimental data of *RI* at 25°C were measured at many values of x_{NaCl} (Ongaratto, 2012).

Then, a regression using Excel™ was used to allow the determination of the relation x_{NaCl} Vs *RI* (Figure 8.5).

Then, just substituting the desired value of *RI* it was possible the calculation of the value of x_{NaCl} required by the models.

So, for x_{NaCl} calculation from *RI* value is used the relation:

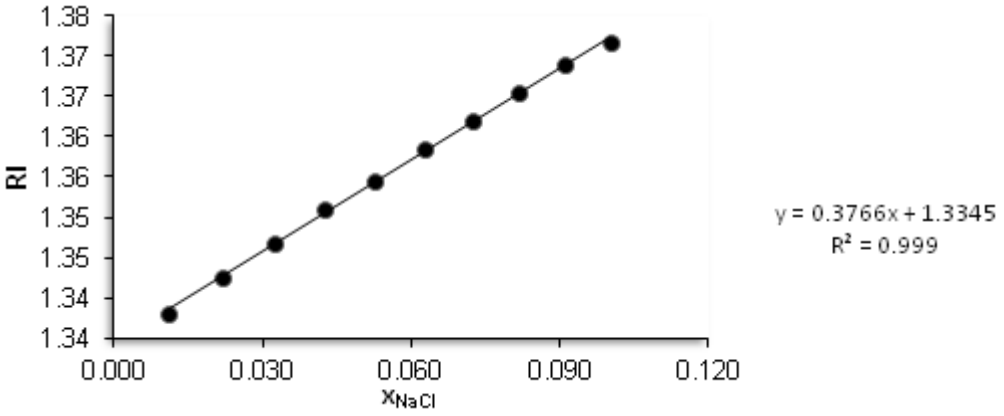

$$x_{NaCl} = a \cdot RI + b$$

Figure 8.5 *RI experimental data at 25°C, at many values of* x_{NaCl} *(Ongaratto, 2012).*

ANNEX G:

Water activity coefficient calculation

Experimental data of water activity coefficient at a wide temperature and concentration range (Pitzer, Neff, Lobo, Robinson) was used in Matlab™ by Prof. Costa to produce a 5 parameters predictive function taking in account short and long range interactions, as well as temperature effect. Then, just substituting the desired value of m_w (water molality) it was possible the calculation of the value of γ_w required by the models. Figure 8.6 shows an example of interpolation obtained with the predictive model.

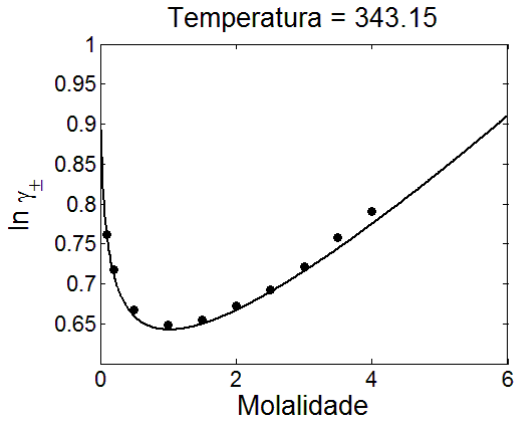

Figure 8.6 *Example of interpolation obtained with the predictive model developed.*

ANNEX H:

Calculation of CO_2 saturation concentration

Regression of CO2 solubility experimental data were used to calculate CO2 saturation concentration in water and pyrophosphate solution (Figure 8.7).

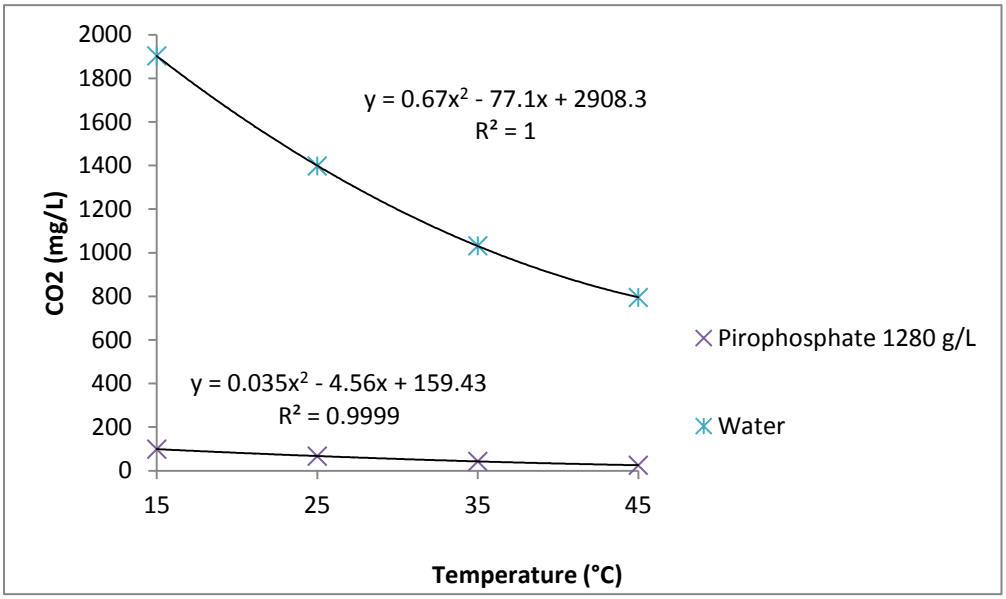

Figure 8.7 *CO2 solubility experimental data in water and pyrophosphate solution.*

Acknowledgment

The author would like to thank his supervisor Ricardo Ongaratto for the helpful guidance on the work.

True gratitude goes to such brilliant professionals Paulo Lage and Cristiano Borges for giving me the precious chance of developing my master thesis work in the Alberto Luiz Coimbra Institute for Graduate Studies and Research in Engineering of the Federal University of Rio de Janeiro and for the precious suggestions.

The author would like to express gratitude to his thesis referent in Italy Fabrizio Bezzo at Padua University, for the support in this academic experience abroad.

True gratitude goes to Prof. Cauê Costa for his unique and helpful contribution for this thesis.

A special thanks goes to old friends Matteo, Gabriele, Patricia, Alessandro, Damiano, Lorenzo, Giacomo, Silvia, Ilaria; to all the new friends of Escola de Quimica and the COPPE lab for being precious mates to share life experiences and laughters and to Antônio Gonçalves Neto (LTFD) for his fundamental technical support to this thesis along all the work.

Deeper gratitude goes to Barbara for the unforgettable moments, to Fatima for caring of me like I was one of her sons and to my parents and my brother for their love, help and for always pushing me to follow my dreams.

True regard goes to COPPE Chemical Engineering program for the financial support provided.

References

1. Richard W. Baker (2004) *Membrane Technology and Applications*, Second Edition. John Wiley & Sons, Ltd.

2. Claudio Patricio Ribeiro Junior (2005) Desenvolvimento de um processo combinado de evaporação por contato direto and permeação de vapour para tratamento de sucos de fruta, Ph.D. Thesis, COPPE/UFRJ, Rio de Janeiro, RJ, BR.

3. Ricardo Schmitz Ongaratto (2012) Processo para concentrar sucos de frutas combinando evaporação osmótica and por contato direto. Ph.D. Thesis, COPPE/UFRJ, Rio de Janeiro, RJ, BR.

4. Cláudio P. Ribeiro Jr., Cristiano P. Borges, Paulo L.C. Lage. Modeling of direct-contact evaporation using simultaneous heat and multicomponent mass-transfer model for superheated bubbles. *Chemical Engineering Science* 60 (2005) 1761 – 1772.

5. Lage P.L.C., Campos F.B. (2004) Advances in direct-contact evaporator design. *Chemical engineering and technology,* v. **27**, n. 1, pp. 91-96.

6. Ribeiro C.P. Jr., Borges C.P., Lage P.L.C. (2005) A new route combining direct-contact evaporation and vapour permeation for obtaining high- quality fruit juice concentrates. Part i: experimental analysis. *Industrial and engineering chemistry research,* v. **44**, n. 17, pp. 6888-6902.

7. Ribeiro C.P. Jr., Borges C.P., Lage P.L.C. (2007) Sparger effects during the concentration of synthetic fruit juices by direct-contact evaporation. *Journal of food engineering,* v. **79**, n. 3, pp. 979-988.

8. Ribeiro C.P. Jr., Lage P.L.C. (2004) Direct-contact evaporation in the homogeneous and heterogeneous bubbling regimes. Part i: experimental analysis. *International journal of heat and mass transfer,* v. **47**, n. 17-18, pp. 3825-3840.

9. Kiepe J., Horstmann S., Fischer K., Gmehling J.. Experimental determination and prediction of gas solubility data for CO_2 + H_2O mixtures containing NaCl or KCl at temperatures between 313 and 393 K and pressures up to 10 MPa. *Ind. Eng. Chem. Res*. 2002**, 41**, 4393-4398.

10. Standard Test Methods for Total and Dissolved Carbon Dioxide in Water (2012) ASTM International.

11. Hancock R. D., Stewart D. (2010) Enhancing the nutritional quality of fruit juices: Advanced technologies for juice extraction and pasteurization. *Biotechnology in functional foods and nutraceuticals*. Edited by Debasis Bagchi , Francis C . Lau , and Dilip K . Ghosh.

12. Ribeiro C.P. Jr., Borges C.P., Lage P.L.C. A combined gas-stripping vapour permeation process for aroma recovery. *Journal of Membrane Science* **238** (2004) 9–19.
13. Global Industry Analysts, Inc. (2012) Fruit and Vegetable Juices: to Global Strategic Business Report, Technical report.
14. Euromonitor (2005) The World Market for Health and Wellness Products, Technical report.
15. FAO (2001) Principes and practices of small- and medium-scale fruit juice processing, Technical report.
16. Kato T., Shimoda M. (2003) Changes in the odors of squeezed apple juice during thermal processing, Elsevier Ltd , Food Res Int **36**(8)9.
17. Myrna O., Nisperos-Carriedo X., Philip E.S. Comparison of volatile flavor components in fresh and processed orange juice. *Journal of Agricultural and Food Chemistry,* **38** (1990), pp. 1048–1052.
18. Cliff M.A., Fukumoto L.R., King M.C., Edwards B.J., Girard B.. Sensory and physico-chemical properties of membrane filtered apple juices. *Journal of Food Quality,* **23** (2000), pp. 171–184.
19. Schreier (1981) Changes of odor compounds during the processing of fruit juices. *Proc. LongAshton Symp,* **7** (1982)355-371.
20. Ramteke, R.S. and Singh, N.I. and Rekha, M.N. and Eipeson, W.E. (1993) Methods for Concentration of Fruit Juices : to Critical Evaluation. *Journal of Food Science and Technology (India),* **30** (6). pp. 391-402.
21. Jariel O., Reynes, M.; Courel, M. Durand, N. Dornier, M. Deblay, P. Comparison of some fruit juice concentration techniques. *Fruits* **51** (6) 437–450.
22. Nisperos-Carriedo M.O., Shaw P.E.. Comparison of volatile flavor components in fresh and porocessed Orange juices. *J. Agric. Food Chem.* **38**(1990) 1048.
23. Ramteke R.S., Eipeson W.E., Patwardhan M.W. Behaviour of aroma volatiles during the evaporative concentration of some tropical fruit juices and pulps. *J. Sci. Food Agric.* **50**(1990)399.
24. Lin J., Roussef L.R., Barros S., Naim M.. Aroma composition changes in early season grapefruit produced from thermal concentration. *Agric. Food Chem.* **50**(2002)813.
25. Karlsson H.O.E., Traghardh G. Aroma recovery during beverage processing. *J. Food Eng* **34**(1997)159.
26. Fleming H.L., Slater C.S., *Pervaporation, Membrane handbook.* Van Nostrand Reinhold, New York, USA (1992) pp 153-159.
27. Merory J., *Food flavorings*, Avi Publishing Company, Connecticut USA 1968.
28. Little A.D., *Flavor: Its chemical, behavioral and commercial aspects*, Charles M. Apt, Colorado, USA, 1977.

29. Nevo Table 1996, Nevo Foundation, Netherlands Nutrition Centre.

30. Umano K., Hagi Y, Nakahara K., Shoji A, Shibamoto T., Volatile constituents of green and ripened pineapple. *J. Agric Foof Chem.* **40** (1992) 599.

31. Werkhoff P., Guntert M., Krammer H., Sommer H., Kaulen J.. Vacuum headspace method in aroma research: Flavor chemistry in yellow passion fruit. *J. Agric. Food Chem.* **46** (1988) 1076.

32. Mannheim C.H., Passy N.. Aroma recovery and retention in liquid foods during concentration and drying – part I – *Processes. Process Biotechnol.*, **10** (1975) 3.

33. D. Smith, C. Ringemberg, E. Olson. *Freeze concentration of fruit juices, Food processing for entrepreneurs series*. Food and Nutrition safety (2006), University of Nebraska.

34. Nonthanum P., Tansakul A.. Freeze concentration of lime juice, Department of Food Engineering, Faculty of Engineering, King Mongkut's University of Technology, *Mj. Int. J. Sci. Tech.* 2008, *1*(Special Issue), 27-37.

35. Jariel, O., Reynes, M., Courel, M., Durand, N., Dornier, M., 1996. Comparaison de quelques techniques de concentration des jus de fruits, *Fruits*, v. 51, n. **6**, pp. 437-450.

36. Zhang, S. Q., Fouda, A. E., Matsuura, T., Chan, K., 1991, Some experimental results and design calculations for reverse osmosis concentration of green tea, *Desalination*, v. 80, n. **2-3**, pp. 211-234.

37. Jiao, B., Cassano, A., Drioli, E., 2004, Recent advances on membrane processes for the concentration of fruit juices: to review, *Journal of Food Engineering*, v. 63, n. **3**, pp. 303-324.

38. Gostoli, C., 1999, Thermal effects in osmotic distillation, *Journal of Membrane Science*, v. 163, n. 1, pp. 75-91.

39. Das Gupta, D. K., Jayarama, K. S., 1996, Studies on the membrane concentration of watermelon juice, *Journal of Scientific and Industrial Research*, v. 55, n. **12**, pp. 966-970.

40. Medina, B. G., Garcia, A., 1988, Concentration of orange juice by reverse osmosis, *Journal of Food Process Engineering*, v. 10, n. **3**, pp. 217-230.

41. World Health Organization, 2003. *World Health Report.*

42. Ribeiro P., Lage P., Borges C.. Recent Advances in Fruit-Juice Concentration Technology. *Innovation in Food Engineering, New Techniques and Products,* CRC Press 2009, 161–221.

43. Chun, K. R.; Seban, R. A. (1971). Heat transfer to evaporating liquid films. *Journal of Heat Transfer* **93** (197): 391–396.

44. Drioli E., Criscuoli A., Molero L., "Membrane distillation", in *Water and Wastewater Treatment Technologies*, [Ed. Saravanamuthu (Vigi) Vigneswaran],

Encyclopedia of Life Support Systems (EOLSS), UNESCO, EOLSS Publishers, Oxford ,UK (2009).

45. Hongvaleerat C., Cabral L.M.C., Dornier M., Reyne M., Ningsanond S.. 2008 Concentration of pineapple juice by osmotic evaporation, *Journal of Food Engineering, v*. 88, n. **4**, pp. 548-552.

46. Onsekizoglu P., Bahceci K.S., Acar J., 2010, The use of factorial design for modeling membrane distillation, *Journal of Membrane Science,* v. 349, n. **1-2**, pp. 225-230.

47. Thanedgunbaworn R., Jiraratananon R., Nguyen M.H., 2007, "Mass and heat transfer analysis in fructose concentration by osmotic distillation process using hollow fiber module", *Journal of Food Engineering,* v. 78, n. **1**, pp. 126-135.

48. Gunko S., Verbych S., Bryk M., Hilal N.. Concentration of apple juice using direct contact membrane distillation. *Deaslination* **190** (2006) 117-124.

49. Bánvölgyi S., Horváth S., Békássy-Molnár E., Vatai G.. Concentration of blackcurrant (*Ribes nigrum* L.) juice with nanofiltration. Department of Food Engineering, Corvinus University of Budapest. *Desalination* **200** (2006) 535–536.

50. Cath T., Childress A.E., Elimelech M.. Forward osmosis: Principles, applications, and recent developments. *Journal of Membrane Science* **281** (2006) 70–87.

51. Echavarrıa A.P., Torras C., Pagan J., Ibarz A.. Fruit Juice Processing and Membrane Technology Application. *Food Eng Rev* (2011) **3**:136–158

52. Joannes Martinus Koen Timmer. (2001) Properties of nanofiltration membranes: model development and industrial application, Ph.D Thesis, University of Eindhoven, NED.

53. Raghavarao, N. Nagara, G. Patil, B. Babu, k. Niranjar. (2005) Athermal membrane process for the concentration of liquid foods and natural colours. Emerging technologies for food processing. Elsevier Ltd. National University of Ireland, Earlsfort Terrace, Dublin.

54. Lefebvre, M.S.M. (1992). Osmotic distillation process and semipermeable barriers therefore. US Patent 5,098,566, 24.

55. Courel, M. Tronel-Peyroz, E., Rios, G.M., Dornier, M., Reynes, M. (2001). The problem of membrane characterization for the process of osmotic distillation. Desalination **140**: 15-25.

56. Shaw, P.E., Lebrun, M., Dornier, M., Ducamp, M.N., Courel, M., Reynes, M. (2001). Evaluation of concentrated orange and passionfruit juices prepared by osmotic evaporation, LEBENSM-WIS, **34**(2) 60-65.

57. Sheng, J., Johnson, R.A., Lefebvre, M.S. (1991). Mass and heat transfer mechanisms in osmotic distillation process, Mass and Desalination, 140, 15-25.

58. Le Than M., Voilley, A., Phantan Luu, R. (1993). Influence de la composition d'un milieu de culture modèle sur Le coefficient de portage vapeur-liquide de substances aromatisantes. Science Aliments, **13**, 699-710.

59. Vaillant R., Jeanton E., Dornier M., O'Brien G.M., Reynes M., Decloux M., (2001) Concentration of passion fruit juice on an industrial pilot scale using osmotic evaporation. J. Food Eng., **47**, 195-202.

60. Kunz W., Benhabiles A., Ben-Aim R.. (1996). Osmotic evaporation through macroporous hydrophobic membranes: to survey of to current research and applications. J. Membrane Sci., 121, 25-36.

61. Petrotos, K. B., Lazarides, H. N., 2001, Osmotic concentration of liquid foods. Journal of Food Engineering, v. 49, n. **2-3**, pp. 201-206.

62. Courel, M., Dornier, M., Herry, J. M., Rios, G. M., Reynes, M., 2000, Effect of operating conditions on water transport during the concentration of sucrose solutions by osmotic distillation, *Journal of Membrane Science*, v. 170, n. **2**, pp. 281-289.

63. Alves, V. D., Coelhoso, I. M., 2006, Orange juice concentration by osmotic evaporation and membrane distillation: A comparative study, *Journal of Food Engineering*, v. 74, n. **1**, pp. 125-133.

64. Badu, B. R., Rastogi, N. K., Raghavarao, K. S. M. S., 2006, Mass transfer in osmotic membrane distillation of phycocyanin colorant and sweet-lime juice, *Journal of Membrane Science*, v. 272, n. **1-2**, pp. 58-69.

65. Cassano. A., Drioli, E., Galaverna, G., Marchelli, R., Di Silvestro, G., Casagnasso, P., 2003, Clarification and concentration of citrus and carrot juices by integrated membrane processes, *Journal of Food Engineering*, v. 57, n. **2**, pp. 153-163.

66. Galaverna, G., Di Silvestro, G., Cassano, A., Sforza, S., Dossena, A., Drioli, E., Marchelli, R., 2008, A new integrated membrane process for the production of concentrated blood orange juice: effect on bioactive compounds and antioxidant activity, *Food Chemistry*, v. 106, n. **3**, pp. 1021-1030.

67. F. L. Martins (2006) Desenvolvimento experimental, modelagem e simulação do processo de evaporação osmótica para concentração de soluções de sacarose contendo aroma de frutas tropicais. Ph.D. Thesis, COPPE/UFRJ, Rio de Janeiro, RJ, BR.

68. Bailey, A. F. G., Barbe, A. M., Hogan, P. A., Johnson, R. A., Sheng, J., 2000, The effect of ultrafiltration on the subsequent concentration of grape juice by osmotic distillation, *Journal of Membrane Science*, v. 164, n. **1-2**, pp. 195-204.

69. Cissé, M., Vaillant, F., Bouquet, S., pallet, D., Lutin, F., Reynes, M., Dornier, M., 2011, Athermal concentration by osmotic evaporation of roselle extract, apple and grape juices and impact on quality, *Innovative Food Science and Emerging Technologies*, v. **12**, n. 3, pp. 352-360.

70. Kozák, Á., Rektor, A., Vatai, G., 2006, Integrated large-scale membrane process for producing concentrated fruit juices, *Desalination*, v. **200**, n. 1-3, pp. 540-542.

71. Thanedgunbaworn, R., Jiraratananon, R., Nguyen, M. H., 2007, Mass and heat transfer analysis in fructose concentration by osmotic distillation process using hollow fiber module, *Journal of Food Engineering*, v. **78**, n. 1, pp. 126-135.

72. Alves, V. D., Koroknai, B., Bélafi-Bakó, K., Coelhoso, I. M., 2004, Using membrane contactors for fruit juice concentration, *Desalination*, v. **162**, n. 1, pp. 263-270.

73. Onsekizoglu, P., Bahceci, K. S., Acar, J., 2010a, The use of factorial design for modeling membrane distillation, *Journal of Membrane Science*, v. **349**, n. 1-2, pp. 225-230.

74. Onsekizoglu, P., BahcecI, K. S., Acar, M. J., 2010b, Clarification and concentration of apple juice using membrane processes: A comparative quality assessment, *Journal of Membrane Science*, v. **352**, n. 1-2, pp. 160-165.

75. Valdés, H., Romero, J., Saavedra, A., Plaza, A., Bubnovich, V., 2009, Concentration of noni juice by means of osmotic distillation, *Journal of Membrane Science*, v. **330**, n. 1-2, pp. 205-213.

76. Cassano, A., Drioli, E., 2007, Concentration of clarified kiwifruit juice by osmotic distillation, *Journal of Food Engineering*, v. **79**, n. 4, pp. 1397-1404.

77. Nagaraj, N., Patil, G., Badu, B. R., Hebbar, U. H., Raghavarao, K. S. M. S., Nene, S., 2006, Mass transfer in osmotic membrane distillation, *Journal of Membrane Science*, v. **268**, n. 1, pp. 48-56.

78. Vaillant, F., Cisse, M., Chaverri, M., Perez, A., Dornier, M., Viquez, F., Dhuique-Mayer, C., 2005, Clarification and concentration of melon juice using membrane processes, *Innovative Food Science & Emerging Techonologies*, v. **6**, n. 2, pp. 213-220.

79. Rodrigues, M. I., Iemma, A. F. (2005) Planejamento de experimentos e otimização de processos: uma estratégia sequencial de planejamentos. 1ª ed. Campinas, Editora Casa do Pão.

80. Vaillant, F., Jeanton, E., Dornier, M., O'Brien, G. M., Reynes, M., Decloux, M., 2001, Concentration of passion fruit juice on an industrial pilot scale using osmotic evaporation, *Journal of Food Engineering*, v. **47**, n. 3, pp. 195-202.

81. Petrotos, K. B., Quantick, P., Petropakis, H., 1998, A study of the direct osmotic concentration of tomato juice in tubular membrane – module configuration. I. The effect of certain basic process parameters on the process performance, *Journal of Membrane Science*, v. **150**, n. 1, pp. 99-110.

82. Celere, M., Gostoli, C., 2004, Osmotic distillation with propylene glycol, glycerol and glycerol-salt mixtures, *Journal of Membrane Science*, v. **229**, n. 1-2, pp. 159-170.

83. Gostoli, C. O., Cervellti, A., Zardi, G., 1999, Gas membrane extraction: a new technique for the production of high quality juices, *Fruit Processing*, v. **8**, n. 10, pp. 417-421.

84. Alves, V.D., Coelhoso, I.M. (2002). Mass transfer in osmotic evaporation: effect of process parameters. *J. Membrane Sci.*, **208**, 171-179.

85. Peinemann K.V., Pereira Nunes S., Giorno L. (2010) *Membrane Technology: Volume 3: Membranes for Food Applications*, WILEY-VCH Verlag GmbH & Co. KGaA, Weinheim.

86. Maruyama T., Yoshida S., Mizushina T., The flow regime transition in a bubble column, *Journal of Chemical Engineering of Japan* **14** (1981) 352–357.

87. Ruzicka M.C., Zahradnik J., Drahos J., Thomas N.H., Homogeneous–heterogeneous regime transition in bubble columns, *Chemical Engineering Science* **56** (2001) 4609–4626.

88. Heijnen J.J, Van't Riet K. (1984) Mass transfer, mixing and heat transfer phenomena in low viscosity bubble column reactors, *Chem. Eng. J.*, **28**, B21-B42.

89. Shah Y.T., Kelkar B.G., Godbole S.P., Deckwer W.D. Design parameters column reactor estimation for bubble, *AIChE J.* (1982) **28** (3) 353.

90. Deckwer W.D., Schumpe A., Improved tools for bubble column reactor design and scale-up, *Chem. Eng. Sci*. **48** (1993) 889–911.

91. Vandu C.O., Krishna R. Influence of scale on the volumetric mass transfer coefficients in bubble columns, *Chem Eng Proc* (2004) **43** (8)987.

92. Rey, G., (1961) Entrainment from submerged combustion evaporator, *AiChE Journal*, v. **7**, n. 2, pp. 299-302.

93. Jacobs, H. R., (1988) Direct-contact heat transfer for process Technologies, *Journal of Heat Transfer*, v. **110**, n. 4b, pp. 1259-1270.

94. Zaida, A. H., Sarma, S. C., Grover, P. D., Heldman, D. R., (1986) Milk concentration by direct contact heat Exchange, *Journal of Food Process Engineering*, v. **9**, n. 1, pp. 63-79.

95. Clift, R., Grace, J. R., Weber, M. E., (1978) *Bubbles, Drops and Particles.* 1 ed. New York, Academic Press.

96. Swindin, N., (1949) Recent developments in submerged combustion, *Transactions of the Institution of Chemical Engineers*, v. **27**, pp. 209-211.

97. Wilke, C. R., Chang, C. T., Ledesma, V. L., Porter, J. W., (1963) Direct contact heat transfer for seawater evaporation, *Chemical Engineering Progress*, v. **59**, n. 12, pp. 69-75.

98. Kurz, G., Güthoff, H., (1987) Submerged combustion gathers a variety of applications, *Process Engineering*, v. **68**, n. 1, pp. 31-32.

99. Cronan, C. S., (1956) Submerged combustion flare anew, *Chemical Engineering*, v. **63**, n. 2, pp. 163-167.

100. Owen, J. J. JR., Moggio, W. A., (1955) Submerged combustion evaporation of neutral sulphite spent cooking liquor, *Tappi Journal*, v. **38**, n. 2, pp. 144-147.

101. Burlyn, Michel (1972) Solute Potentials of Sucrose Solutions. *Plant Physiol.* (1972) **50**:196–198.

102. Michaels et al (1998) Methods and apparatus for osmotic distillation. Patent number 5824223, Rentiers Machinery Proprietary Ltd.

103. V.M.M. Lobo, (1975) *Electrolyte Solutions: Literature Data on Thermodynamic and Transport Properties - Vol. I and II*, Coimbra Editora, Coimbra.

104. Achilli, Y T. Cath, A. E. Childress (2010) Selection of inorganic-based draw solutions for forward osmosis applications. *Journal of Membrane Science,* **364** (1−2), 233−241.